SAPIENZA
UNIVERSITÀ DI ROMA

The RSB order parameter in finite-dimensional spin glasses. Numerical computation at zero temperature

Scuola di dottorato Vito Volterra

Dottorato di Ricerca in Fisica – XXXI Ciclo

Candidate

Francesco De Santis
ID number 0000

Thesis Advisor

Prof. Giorgio Parisi

A thesis submitted in partial fulfillment of the requirements
for the degree of Doctor of Philosophy in Physics

31 July 2019

Thesis defended on 09 September 2019
in front of a Board of Examiners composed by:

Prof. Andrea Cavagna (chairman)

Prof. Matteo Marsili

Prof. Silvio Franz

The RSB order parameter in finite-dimensional spin glasses. Numerical computation at zero temperature

Ph.D. thesis. Sapienza – University of Rome

ISBN: 000000000-0

This thesis has been typeset by LaTeX and the Sapthesis class.

Version: September 6, 2019

Author's email: francescodesantis.fds@gmail.it

Abstract

This thesis focuses on the computation of the overlap distribution which characterizes spin glasses with finite connectivity upon an RSB transition at zero temperature. Two models are studied: the $J\pm$ Bethe lattice spin glass and the Edwards-Anderson spin glass in three dimensions with *random regular* bond dilution, a random dilution with the constraint of fixed connectivity $z = 3$. The overlap distribution is the spin glass order parameter and its form has not been derived yet for models other than mean-field. The approach is based on the study of the effects induced by a bulk perturbation on the energy landscape. In ultrametric spin glasses, the distribution of the excited states is known to be related to the order parameter through a universal formula which is used for deriving the order parameter from the experimental distributions. Besides, the finite-size corrections to the ground state energy are computed for the two models.

Contents

Introduction

The reason why spin glasses have dominated the scene of Statistical Mechanics of Disordered Systems in the last forty years is the complexity of behaviors they manifest even in the simplest form of mean-field approximation. Like glasses, below a certain critical temperature, these systems condensate in an exponential multitude of frozen configurations which are different from each other and not related by any simple symmetry. If one had to classify all the possible states, the organization of these frozen states would remind more of the branching process of a tree than some casual distributions of points in space. Such complexity was frankly unexpected when the model was formulated for the first time by Edwards and Anderson in the seventies [1] as little more than a purely theoretical problem with few practical applications. The subject turned out to be a formidable challenge for physicists and mathematicians, yielding to the formulation of new theories and methods for building a more general Theory of Glasses.

In this respect, spin glasses are probably the simplest realization of a glass. In the Edwards-Anderson (EA) original formulation, a spin glass is nothing more than a collection of Ising spins on a lattice, their nearest-neighbor interactions being a random distribution of ferromagnetic and anti-ferromagnetic bonds. In other words, the Edwards-Anderson spin glass is an Ising model, very well known in Statistical Mechanics, with a pinch of randomness added to the Hamiltonian. As simple as it could seem, this is one of the most complicated models to be approached and its thermodynamics has not been fully understood yet, with a solution being available only in more than six dimensions. In this respect, the infinite-dimensional spin glass is a simplified version of the EA model introduced by Sherrington and Kirkpatrick (SK) [2] as a starting point for building a mean-field solution. Nevertheless, finding the correct solution to this model required a great effort and took several years. The exact solution was found by Parisi [3, 4] in a particular formulation known as *Replica Symmetry Breaking* (RSB)[5], whose physical implications were not immediately understood. When the mystery was solved few years later[5, 6], an unexpected scenario appeared, as the spin glass phase turned out to be organized in a large number of states different from each other, organized in a complex hierarchy of clusters known as *ultrametric* structure [7].

Many advances have been made since then. First of all, numerous results found initially with a heuristic approach, like the replica method, have been rigorously proved with a more robust mathematical formulation [8, 9], almost twenty-five years after the formulation of the theory. Moreover, new techniques have been forged to extend the theory beyond the mean-field level. The cavity method [10, 11] allows to reformulate the original spin glass problem in a probabilistic framework providing a

bridge with Combinatorial Optimization [12–16]. Moreover, the spin glass theory has found a wide range of applications in fields ranging from physics to very different areas, like supercooled liquids [17–19], photonics [20, 21], random matrices [22–24], random interfaces [25], inference [26–28], signal processing[29], neural networks [30–33], immunology [34, 35], epidemic spreading [36, 37], finance [38], game theory [39, 40], quantum algorithms [41], collective behavior [42, 43] and biological networks [44].

The problem of formulating a finite-dimensional theory remains. In this respect, finite-dimensional models represent a more realistic version of spin glasses, where each spin can interact only with a limited number of neighbors, and one wonders how many of the remarkable features of the mean-field description would survive in these models. The theoretical task, however, is not easy. In order to descend to finite-dimensions, one should consider fluctuations around the mean-field solution, a problem studied in the Renormalization group approach [45], whose goal is to compute the upper critical dimension above which the mean-field solution provides a meaningful description of the spin glass transition. It is known that for the EA model the upper critical dimension is $d_u = 6$.

Several conjectures have been made about the behavior in dimension lower than six. The investigation in this regime is mostly based on the comparison between numerical evidence on systems of finite-size and the predictions from Finite Scaling Theory (FSC). In the RSB theory, small excitations of finite energy cost produce a global rearrangement of the system whose interface is space-filling, even in the thermodynamic limit. In the Droplet Scaling Theory, or Droplet Model (DM) [46–48], a very different scenario is conjectured, where excitations have the form of compact droplets with a fractal-dimensional interface, whose cost grows with the size of the system.

Unfortunately, the complications which arise in the numerical investigation at low temperature, limit the size of the systems which can be studied. Two main approaches are usually taken. One could either thermalize the system starting from high temperature and performing a simulated annealing (or analog technique based on a Monte-Carlo dynamics), or perform a direct calculation of ground states and proceed with a zero-temperature analysis. In the first case, critical slow-down phenomena arise which make the algorithm very inefficient as the temperature decreases. The second approach has proved to be very useful in the last twenty years, as very effective algorithms for the ground states computation have been borrowed from computer science.

The purpose of this thesis is two-fold. On one side it constitutes a review of the efforts which have been made until today to formulate a finite-dimensional description of spin glasses, focusing mostly on the numerical approach and on the results collected in favor of the different theoretical conjectures. On the other side, we provide an original contribution to the ongoing investigation by deriving the overlap distribution at zero temperature of two models: the Bethe lattice spin glass, and the diluted Edwards-Anderson model in three dimensions. The overlap distribution has great importance in the characterization of the spin glass phase since it constitutes the physical order parameter of the spin glass transition. In other words, the whole information about the organization of the states is encoded within this distribution. The analytical derivation of this quantity is possible only in mean-field models, and its numerical computation has been tried in different contexts. The method adopted

in this thesis was proposed by Franz and Parisi [49], and is based on the effects induced by a bulk perturbation on the energy landscape. The purpose of the analysis is to gather new information about the nature of spin glasses which deviate from the mean-field description.

This thesis is organized as follows:

PART I : In the first part the fundamentals are introduced and a course is set from mean-field theory to finite-dimensional systems, passing through diluted systems.

In *Chapter 1*, the general formalism is introduced, providing notions of graph theory and presenting a general introduction to spin glasses and disordered systems. Moreover, a connection between Spin Glass Theory and Combinatorial Optimization is presented to show the extent of the theory.

In *Chapter 2*, the mean-field theory of spin glasses is presented through the introduction of two standard models: the Sherrington-Kirkpatrick model and the Bethe lattice spin glass. The two main approaches used in the mean-field theory are reviewed: the Replica approach and the Cavity method. Moreover, one of the most important concepts of spin glass theory will be introduced: the spin glass order parameter.

In *Chapter 3*, the state of the art of the investigation at finite dimension is presented, focusing on the numerical approach and on the scaling properties of the ground states.

PART II : In this part, the main results of the numerical simulations concerning several aspects of spin glasses at finite dimension and finite connectivity are presented.

In *Chapter 4*, the computational setup and the numerical approach are presented, together with the first results of the simulations and a short tentative study of the ultrametricity.

In *Chapter 5*, the first original contributions of this thesis are presented as the finite-size corrections to the ground state energy of the models are calculated and discussed.

In *Chapter 6*, the overlap distribution of the models is derived from a direct computation of the ground states. As the technique adopted for the computation had never been used before for these models, the results presented in this chapter are an original contribution to the ongoing investigation.

In *Chapter 7*, some conclusions and perspectives of the present work are discussed.

The project that forms the basis for this thesis was developed gradually during the years of the doctorate. The initial idea suggested by Giorgio Parisi, my thesis advisor, involved the derivation of the RSB order parameter of the Bethe lattice

from the overlap distribution induced by a bulk perturbation. The starting point consisted in developing and refining the computational framework, and preparing the ground for simulations on a scale large enough to provide statistically significant results. This part was completed by the end of the first year, and the results obtained were in agreement with the presence of an RSB transition at zero temperature at the predicted critical field. During the second year, my advisor suggested that the same method could be used for studying a bond-diluted finite-dimensional model with a degree distribution similar to the one of the Bethe lattice. At the same time, I started to study the finite-size corrections to the ground state energy and the spin glass susceptivity near the critical field. This latter was addressed by studying the scaling properties of the excitations induced by one spin reversal. In this case, the preliminary results showed that the method was affected by excessive noise and the study was postponed for further investigation. The study was refined during the final year of the doctorate, which was also spent on verifying the obtained results. In particular, the results relative to the spin glass models were compared with the results obtained in the random field case, where no RSB transition is expected. Moreover, the consistency of the method for deriving the order parameter was tested and confirmed by a more detailed analysis of the experimental distributions. In conclusion, the different results obtained over the course of these few years of doctorate fall into the branch of finite-dimensional studies. Hopefully, they may provide a useful tool of investigation for deriving a more general theory of spin glasses.

Part I

General Introduction

Chapter 1

Disordered systems

1.1 Elements of Graph Theory

Graphs are mathematical structures able to represent very effectively networks of relationships between elements. The concept of graph was introduced already in the 18th century by Euler to study the problem of the *Seven bridges of Königsberg*, and formalized in the next two centuries with the works of Cayley on trees, König, and Polya [50]. The probabilistic approach that brought to the formulation of modern *random graph theory* [51, 52] started with the article of *Erdös and Rényi* on random graphs [53]. Beside the applications in mathematics and physics, graph theory has proven very effective at modeling systems of various nature, from Computer Science to Biology, Finance and Social Science[54–57]. In the context of disordered systems, graph theory provides a useful notation for defining the underlying structure of a model and powerful methods and theorems for characterizing its topology.

In this section, we introduce the basic concepts and the notation which will be used very often throughout the rest of this thesis. For a more detailed introduction to Graph Theory we refer to [52, 58].

1.1.1 Fundamentals

Basic definitions. A *graph* $G(N, M) = G_{N,M} = (\mathcal{V}, \mathcal{E})$ consists of a set $\mathcal{V} \neq \emptyset$ of N *vertices* (or *nodes*) and a set $\mathcal{E}$ of M edges (or *links*). A node is usually identified by its order i in $\mathcal{V}$, such that $\mathcal{V} = \{1, \dots, N\}$, while the edges are represented as pairs of elements of $\mathcal{V}$. If the pairs are unordered then the graph is *undirected* and the edges are represented as lines connecting the nodes, otherwise the graph is *directed* and the edges are represented as arrows.

An edge l is said to be *incident* in the node i if i is one of the *end-nodes*. Two nodes joined by an edge are said to be *adjacent* or *neighboring*. The set of vertices incident in a node i is called *adjacency* or *neighborhood* of i and is denoted ∂i. An edge of the type (i, i) is called *self-loop* (or simply *loop*). If two nodes are joined by more than one edge, then the link is a *multi-edge*. A graph which does not contain either loops or multi-edges is said to be *simple*, otherwise is called *multigraph*. The number of edges M in an undirected graph ranges from zero (*edgeless* graph) to $\binom{N}{2} = N(N-1)/2$ (*fully-connected* graph). The graph is said to be *sparse* if

$M \ll N^2$ (or M remains finite in the $N \to \infty$ limit), or *dense* if $M = \mathcal{O}(N^2)$. Moreover, if a mapping $w : \mathcal{E} \mapsto \mathbb{R}$ is defined, then the graph is said to be *weighted*. In simple graphs, the *weights* are denoted $w(i,j) \equiv w_{ij}$ and may specify the *cost, capacity* or a measure of *distance* if the graph is embedded in a metric space. In the rest of the thesis, we will consider simple graphs which are undirected and unweighted, unless differently specified.

A *subgraph* $G'(\mathcal{V}', \mathcal{E}')$ is a graph such that $\mathcal{V}' \subseteq \mathcal{V}$ and $\mathcal{E}' \subseteq \mathcal{E}$. If $\mathcal{E}'$ contains all the edges incident in the nodes of $\mathcal{V}'$ which are contained in $\mathcal{E}$, then G' is said to be the *subgraph induced by* $\mathcal{V}'$, denoted $G' = G[\mathcal{V}']$. A subgraph is *maximal* with respect to a property if it cannot be extended without losing that property.

Node degree and degree distributions. The cardinality of the adjacency of a node is said *connectivity* of *node degree*: $deg(i) \equiv k_i = |\partial i|$. If $k_i = 0$ the node i *isolated*; if $k_i = 1$ the node is a *leaf*. It is convenient to consider the *degree distribution* of a graph, defined as the frequency distribution:

$$p_G(k) \equiv \frac{1}{N} \sum_{i \in \mathcal{V}} \delta(k - k_i), \quad k \in \mathbb{N} \tag{1.1}$$

The *mean degree* is

$$z_G \equiv \frac{1}{N} \sum_{i \in \mathcal{V}} = \sum_{k \geq 0} p_G(k) k \tag{1.2}$$

Paths and cycles. A *path* W_ℓ of length ℓ is an ordered sequence of vertices $W_\ell = (i_0, i_1, \ldots, i_\ell)$ such that $(i_n, i_{n+1}) \in \mathcal{E}$, $\forall n = 0, \ldots, \ell - 1$. A path is *simple* if each node is crossed only once by the path. The *distance* between two nodes is defined as the length of the shortest path between them. The maximum distance of the graph is said to be the *diameter* of the graph. A path is called a *cycle* if $i_0 = i_\ell$, otherwise is an *open* path. A graph with no cycles is called *acyclic*.

Trees. An acyclic graph is called a *forest*, and a connected forest is called a *tree*. In a tree, any two vertices are connected by only one path. Moreover, if an edge is removed from a tree, the resulting graph is disconnected; if an edge is added to the tree, a cycle is formed, and the graph is not a tree anymore. Trees contain always at least one leaf with degree 1.

In *rooted* trees, a vertex is distinguished from the others and called a *root*. The *depth* of a node is defined as its distance from the root. In rooted trees, there is an orientation for classifying the nodes which goes from the root to the leaves. With respect to a node i, the nodes on the path to the root are called *ascending* nodes, while the ones on the path to the leaves are called descending nodes. The *parent* of a node is its neighboring ascendant, while the *child* of a node is one of the adjacent descendants. Two nodes are *siblings* if they share the same parent.

A *spanning tree* of a graph is a tree subgraph which contains all the vertices of the graph.

Other topological properties A graph is *connected* if for any pair of nodes i, j there exists a path between them. A graph is *K-partite* if $\mathcal{V}$ can be partioned in K subsets of disconnected graphs. The *giant component* of a graph is a connected portion of the graph which contains a number $\mathcal{O}(N)$ of nodes.

Matricial representation. A graph can be completely defined an *adjacency matrix* A, an $N \times N$ matrix whose coefficients A_{ij} are equal to 1 if $(i,j) \in \mathcal{E}$, 0 otherwise. The adjacency matrix of a simple graph is *symmetric* and *zero-diagonal*. Moreover, the sum across the i-th row or column is equal to the k_i. An interesting property of the adjacency matrix of a simple graph is that its powers A^l are related to the paths of length l between the nodes. The coefficient A^l_{ij} is equal to the number of *directed* paths between i and j. The coefficients A^l_{ii} are equal to twice the number of cycles of length l passing through i. In weighted graphs, the coefficients of the adjacency matrix may be the weights: $A_{ij} = w_{ij}$.

A graph can be alternatively represented by the *incidence matrix* B, a $N \times M$ matrix whose entries B_{ik} are 1 if the edge $e_k \in \mathcal{E}$ is incident in $i \in \mathcal{V}$. Typically, this representation is more expensive in terms of storage space in computational applications, and a representation in terms of the adjacency matrix is preferred. The adjacency matrix of sparse graphs is also sparse, and in practical applications is substituted by *adjacency list* $\{a_i\}_{i\in\mathcal{V}}$ in which every vector a_i is the list of the adjacent nodes.

1.1.2 Random Graphs

In 1959, Erdös and Renyi introduced a new probabilistic approach to graph theory [53], with the purpose of studying the properties of graphs as a function of the increasing number of random connections, founding a new branch which developed independently as *random graphs theory*. The approach is based on the definition of a probability space on the set of graphs $\mathcal{G}$ with N vertices with a specific probability measure $P[G]$, which together define a *graph ensembles*. An instance or realization of a particular element of the ensemble is a graph $G \in \mathcal{G}$ sampled from the distribution $P(G)$ following a specific random process.

Due to the presence of structural disorder, one is usually interested in the behavior of the *typical* instance of the ensemble. Thus, it is convenient to define the *average over the ensemble* of a property O:

$$\mathbb{E}[O_G] \equiv \overline{O} = \sum_{G\in\mathcal{G}} O_G P[G] \tag{1.3}$$

In the following, we introduce two ensembles particularly important in the theory of spin glasses.

Erdös-Renyi (ER) ensemble: In their first article [53], Erdös and Renyi proposed a model for generating random graphs with N nodes and M edges, which we denote $G^{ER}_{N,M}$. Starting with an edgeless graph with N nodes, ER graphs are generated by adding randomly M edges, prohibiting loops or multi-edges. A different ensemble $G^{ER}_{N,p}$ is generated by following a different procedure. Starting from a set of N disconnected nodes, each of the $N(N-1)/2$ edges is added with probability $0 < p < 1$. This ensemble contains graphs with a different number of links, the average being $\binom{N}{2}p$, and the probability of a graph with M edges is:

$$P[G] = p^M (1-p)^{N(N-1)/2-M} \tag{1.4}$$

The $G^{ER}_{N,M}$ and $G^{ER}_{N,p}$ models coincide in the $N \to \infty$ limit, and they have a strong analogy, respectively, with the canonical and grand canonical ensemble in Statistical Mechanics [59].

The probability that a node i has $k = k_i$ edges is the binomial distribution:

$$P(k_i = k) = \binom{N-1}{k} p^k (1-p)^{N-1-k} \tag{1.5}$$

where p^k is the probability for k edges to be incident in i with independent probability p, $(1-p)^{N-1-k}$ is the probability of *not* having the remaining $N-1-k$ edges, and $\binom{N-1}{k}$ is the number of different ways of selecting the neighboring nodes. Since all the nodes are statistically equivalent, in the large N limit and fixed $z =< k >$, the degree distribution tends to the Poissonian distribution:

$$P(k) = \frac{e^{-z} z^k}{k!} \tag{1.6}$$

For this reason, ER graphs are called *Poissonian random graphs.*

Random Regular Graph (RRG) ensemble : The ensemble of the *z-regular random graphs* $G^{RRG}_{N,z}$ (with $3 \leq z \leq N$) has uniform measure over the random graphs where each of the N nodes has fixed degree $k_i = z$. The number of edges is $M = \frac{Nz}{2}$, and Nz must be an even number.

Since most of random graphs are non-regular, it is important to implement the selection of the RRGs in an unbiased way, such that the samples are drawn with a uniform distribution over the $G^{RRG}_{N,z}$ ensemble. The standard method was proposed by Bollobás [60], and goes under the name of *configuration model*, or *pairing model*. One starts with a partition of Nz points called *half-edges* in N *cells* of z elements, and proceeds by pairing the half-edges through a random matching. The RRG is generated by contracting each of the N points belonging to different cells into one point. In general, there is a finite probability to obtain a multi-graph, especially for large values of z. In this case, the graph is discarded and the procedure is repeated from the beginning. Due to the possibility of sampling a non-simple graph, this method is computationally expensive and gets exponentially slow with increasing z. Faster algorithms which preserve the uniform measure over the ensemble in the large N limit have been proposed in [61, 62]. In particular, the algorithm can be simplified by rejecting just the last matching which brings to a multi-graph, without repeating the whole procedure. This is the method which has been used for generating the RRG samples in this thesis.

The configuration model, though, provides a uniform measure over the ensemble and can be used for generating random graphs from the ensemble $G^{CONF}_{N,D}$ with $D = \{k_i\}_{i=1}^N$ any given degree distribution [63].

Connectedness. The connectivity properties of random graphs are subject to a dramatic change upon a change of the parameter p below a critical value $p_c = 1/N$.

Let us consider the $G^{ER}_{N,p}$ model, whose graphs have an average degree $z =< k >$. Erdös and Renyi proved that *almost surely* [1]:

- if $p < p_c$, then the graph is disconnected in components not larger than $\mathcal{O}(\ln N)$ with no more than one cycle;
- if $p = p_c$, then the larges component has size $\mathcal{O}(N^{2/3})$;
- if $p > p_c$, then the graph has a giant component of size $\mathcal{O}(N)$ with $\mathcal{O}(N)$ cycles, and there are no components larger than $\mathcal{O}(\ln N)$ and more than one cycle.

From the statistical physics point of view, the transition at p_c has the typical features of a second-order phase transition, and if the size of the largest component is chosen as order parameter, then the transition falls in the same universality class as mean-field percolation transitions. With respect to the property of connectedness in $G^{ER}_{N,p}$, a random graph is almost surely connected if $p \geq \frac{\ln N}{N}$. In the $G^{RRG}_{N,z}$ ensemble, almost any graph is connected for $z \geq 3$.

Local tree topology. In the context of statistical physics, one of the most important properties of random graphs concerns the density of cycles of finite length. In this respect, the probability of finding C_ℓ cycles in a random graph is finite in the $N \to \infty$ limit, if ℓ is kept constant.

In random regular graphs, a given sequence of variables $Y_3, \ldots, Y_m$ representing the number of cycles of length $3 \leq \ell \leq m$, tend asymptotically to random variables with Poisson distribution [51, 64] and mean:

$$\lambda_\ell = \frac{(z-1)^\ell}{2\ell} \tag{1.7}$$

As the density of cycles of finite length decreases with the size of $G^{RRG}_{N,z}$ graphs, given any node i, there exist a distance R such that the subgraph induced by the nodes within distance R from i is almost surely a tree. In spin glass theory this property is crucial, since it grants that the frustration affects the system only on large scale, permitting to neglect the correlation between spins at short distance. In this regard, a spin glass model defined on a random graph is a *Bethe lattice spin glass*, and will be studied in detail in Section 2.2.

1.1.3 Factor graphs

The representation of systems where local interactions involve more than two variables requires a more general class of bipartite graphs called *factor graphs* [12]. Factor graphs are normally used for representing the p-spin model and some optimization problem (see Section 1.2.3).

Let us consider a set of N variables $\underline{x} = \{x_1, \ldots, x_N\}$ taking values in a finite set X, and a probability measure defined over the space of the configurations :

$$P[\underline{x}] = \frac{1}{Z} \prod_{a=1}^{M} \psi_a(\underline{x}_{\partial a}) \tag{1.8}$$

[1] In probability theory, a property is *almost sure* if it appears with probability one in the large N limit, or in other words if the set of instances where the property is violated has zero measure in the probability space.

where ψ_a are special *compatibility functions* which depend on the nature of the problem, defined on a subset ∂a of the N variable indexes.

A *factor graph* is a bipartite graph which provides an effective representation of the joint probability (1.8). Factor graphs consist of two groups of vertices:

- *variable nodes*, which correspond to the N variables and whose indexes are denoted $i, j, k, l, ...$
- *function nodes*, which correspond to M interactions between nodes, denoted $a, b, c, ...$, each one involving a subset of variable nodes $\partial a, \partial b, \partial c$

Each variable node is connected by edges to all the function nodes in which it appears, and vice versa.

In spin glasses with pairwise interactions, the function nodes are trivial, since they connect only 2 spins. ($|\partial a| = 2$), and simple graphs provide a good representation. In p-spin glasses with $p > 2$, each function node a has adjacency $\partial a = \{i_1, \dots, i_p\}$ and contributes to the Hamiltonian with a term $E_a = -J_{i_1,\dots,i_p}\sigma_{i_1} \dots \sigma_{i_p}$. Factor graphs representation provides a powerful connection between statistical physics and combinatorial optimization.

1.2 Spin glasses

Spin glasses were introduced in the early seventies as a class of magnetic materials with a peculiar response to an oscillating external field. For these systems, the susceptibility has a cusp at a critical temperature T_c, a behavior qualitatively different from ordinary magnetic materials [65]. This singular behavior is explained in terms of a phase transition due to the *freezing* of the magnetic dipoles of the samples. Like in ordinary ferromagnetic materials, the physical origin of these dipoles is the *spin* of the electrons, with the difference that the couplings between the spins are somehow irregular. This irregularity can be accounted for by introducing two ingredients in an ordinary d-dimensional ferromagnetic Ising model: *disorder* and *frustration*. The disorder is introduced in the form of random anti-ferromagnetic bonds, according to some probability distribution. The frustration is due to the presence of closed cycles in the graph along which it is not possible to satisfy simultaneously all the bonds. This results in the impossibility of minimizing all the terms of the Hamiltonian at the same time.

The systematic study of spin glasses started with the articles of Edwards and Anderson [1] and Sherrington and Kirkpatrick [2]. Since then, spin glasses have gained importance in Statistical Mechanics as representative of a more general class of disordered systems, ranging from supercooled liquids, glass forming, structural glasses, optimization problems, and many other models. In this context, many interesting phenomena concerning glassy systems were discovered for the first time in mean-field spin glasses, models where the mean-field approximation is exact.

Before proceeding further, it is convenient to summarize the most important aspects which account for the *glassy behavior* of spin glasses:

- Spin glasses undergo a phase transition at critical temperature T_c. The transition from the paramagnetic phase to the *spin glass phase* is characterized by the appearance of *frozen disorder* in which the local magnetization is non-zero but the total magnetization is null.

- The energy landscape in the spin glass phase is *rough* as it consists of many valleys and barriers. In the thermodynamic limit, the barriers are eventually infinite, and the ergodicity is broken in the system. The Gibbs state does not describe anymore the system at the equilibrium and the Boltzmann measure is decomposed in a sum of *pure states*, corresponding to the measures restricted to ergodically disconnected regions of the space of the configuration.

- The out-of-equilibrium behavior is characterized by a different type of transitions which occur in general at different temperatures from T_C. The dynamic evolution of the systems is subject to a critical slowing down upon cooling below the critical temperature starting from high temperature. The dynamics is characterized by history-dependent response and aging.

- The mean-field solution of the SK model provides a scenario known as *replica symmetry breaking* (RSB), in which all the states are macroscopically different and show a form of non-trivial organization. Due to *ultrametricity*, the states are organized in a structure of clusters with respect to their mutual distances. This hierarchy can be described by representing the states as the leaves of a

rooted tree and the clusters as the intermediate nodes.

In this section, we will introduce a mathematical definition of disorder and present the main theoretical models of spin glasses. Moreover, we will give a brief review of a different class of disorder systems encountered Optimization. The analogy between spin glasses and optimization problems has widely influenced the development of both Physics and Computer Science, as concepts, methods, and algorithms have been shared to build a more general theory of disordered systems.

1.2.1 Disorder

Quenched disorder. In real disordered systems, different types of variables are normally characterized by different dynamic time scales τ. The variables subject to thermal fluctuations, like spins in magnetic systems, follow a *fast* thermal dynamics, their values changing in times of order τ_{eq}. The system is considered at equilibrium for times $t_{eq}/\tau_{eq} \gg 1$. On the other hand, the variables describing the disorder are governed by much slower dynamics, with time scale $\tau_q \gg \tau_{eq}$. For all practical purposes, these variables are considered frozen, or *quenched*, as they are constant for $t < t_{eq}$. In this case, a sample of a disordered system is characterized by a specific configuration of quenched variables.

When describing spin glasses, we will consider two types of disorder. The first one consists in a certain amount of randomness introduced in the mutual interactions between the variables. For a given sample, the coefficients of the coupling matrix J are i.i.d. quenched random variables drawn from a probability distribution $P(J)$ which depends on the model considered. In infinite-range models and in the d-dimensional Edwards-Anderson model, this is the only type of disorder present in the system.

The second type of disorder is structural, as randomness is introduced in the *adjacency matrix* of the graph which describes the lattice. In *Erdos-Reiny* random graphs two nodes are connected with probability p, and the distribution of the node degrees is Poissonian. In *random regular graphs* the nodes are connected at random, but the number of neighbors of each node is kept constant. In *diluted graphs* the edges are removed with a certain probability starting from a *d-dimensional* regular lattice. In the next chapters we will consider a sort of *random-regular* dilution for the regular lattice, obtained by keeping the number of neighbors of each node constant $z < 2D$.

Unless differently specified, in the rest of this thesis we will assume that every form of disorder is contained in the matrix J. A null entry $J_{ij} = 0$ will denote a missing bond between the sites (i, j), while a non-zero entry will denote both the presence of an edge in the underlying graph ($A_{ij} = 1$) and the coupling between the two sites.

The average over the disorder. Let us consider a given sample characterized by a specific realization of J, and let us consider an observable O_J describing some thermodynamic property of the sample. Due to the presence of disorder, O_J is different when calculated on two different samples with different realizations of J. When dealing with disordered systems, though we are interested in the behavior of the *typical sample*, whose properties are supposed to be described by quantities

which are averaged over the disorder distribution. In our case, we will denote such averages for an observable as:

$$O = \overline{O_J} = \lim_{N\to\infty} \int O_J P(J) dJ \tag{1.9}$$

This averages are relevant for describing the whole ensemble only if the fluctuations can be kept under control. For instance, as in ordinary statistical mechanics we know that the relative fluctuations of the energy around its thermal mean value are of order $O(N^{-1/2})$, we also expect that the fluctuations of relevant quantities between different systems go to zero in the thermodynamic limit. If the sample-to-sample fluctuations vanish in the thermodynamic limit, then the observable is said to be *self-averaging*. If we know that quantities of interest are self-averaging, then we can expect the same results in experiments on different macroscopic samples. Moreover, a theoretical computation of the mean value of such quantities over the whole ensemble gives the same results in all of the experiments. Normally, extensive observables such as the free-energy are well-behaved, in the sense that their associated densities are *self-averaging* in the thermodynamic limit.

However, not all the observables are *self-averaging*. In some cases, the *atypical samples* give a finite contribution to the average even in the thermodynamic limit. In this case, the sample-to-sample fluctuations do not vanish for $N \to \infty$ and the average over the disorder cannot be assumed to be representative of the behavior of the single sample. An example of non-averaging observable is the overlap distribution in spin-glasses, which will be introduced in the next sections.

Quenched and annealed averages. Let us consider a system described by Hamiltonian H_J, whose equilibrium distribution is characterized by the usual Boltzmann measure, and let Z_J be the partition function:

$$Z_J(\beta) = \mathrm{Tr}_\sigma e^{-\beta \mathcal{H}_J} \tag{1.10}$$

where β is the inverse temperature, and the trace involves the sum over all the configurations of the Boltzmann measure.

We are interested in computing the averaged free-energy density:

$$f = \overline{f_J} = -\lim_{N\to\infty} \frac{1}{\beta N} \overline{\log Z_J} \tag{1.11}$$

The presence of the logarithm here is crucial. The average over the logarithm of the partition function is a *quenched average* and it turns out to be more complicated than the simpler *annealed average* $\overline{Z_J}$. In the second average, the quenched variables and the thermal variables are treated in the same way. However, we know that quenched variables do not participate in the thermalization of the system and that they must be considered constant in the typical time-scale needed for reaching the equilibrium. For this reason, the two averages have very different physical meaning and cannot be exchanged.

1.2.2 Spin glass models

A spin glass is defined as a set of N variables $\sigma = \sigma_{ii=1,\dots,N}$ located on the vertices of a graph G. If the interactions between the variables are pairwise, then G is a

simple graph with only one type of vertices (representing spin variables), and the edges of the graph represent pairs of interacting spins. If more than two spins are involved in the interactions, like in the more general p-spin model then G is a factor graph. In this thesis, we will consider only models with 2-spin interactions and Ising variables $\sigma_i = \pm 1$, unless differently specified.

Given these premises, let us consider an Ising spin glass defined on a simple graph $G = (\mathcal{V}, \mathcal{E})$:

$$\mathcal{H}_J[\sigma] = -\sum_{(i,j)\in\mathcal{E}} J_{ij}\sigma_i\sigma_j - \sum_{i\in\mathcal{V}} h_i\sigma_i \tag{1.12}$$

The coefficients J_{ij} are i.i.d. quenched random variables drawn from a probability distribution $P(J)$, different from zero only in correspondence of an edge. We will assume that the coupling matrix J is symmetric ($J_{ij} = J_{ji}$) and has zero-diagonal ($J_{ii} = 0$).

Two distributions of disorder are usually considered:

- *Gaussian distribution* with mean $\overline{J}$ and variance $\overline{J^2}$:

$$P(J) = \frac{1}{\sqrt{2\pi\overline{J^2}}} e^{-\frac{J-\overline{J}}{2\overline{J^2}}} \tag{1.13}$$

- *Bimodal distribution* with zero mean and variance 1:

$$P(J) = \frac{1}{2}\delta(1-J) + \frac{1}{2}\delta(1+J) \tag{1.14}$$

In some cases we will mention *biased* models in which $\overline{J} \neq 0$, otherwise we will consider $P(J)$ with zero mean.

We also consider four different models:

Sherrington-Kirkpatrick (SK) model [2]: In the *fully-connected* model all the J_{ij} coefficients are different from zero and drawn from a Gaussian or Bimodal distribution with variance $N^{-\frac{1}{2}}$. This ensures that the energy density does not diverge in the thermodynamic limit when the number of terms in the Hamiltonian grows as $\mathcal{O}(N^2)$. The mean-field theory gives exact results for this model in the $N \to \infty$ limit [66].

Bethe lattice (BL) model [10, 11]: The model is typically defined on a random regular graph with coordination number z. As the number of edges is $Nz/2$, the variance of the $P(J)$ distribution is finite and typically set to $z^{-1/2}$ in order to have a good limit $z \to \infty$. Due to the topology of the underlying graph, the correlations can be neglected in the thermodynamic limit, and the mean-field theory is valid for this model.

Long range (LR) model [67]: The model is defined on a d-dimensional lattice, and the interactions are limited within a radius R from each site. The variance of the disorder distribution is therefore set to $1/R^{D/2}$. In this model, the corrections to the mean-field theory are small if R is large. However, the corrections might change the large distance behavior of the correlation functions, and the phase transition might disappear. Normally the long-range model

represents a good candidate for interpolating between the mean-field results and the short-range model [68].

EDWARDS-ANDERSON (EA) MODEL [1, 69]: The model is defined on a d-dimensional lattice with nearest-neighbors interactions, and the variance is normally $D^{-\frac{1}{2}}$. The correlations to the mean-field theory are large, and no spin glass transition is expected in $d = 1, 2$ (the lower critical dimension is $d_c = 2.5$) [70]. The upper critical dimension above which the mean-field describes correctly this model is $d_u = 6$. The behavior at lower dimension is still debated, and the investigation relies mostly on numerical methods.

From the analytical point of view, the four models have been presented in order of difficulty, the infinite-range model being the simplest and the first to be solved, and the others presenting difficulties in the computation of the corrections to the mean-field theory. Although they belong to different universality classes, the first two being mean-field models, the last two being short-range models, with respect to the free energy, all the models tend to the SK model respectively for $z \to \infty, R \to \infty, d \to \infty$.

1.2.3 Optimization

The main concepts and phenomena which characterize spin glasses are analogous to the ones encountered in Combinatorial Optimization, where three types of problems are normally considered:

- *optimization problems*, which consist in finding an optimal solution;
- *evaluation problems*, which consist in determining the cost of an optimal solution;
- *decision problems*, consisting in comparing the cost of two solutions with respect to their cost.

In this section we illustrate the analogies between Spin Glass Theory and Optimization, reviewing some of the most common models.

Some concepts introduced in this chapter will be encountered in Chapter 6.4, where the problem of computing spin glass ground states will be addressed.

Computational Complexity. *Computational complexity theory* classifies problems according to their difficulty in terms of the amount of computational resources needed to solve them.

To evaluate the overall hardness of a problem, for instance, we might consider the time required by an algorithm to solve the worst instance, i.e. the one which takes the longest time t_N to be solved, out of all the instances with the same size. Moreover, it is usually important to compare two problems in terms of their *hardness*. A problem A is said to be *not harder than* B, if any instance of A can be turned in an instance of B, in polynomial time. This operation is called *polynomial reduction* and sets a class of equivalence for problems. In this regard, computational problems are generally classified according to the following *computational complexity classes*:

Class P It's the class of polynomial problems, whose running time is bounded from above by a fixed polynomial, $T_N = O(N^k)$. These problems are considered *simple* and they can be solved by *efficient* algorithms.

Class NP : Non-deterministic polynomial problems can be solved in polynomial time by algorithms that can run in parallel on an arbitrarily large number of processors. This means that in general, these problems are not solvable in polynomial time but, if a positive instance of the decision problem is found, then it can be verified in polynomial time.

Class NP-complete : A problem A is *complete* for a class if (a) it belongs to the class and (b) any problem of the class is not harder than A. In this respect, NP-complete problems are the hardest problems in the class NP and if a problem is found to be NP-complete, then all the others cannot be harder than this one.

NP-hard : The problems which do not belong to the previous classes are NP-hard. These problems are at least as difficult as NP-complete problems.

Finding the exact ground state of a spin glass is an NP-hard problem, except in

few cases. As a consequence, exact algorithms can be used only for small systems ($N \sim 10^2$) under certain assumptions. For larger systems heuristic methods are used. A review of these methods will be given in Chapter 4.

Optimization problems. A combinatorial optimization problem is defined by a set of possible instances - a finite set of allowed configurations - and a *cost function*. The latter is a real-valued function E defined over this set, which corresponds to the energy in the spin glass case. Solving an optimization problem corresponds to finding the *optimal* configuration which is a global minimum (ground state) for the cost function. In this respect, solving an optimization problem corresponds to finding its equilibrium state at zero temperature.

Search algorithms are used in Computer Science to solve optimization problems by exploring the space of configuration. As the size of the space grows exponentially with N, a minimization procedure must be defined, an algorithm which dynamically explores the space starting from a configuration, evolving towards the optimal solution until the cost function reaches its minimum.

The optimization problems which are interesting in the context of spin glasses are the ones with a *glassy* energy landscape. In these systems, the cost function is non-convex and has many valleys. As a consequence, the dynamics of solving algorithms is affected by meta-stable states and ergodicity breaking.

Hereafter, we introduce some of the most common optimization problems which share similarities with glasses.

Assignment : Given two different sets of N elements, for example N persons and N jobs, and a *affinity* matrix C_{ij} which defines the affinity between pair of elements belonging to different sets, the problem consists in finding the *assignment* which maximizes the total affinity. A configuration is characterized by a permutation of the N indexes, therefore the size of the space of solutions is $N!$. The cost of a permutation p is $\sum_i C_{ip(i)}$. These problems belong to the class P and can be solved in times of order $\mathcal{O}(N^3)$ [12].

Satisfiability The satisfiability problem consists in determining whether there exists a set of N boolean variables which satisfies a set of logical constraints (decision problem) or to find the configurations which minimize the number of violated constraints (optimization problem). The logical constraints are expressed in a special form which contains only logical OR and NOT operators applied to k variables per time, called *k-clause*. Satisfiability problems where all clauses have the same length k are said k-SAT problems. The 2-SAT decision problem is known to be easy, while in the general case the problem is class NP-complete.

The 2-XORSAT problem in which every variable appears exactly in z random equations (with $M = Nz/2$ total equations) is equivalent to the solving the spin glass problem on the Bethe lattice.

Coloring The q-coloring decision problem consists in finding whether the vertices of a graph can be colored using q colors in such a way that there are no neighboring vertices with the same color. A similar problem is the *vertex-covering* problem which consists in using the least possible number of pebbles

to cover the vertices of a graph in such a way that every edge has an end-point covered.

Random Simple Matching: Given an unoriented graph $G(\mathcal{V}, \mathcal{E})$, a matching $\mathcal{M}$ is a set of edges having the property that no two edges in $\mathcal{M}$ have an ending in common. A vertex v is *matched* if there is an edge incident to v in the matching, otherwise v is *unmatched*. A matching is perfect if every vertex of G is matched.

Usually a function $l(e) : E \to R$ is defined, which can be thought of as a distance, a weight or the cost of a single matching. The cost function is thus $L_{\mathcal{M}} = \sum_{e \in \mathcal{M}} l(e)$, the total length of a matching $\mathcal{M}$. The matching problem consists in finding the cheapest matching which minimizes $L_{\mathcal{M}}$.

If the vertices are N points drawn at random in a d-dimensional cube, then the problem is known as *random Euclidean matching* problem. In this case, the cost $l(e)$ of an edge is the usual Euclidean distance between two points.

The mean field approximation of the problem has been investigated in [13, 14, 71–74].

Minimum/Maximum cut Given a graph $G(V, E)$, the MIN-CUT (MAX-CUT) problem consists in finding the cut $C(S, T)$ of minimum (maximum) weight which partitions V into two subsets S, T. In Ising spin glasses, where the spins can be assigned to one of the two subsets according to their value $\sigma = \pm 1$, this problem corresponds to finding the cut which minimizes the number of broken bonds, i.e. the ground state. If there is no frustration in the system, there are algorithms which solve the problem in polynomial time. The problem is classified simple and can be solved in polynomial time. The MIN-CUT problem will be introduced in more detail in Section 4.2 and in Appendix C.

Chapter 2

Mean-field scenario

A standard procedure adopted in Statistical Mechanics for deriving the thermodynamic properties of a model consists in studying its *mean field approximation*, a 'simplified' version of the problem. Since the complications derive usually from the presence of correlations in the system, in the mean-field approximation the partition function is assumed to be in some way factorizable, at the cost of neglecting correlations. At this level, the expressions for the free-energy and the correlation functions are derived in the thermodynamic limit by solving a set of saddle point equations in terms of the order parameter. In general, correlations are not neglectable and correlations must be eventually reintroduced in the model in a second stage by calculating the corrections to the mean-field approximation. Models which are exactly solvable in the mean-field theory are said *mean-field* models.

The purpose of this chapter is to introduce the main results achieved in the mean-field theory of spin glasses by means of two equivalent although formally very different methods. The replica approach was historically the first one to be used for solving the Sherrington-Kirkpatrick fully connected model, already introduced in the previous section, but the results required several years for obtaining a physical interpretation. The cavity method is a more intuitive probabilistic approach which was introduced few years later [13] and proved to be particularly effective for deriving the mean-field approximation of the Bethe lattice [10, 11] and in general to be implemented on optimization problems defined on sparse graphs.

2.1 The Sherrington-Kirkpatrick model

2.1.1 The replica approach

We consider a system of N Ising spins, with random interactions J drawn from a probability distribution $P(J)$, eventually in a random external field h, (see Sec. 1.2.2), with general Hamiltonian:

$$\mathcal{H}_J[\sigma] = -\sum_{(i,j)} J_{ij}\sigma_i\sigma_j - \sum_i h_i\sigma_i \tag{2.1}$$

where σ is a configuration of the system. For a system at equilibrium at temperature T, the probability measure over the space of configurations is the usual Boltzmann-

Gibbs distribution:

$$P_J[\sigma] = \frac{1}{Z_J} e^{-\beta \mathcal{H}[\sigma]}, \quad Z_J = \mathrm{Tr}_\sigma e^{-\beta \mathcal{H}[\sigma]} \tag{2.2}$$

where $\beta = 1/T$ is the inverse temperature and Z is the partition function. The partition function depends on the Hamiltonian H_J, and therefore on the particular realization of the disorder. However, as already seen in Sec. 1.2.1, one is usually interested in the behavior of the typical sample, and therefore thermodynamic quantities should be averaged over the $P(J)$ distribution. The free energy is thus given by Eq. (1.11):

$$f = \overline{f_J} = -\lim_{N\to\infty} \frac{1}{\beta N} \overline{\log Z_J} \tag{1.11}$$

The computation of $\overline{\ln Z_J}$ is not straightforward, and requires a mathematical workaround known as *replica trick*. The method is based on the identity:

$$\log Z = \lim_{n\to 0} \frac{Z^n - 1}{n} \tag{2.3}$$

where Z^n is the *replicated* partition function, which takes into account the space of n identical independent replicas. The free-energy density is thus:

$$f = -\lim_{N\to\infty} \lim_{n\to 0} \frac{1 + \overline{Z_J^n}}{n}, \quad Z_J^n = \mathrm{Tr}_{\sigma^n} e^{-\beta \mathcal{H}_J^n} \tag{2.4}$$

where $\mathcal{H}^n = \sum_{a=1}^n \mathcal{H}_J[s^a]$ is the replicated Hamiltonian. Proceeding with the mean field approach, one first averages over the disorder, obtaining an integral which depends on a different Hamiltonian in which replicas are coupled. In this respect, it is convenient to introduce the *overlap between replicas*:

$$q_{ab} = \frac{1}{N} \sum_i \sigma_i^a \sigma_i^b \tag{2.5}$$

The averaged replicated partition function is:

$$\begin{aligned} Z_n = \overline{Z_J^n} &= \int \prod_{a<b} dQ_{ab} \sqrt{\frac{N\beta^2}{2\pi}} \exp -N A[Q] \\ A[Q] &= -n\beta^2/4 + \beta^2/4 \sum_{1\le a<b\le n} Q_{ab}^2 - \ln Z[Q] \\ Z[Q] &= \sum_{\{S\}} \exp -\beta H[Q,\sigma] \\ H[Q,\sigma] &= -\beta \sum_{1\le a<b\le n} Q_{ab}\sigma^a\sigma^b - h\sum_{a=1}^n \sigma^n \end{aligned} \tag{2.6}$$

where Q is a $n \times n$ matrix whose coefficients represents couplings between replicas. The particular form of the partition function suggests that its thermodynamic limit can be computed through the saddle-point method, therefore:

$$f_n \equiv \lim_{N\to\infty} \frac{1}{\beta N n} \ln Z_n = \frac{1}{\beta n} \min A[Q] \tag{2.7}$$

The minimum of $A[Q]$ is found by solving a set of saddle points equations:

$$\frac{\partial A}{\partial Q_{ab}} = 0 \tag{2.8}$$

under the condition that the all the eigenvalues of the Hessian matrix $\mathbb{H}_{abcd} = \partial^2 A/\partial Q_{ab}\partial Q_{cd}$ are non negative. The saddle-point equations admit multiple solutions related by a symmetry, a concept known in Statistical Mechanics as *symmetry breaking*. In this case, a solution $A[Q]$ should be invariant under the group of permutations of all replicas, called *replica group*. A solution is *Replica Symmetric*(RS) if the value of Q_{ab} does not depend on the indexes a, b. As soon as the non-diagonal elements of Q_{ab} depend on the indexes the replica symmetry is broken.

Replica Symmetric Solution. The simplest choice is to assume that all the replicas are equivalent:

$$\forall a, b, a \neq b : Q_{ab} = q; \qquad \forall a : Q_{aa} = 0 \tag{2.9}$$

This assumption is called *Replica Symmetric Ansatz* (RS). The last step consists in calculating the $n \to 0$ limit of the replicated functions to obtain the thermodynamic quantities. We remark that the original order of the limits $N \to \infty$ and $n \to 0$ is here inverted, an operation which in principle is not straightforward and which was proved to be correct only twenty-five years after the formulation of the problem [75, 76].

At zero magnetic field, the analytical continuation of the solution of the equation $dA/dq = 0$ provides a solution $q = 0$ for $T > T_C = 1$, and $q \neq 0$ for $T < T_C = 1$. Soon after the formulation of the RS solution [2] it was clear that the results presented some inconsistencies which led, for instance, to a negative entropy in the low temperature phase. The main problem is that the RS solution becomes unstable when positive eigenvalues of the Hessian matrix appear [77]. The instability appears along the critical *de Almeida-Touless* line (dAT line) $h_c(T)$ defined on the h, T plane. While the RS solution is stable above the dAT line, below the line the correct solution is achieved by a procedure known as *replica symmetry breaking* (RSB). In the SK model, the AT line diverges at $T = 0$, implying that there is no transition at zero temperature and the system is the RSB phase. This is an effect of infinite-range interactions, and in dilute models with finite connectivity the $h_c(T)$ line converges to a finite value for $T \to 0$.

Replica Symmetry Breaking. The RSB solution was formulated by Parisi in a series of articles [3, 4, 78] published few years after the original article of Sherrington and Kirkpatrick. The solution is found by an iterative approach which we illustrate for the first step.

At the first step (1RSB) the n replicas are grouped into k blocks of m_1 elements, such that $k = n/m_1 \in \mathbb{N}$. The 1RSB ansatz is:

$$\begin{cases} Q_{ab} = q_0 & \text{if} \quad I(a/m_1) = I(b/m_1) \\ Q_{ab} = q_1 & \text{if} \quad I(a/m_1) \neq I(b/m_1) \\ Q_{aa} = 0 & \text{if} \quad a = b \end{cases} \tag{2.10}$$

Now every line has $m_1 - 1$ off diagonal elements with coefficient q_1 and $n - m$ with coefficient q_0. The free energy is now a function $A[Q] = A(q_0, q_1, m_1)$, which must be

minimized with respect to all the parameters to obtain a saddle-point solution. Even at this first stage, the results are much more satisfactory than the ones obtained with the RS solution, in terms of the corrections to the free energy, which is much more similar to the value obtained numerically, in terms of the entropy, which reduced by a factor ten, and in terms of the stability of the solution.

The procedure can be iterated at further levels of RSB. At each new level k, the diagonal blocks are partitioned hierarchically, and new parameters m_i, q_i are introduced in the model. The *full RSB* solution is found in the $k \to \infty$ limit. At each step, once the saddle-point solution is found, other equivalent solutions are found by a permutation of the replicas into each group, or by a permutation of the groups of replicas. This means that the group which leaves Q invariant is $(S_m)^{\otimes n/m} \otimes S_{n/m}$, where $(S_m)^{\otimes n/m}$ is the direct product of the permutations group of m replicas with itself.

The order parameter $Q(x)$ becomes a piecewise function defined by:

$$Q(x) = q_i \text{ if } m_i < x < m_{i+1} \tag{2.11}$$

In the $k \to \infty$ limit it becomes eventually a continuous function:

$$Q(x) = \begin{cases} q_m & \text{if} \quad x < x_m \\ q(x) \text{ with } dq/dx > 0 & \text{if} \quad x_m < x < x_M \\ q_M & \text{if} \quad x > x_M \end{cases} \tag{2.12}$$

In general, $x_m \to x_M$ when the system approaches the dAT line from below, and the two values collapse above the dAT line. The *full RSB* solution is stable at low temperature and provides physically consistent thermodynamic quantities which are in very good agreement with the numerical simulations.

2.1.2 The spin glass order parameter

The meaning of RSB remains quite obscure as long as only replicas are involved, but it gets a clearer physical interpretation when the order parameter is expressed in terms of the overlap between *states* rather than replicas. The nature of the states in the spin glass phase is better understood in the *TAP approach*, introduced by Thouless, Anderson and Palmer [66, 79]. The results obtained within the TAP approach are not completely satisfactory but present the spin glass phase as characterized by a rough free-energy landscape with a large number of valleys. As the barriers become infinitely high in the thermodynamic limit, the ergodicity is broken, and the space of configurations is fragmented into pure states.

The usual Boltzmann measure must be decomposed in a sum of pure states:

$$< \cdot >= \sum_\alpha w_\alpha < \cdot >_\alpha \tag{2.13}$$

In this sense the Gibbs state is not an equilibrium state, but rather a mixture of equilibrium states.

In order to describe to what extent two states differ from each other, a notion of distance or similarity between states is needed. The overlap between two states is

defined:

$$q^{\alpha\beta} = \frac{1}{N}\sum_{i=1}^{N} m_i^{\alpha} m_i^{\beta} \tag{2.14}$$

where m^{α} and m^{β} are the magnetization of the system in two different states. The self-overlap $q_{\alpha\alpha}$ is the Edwards-Anderson order parameter:

$$q_{EA} = q_{\alpha\alpha} = \frac{1}{N} < \sigma_i >_{\alpha}^{2} \tag{2.15}$$

and is supposed to be the maximum value of overlap. The probability for two random states to have overlap q is given by:

$$P_J(q) = \sum_{\alpha,\beta} w_{\alpha} w_{\beta} \delta(q - q^{\alpha\beta}), \quad P(q) = \overline{P_J(q)} \tag{2.16}$$

It is convenient to define the integrated distribution:

$$x(q) = \int_{-1}^{q} P(q')\, dq' \tag{2.17}$$

which verifies: $x(q_m) = 0,\ x(q_M) = 1$. We recall that in the replica framework the order parameter is given by the $n \times n$ matrix Q_{ab} representing the overlaps between replicas. In the $n \to 0$ limit the parameter becomes a continuous function $Q(x)$ defined between 0 and 1. The physical interpretation of the replica symmetry breaking was given in [4], where it was shown how the inverse function $q(x)$ of the integrated probability (2.17) is the same function as $Q(x)$. In this respect, $P(q)$ is the physical spin glass order parameter.

When the parameters h, T are above the dAT line, the spin glass phase is simple, since it consists only of one state. Thus, in the RS phase the overlap distribution has a sharp peak on the self-overlap:

$$P_{RS}(q) = \delta(q - q_{EA}) \tag{2.18}$$

This is also the case also of the paramagnetic phase, where $q_{EA} = 0$.

Below the AT line, the RS solution is unstable, and the number and nature of the states depend on the particular spin glass model. In general the different models can be classified in two main categories, according to the type of RSB transition[12]:

Continuous Glass Transitions (full RSB). In this case, $P(q)$ has form:

$$P(q) = x_m \delta(q - q_m) + x_M \delta(q - q_M) + \tilde{P}(q) \tag{2.19}$$

where $\tilde{P}(q)$ is a smooth continuous function defined in the interval $[q_m, q_M]$.

Discontinuous Glass Transitions (1RSB). In this case, as the AT line is crossed, a new peak appears in q_1 at a value different from q_0 which characterized the RS phase. The width $q_1 - q_0$ does not vanish as the system approaches the AT line, but rather the *mass* $x_1 \to 0$.

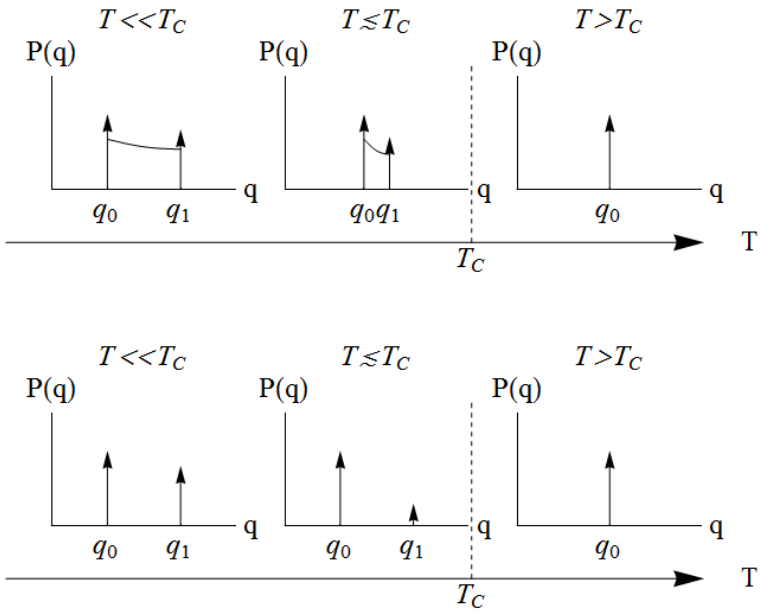

Figure 2.1. Overlap distribution in a continuous (top) and discontinuous (bottom) phase transition. The arrows indicate discrete delta distributions.

Several models have been studied with replica and cavity method and continuous transitions are typically observed in ordinary spin glasses with 2-spin interactions and in vertex coloring problems. Discontinuous transitions are observed in the spherical p-spin model with $p \geq 3$, in random SAT problems and structural glasses.

The two-peaks structure of the 1RSB scenario has a simple geometrical interpretation. When two configurations are independently chosen from the Boltzmann measure, the overlap is with high probability q_0, or q_1. This means that the Boltzmann measure concentrates in small regions of the configuration space, and the states can be clustered. With high probability, two independent random configurations in the same cluster have overlap q_1, and two configurations in distinct clusters have overlap q_0.

2.1.3 Ultrametricity

Beside the two spin correlations, one could study higher degrees of correlation and the related probability distribution. When the overlap between three spins is considered, for instance, remarkable properties appear in the spin glass phase.

Let us consider the distances between three randomly chosen states of a spin glass. The joint distribution of their mutual overlaps, in the replica formalism, is:

$$P(q_1, q_2, q_3) = \overline{P_J(q_1, q_2, q_3)} = \lim_{n\to 0} \frac{1}{n(n-1)(n-2)} \sum_{abc} (Q^{ab} - q_1)(Q^{ac} - q_2)(Q^{bc} - q_3) \tag{2.20}$$

In the RSB parametrization it becomes:

$$\begin{aligned} P(q_1,q_2,q_3) =& \frac{1}{2}P(q_1)x(q_1)\delta(q_1-q_2)\delta(q_3-q_1)+ \\ &+\frac{1}{2}P(q_1)P(q_2)\delta(q_1-q_2)\delta(q_3-q_1)+ \\ &+ \textit{ permutations} \end{aligned} \tag{2.21}$$

This distribution implies that either the three states are mutually equidistant or that two of the separations are equal and greater then the third. This property reveals a hierarchical structure in the overlaps between the various phases and it is known as *ultrametricity*.

A space $\mathcal{M}$ is *ultrametric* if the triangular inequality typical of the Euclidean space is replaced by the ultrametric condition:

$$d(x,z) = \max[d(x,y), d(y,z)], \quad \forall x,y,z \in \mathcal{M} \tag{2.22}$$

In unltrametric spaces, three points chosen at random form either an equilateral or an isosceles triangle with two sides longer than the third. An ultrametric ordering can be described by establishing a one-to-one correspondence between the points of the space and the end tips of the branches of a rooted tree. The distance between two points is proportional to the level at which the corresponding branches converge. An alternative consists in partitioning the space in clusters of equally distant points. Under ultrametricity, it can be shown that such a partition would cover the entire space in disjointed clusters of states.

2.1.4 The ultrametric tree of states

The arguments of the previous chapter show that the replica symmetry breaking yields the property of ultrametricity in the space of configurations. In this respect, ultrametricity is a more general geometric property, the *simplest* form of non-trivial organization arising in systems which admit a *taxonomic* classification [80]. Two questions arise at this point: the first is whether there is a more profound property of spin glasses which yields RSB *and* ultrametricity as a consequence; the second is whether there is a set of assumptions which, together with ultrametricity, are equivalent to RSB. The first question was answered by Guerra [81–83], who derived a set of *stochastic stability* identities, related to the stability of the system against a generic perturbation. In this respect stochastic stability is a theorem which has been proved to be valid in mean-field spin glasses, providing a more general explanation for RSB. The answer to the second question is that RSB can be obtained in an ultrametric system by considering generalized random free energies for the clusters of the system [5].

For a given cluster I, the "free energy" F_I is defined by:

$$W_I = \frac{e^{-\beta F_I}}{\sum_K e^{-\beta F_K}} \tag{2.23}$$

F_I cannot be derived by solving this equation, but it is possible to guess the distributions of the F_I's at each level, and then check *a posteriori* that they return

the correct W_I distributions found with the replica computation. The definition of the random free energies is presented in more detail in Appendix A, where the results of [5] are shown.

The general procedure consists in performing the computation over a rooted tree with depth k and a finite number of branches, where a well-defined overlap scale q_i is assigned to each level, and then perform the limit of continuum branching for obtaining the whole continuous spectrum. In the case of a tree with k branches, we consider two sets of parameters $0 < q_0 < q_1 < ... < q_k < 1$ and $0 < x_0 < \ldots < x_k$, where $x(q)$ is the integrated overlap probability. The foliation of the tree follows an iterative stochastic process known as *Derrida-Ruelle* cascade [84, 85]. An overall scale $F^{(0)}$ is associated with the *grand-ancestor* at the top of the tree, the common root of all the configurations. Then, at the level q_1, each of the clusters is associated with a random independent, identically distributed free energy scale $F_I^(1)$, such that the average number of states with free-energy in the interval $F^{(1)}, F^{(1)} + dF^{(1)}]$ is:

$$d\mathcal{N}^{(1)}(F^{(1)}) = e^{\beta x(q_1)(F^{(1)} - F^{(0)})} dF^{(1)} \tag{2.24}$$

The process is iterated at various scales. Once the $F_I^{(l)}$ at the level q_l have been chosen, the $F_J^{(l+1)}$ at level q_{l+1} of the subclusters J within each cluster I have again i.i.d. random free energy scales whose average number in the interval $F^{(1+1)}, F^{(1+1)} + dF^{(1+1)}]$ is:

$$d\mathcal{N}^{(l+1)}(F^{(l+1)}) = e^{\beta x(q_l)(F^{(l+1)} - F_I^{(l)})} dF^{(1+1)} \tag{2.25}$$

where the dependence on the super-cluster I is contained in $F_I^{(l)}$.
The last level at the scale q_k represents the configurations, whose F variables are the energies, while the variables at the q_{k-1} level are the "true" free-energies of the pure states. We notice that since $x(q)$ at the last level is one, the configuration energies have a distribution proportional to $e^{\beta E}$. This distribution becomes relevant at zero-temperature, where a similar construction is considered in terms of the energy of the configurations. The zero temperature case is treated in Appendix B and is widely discussed in Chpater 6.

The most important results regarding the foliation of the tree can be summarized in the following observations:

- the process has a characteristic of self-similarity, as the distribution of the thicknesses is formally the same at any level, changing only for the distribution of the values of $x(q)$;
- the distributions are universal, since they depend on the parameters of the system (temperature, field and other parameters of the Hamiltonian) only through the $x(q)$ parameters;
- the distribution of the thickness at each level of branching is not homogeneous, since it consists of few dominating branches which contribute to a large part of the total thickness, and an infinite number of branches which account for a small part of it.

This construction has a character of universality, since the weights W of the branches are given by a very general definition.

2.1.5 Non self-averageness of the overlap distribution

One of the most important consequences of the RSB scenario consists in the non-triviality of the averaged overlap distribution $P(q)$ and of the sample-dependent ones $P_J(q)$. An even more interesting aspect regards the non-vanishing sample-to-sample fluctuations of $P_J(q)$, which results in $P(q)$ being non self-averaging. In this section, we follow the arguments of [6] for justifying this last statement and show that the fluctuations

$$\overline{P_J(q_1)P_J(q_2)} - \overline{P_J(q_1)}\;\overline{P_J(q_2)} \tag{2.26}$$

do not vanish in the thermodynamic limit.

One starts by considering the joint probability of finding four replicas $a_1, ...a_4$ with mutual overlaps $q_1 = q^{a_1 a_2}$, $q_2 = q^{a_3 a_4}$ distributed as $P(q_1, q_2)$. The computation is done by first considering the moment-generating function (Laplace Transform) of $P(q)$:

$$g(y) = \int dq P(q) e^{yq} \tag{2.27}$$

In the replica framework:

$$g(y) = \lim_{n\to 0} \frac{1}{n(n-1)} \sum_{a\neq b} e^{yQ_{ab}} = \int_0^1 e^{yQ(x)} dx \tag{2.28}$$

The formula can be generalized:

$$\begin{aligned} g_J(y_1, y_2) = \int dq P(q) e^{y_1 q_1 + y_2 q_2} P_J(q_1, q_2) = \\ = < e^{\frac{1}{N}\sum_i y_1 \sigma_1^i \sigma_2^i + y_2 \sigma_3^i \sigma_4^i} >_{H_4} \end{aligned} \tag{2.29}$$

where we have considered four identical copies of the system with variables $\sigma_1, ..., \sigma_4$ and the average over the hamiltonian $H_4(\sigma_1, \sigma_2, \sigma_3, \sigma\_4) = \sum_{i=1}^4 H(\sigma_i)$. The average over the disorder is computed using replicas:

$$\begin{aligned} g(y_1, y_2) &= \lim_{n\to 0} \frac{1}{n(n-1)(n-2)(n-3)} \sum_{a\neq b\neq c\neq d} e^{y_1 Q_{ab} + y_2 Q_{cd}} = \\ &= \lim_{n\to 0} \frac{1}{n(n-1)(n-2)(n-3)} Tr[A(y_1)A(y_2)] \end{aligned} \tag{2.30}$$

where $A_{ab}(y) = e^{Q_{ab}}(1 - \delta_{ab})$. In the $n \to 0$ limit we substitute $m_i \to 0 < x < 1$, $Q_i \to Q(x)$ finding finally:

$$\overline{P_J(q_1)P_J(q_2)} = \frac{1}{3} P(q_1)\delta(q_1 - q_2) + \frac{2}{3} P(q_1)P(q_2) \tag{2.31}$$

2.2 The Bethe lattice spin glass

The results presented in the previous sections are valid in mean-field models, and precisely they have been obtained for the SK model. The reason why the mean-field solution is exact in the SK model is due to the full connectivity of the model. In the thermodynamic limit, the density of bonds is extensive, and the energy density is kept finite by considering a $P(J)$ with variance $\mathcal{O}(N^{-}1)$. In order to define a more realistic model of spin glass, models with finite connectivity should be taken into account. One way of proceeding is to consider *diluted systems* in which the density of bonds is kept finite in the thermodynamic limit. These models are defined on sparse graphs such as the ones defined in Section 1.1, and are known in Statistical Mechanics as *Bethe lattice*.

These lattices are related to the Bethe approximation, a method invented by Bethe to deal with ferromagnetic models. The method consists in creating a *cavity* by removing a spin, an operation that leaves the neighboring spins uncorrelated. This approximation is not exact in the general case [1] due to the presence of possible correlations which might due to the presence of cycles in the system. A model where the Bethe approximation is exact in the thermodynamic limit is a Bethe lattice.

In ferromagnetic models, a Bethe lattice can be defined as the internal of a *Cayley* tree with coordination number $k+1$. The graph generated starting from a root, adding $k+1$ neighbors on a first layer, and then adding iteratively z new neighbors on a new layer for each leaf of the previous step. Due to the absence of cycles, correlations can be neglected in this model, and the Bethe approximation is exact.

In spin glass models, however, cycles are needed to implement frustration. In a Cayley tree, this can be partially done by imposing boundary conditions, but the model would present a strong heterogeneity due to the different distance of the nodes from the boundary and would be poorly realistic. In this respect, random regular graphs are excellent candidates, with a homogeneous topology and constant coordination number z. Moreover, in the thermodynamic limit, the density of cycles of finite length goes to zero (see Section 1.1), yielding a local tree-like topology. This is a sufficient condition for a random regular graph to be a Bethe lattice.

An approximated solution of the model was found by Mèzard and Parisi using the cavity method in both finite and zero temperature [10, 11]. If correlations are neglected, the method is equivalent to the Bethe approximation and provides the RS solution of the model. Moreover, the 1RSB corrections can be computed within the cavity method, providing a solution which is in very good agreement with the numerical data. In the following, we review the main results found in the mean-field approach to the Bethe lattice as presented in [11], focusing on the description at zero temperature.

2.2.1 The cavity method at zero temperature

The cavity method was developed initially in the context of spin glass theory as a generalization of the Bethe-Peierls approximation which would take into account the

[1] The Bethe approximation is exact in the 1-dimensional chain and in infinite dimensions, where the mean-field approximation is recovered

effects of the replica symmetry breaking. Although it is in principle equivalent to the replica method, it has some advantages. In the first place, it proceeds through standard probability analysis, making explicit all the hypothesis involved in it. Furthermore, the average over disorder is performed at the end, in contrast with the replica method, permitting the computation of the order parameter on each site for a given sample. Roughly speaking, the cavity method works by induction, assuming that some properties are verified in a N spins system, and showing that these are self-consistently reproduced in a system of size $N+1$.

Cavity graphs. Let us consider a Bethe lattice spin glass defined on a random regular graph $G_{N,z}^{RRG}$ of size N and connectivity $z = 3$, described by the usual Hamiltonian. We are interested in computing:

- the asymptotic value of the energy density of the *global ground state* GGS, defined as the configuration with minimum energy:

$$U = \lim_{N\to\infty} \frac{E_N}{N} \tag{2.32}$$

- the asymptotic value of the energy density of a *local ground state* LGS, defined as a configuration whose energy cannot be decreased by flipping a finite number of spins in the thermodynamic limit.

We start by considering a *cavity graph*, an intermediate graph $G_{N,q}$ where q randomly chosen *cavity* spins have only k neighbours, while the other $N-q$ spins have $k+1$ neighbours. Cavity spins are fixed $\sigma_1, ..., \sigma_q$ and the global ground state (GGS) energy of the corresponding spin glass model depends on their values. We would like to determine the energy cost needed for going from the cavity graph to the original Bethe lattice upon adding edges or nodes. More precisely, we define the basic operations:

- *Iteration*: performed by adding a new spin σ_0 of fixed value into the cavity, connecting it to k cavity spins $\sigma_1, ..., \sigma_k$, and optimizing their values. In this way we perform the transofrmation $\mathcal{G}_{N,q} \to \mathcal{G}_{N+1,q-k+1}$.
- *Link addition*: no new node is added but a single link between two existing randomly chosen cavity spins, and by optimizing their values. This corresponds to $\mathcal{G}_{N,q} \to \mathcal{G}_{N,q-2}$. Let ΔE_L be the average energy shift of the GGS for a single link addition.
- *Site addition*: a new spin σ_0 is added into the cavity and $k+1$ cavity spins are connected to it. By Optimizing the values of the $k+2$ spins we perform $\mathcal{G}_{N,q} \to \mathcal{G}_{N+1,q-k-1}$ Let ΔE_S be the average GGS energy shift for a single site addition.

Starting from $\mathcal{G}_{N,2(k+1)}$ and performing $k+1$ link additions we get $\mathcal{G}_{N,0}$. Starting from the same graph and performing 2 site additions we get $\mathcal{G}_{N+2,0}$. The average energy shift when going from N to $N+2$ is then:

$$E_{N+2} - E_N = 2\Delta E_S - (k+1)\Delta E_L \tag{2.33}$$

Since total energy is asymptotically linear in N, it follow that:

$$U = \lim_{N\to\infty} E_N/N = \frac{E_{N+2} - E_N}{2} = \Delta E_S - \frac{k+1}{2}\Delta E_L \tag{2.34}$$

Bethe approximation. The basic assumption of the RS solution is that the various cavity spins become uncorrelated in the large N limit. This is reasonable if $q \ll N$, since the distance between two randomly chosen cavity spins is large enough to assume they are uncorrelated. An important assumption is thus that the perturbation corresponding to the variation of one of the cavity spins remains localized and it does not propagate to the whole lattice. Formally we assume that, at the RS level, the GGS energy of a $G_{N,q}$ is an addictive functions of the values of the q cavity spins:

$$E(\{\sigma\}) = E^0 - \sum_{i=1}^{q} h_i \sigma_i \tag{2.35}$$

where h_i is the sample-dependent *local cavity field*. In random regular graphs we assume that h_i are independent identically distributed random variables distributed as $P(h)$. In general, there is no simple expression for the cavity fields, since they are related to the difference in energy of two GGS with flipped cavity spins, which may differ in an arbitrarily large number of spins. The quantity $E(\sigma)$ is computed by minimizing the energy as a function of the other $N - q$ spins at fixed values of the q cavity spins. Under these assumptions, a self-consistent equation for this distribution is obtained by considering an iteration: we add a new spin in the cavity, fix its value to σ_0 and connect it to k cavity spins through a new set of coupling constants $J_1, ..., J_k$. The field acting on each $\sigma_{i\in\{1,...,k\}}$ is $h'_i = h_i + J_i\sigma_0$ and the spins must align with the field in order to minimize its energy. The energy of the link $< 0i >$ is:

$$\epsilon_i = \min_{\sigma_i} h'_i \sigma_i = -|h'_i| \equiv -a(J_i, h_i) - \sigma_0 u(J_i, h_i) \tag{2.36}$$

where:

$$\begin{aligned} u(J_i, h_i) &\equiv \frac{1}{2}(|h_i + J_i| - |h_i - J_i|) \\ a(J_i, h_i) &\equiv \frac{1}{2}(|h_i + J_i| + |h_i - J_i|) = |h_i + J_i| - |u(J_i, h_i)| \end{aligned} \tag{2.37}$$

Therefore the new local field acting on σ_0 is given by:

$$h_0 = \sum_{i=1}^{k} u(J_i, h_i) \tag{2.38}$$

In this way a recursion equation is found for the distribution $P(h)$:

$$P(h) = \overline{\int \prod_{i=1}^{k} [dh_i P(h_i)] \delta\left(h - \sum_{i=1}^{k} u(J_i, h_i)\right)} \tag{2.39}$$

where the average is performed both over $P(J)$ and the G^{RRG} ensemble.

In the $\pm J$ model the local fields are integer numbers and the symmetry of J yields asymmetric form for $P(h)$. In this case the functions u and a have simpler form:

$$\begin{cases} a(J,h) = |h|, & u(J,h) = \text{sign} Jh, & \text{if } h \neq 0 \\ a(J,h) = 1, & u(J,h) = 0, & \text{if } h = 0 \end{cases} \implies P(h) = \sum_{k=-r}^{+} r p_r \delta(h - r) \tag{2.40}$$

Moreover, due to the symmetry of $P(h)$ is $p_+ = p_-$. In the simple case $z = 3$ ($k = 2$), it is found that $p_0 = 1/3, p_1 = 2/9, p_2 = 1/9$ and the energy of the ground state is $E \approx -1.278$.

Even if the fields are integers, equations (2.39) admit some solutions which are not only distributed over integers but also have a continuous part. A detailed computation shows that if one starts from integer fields plus a small correction, at zero temperature, the corrections are amplified in the iteration until the final distribution is no more concentrated near the integers. In other words, a small variation of the field in one point propagates and leads to a large instability over the whole lattice. This is assumed to be a clue that the RS solution is incorrect, and that the artifact would disappear in the full RSB solution.

1-RSB The RS solution cannot be correct because the hypothesis that the GGS is stable upon the addition of a new site or new links is incorrect. The energy landscape of the system and therefore the probability distributions are subject to an abrupt change, definitely not smooth, which should be taken into account. This is due to the existence of several *local ground states* (LGS) whose energies cannot be lowered by flipping a finite number of spins, in the large N limit. In general, LGS are stable upon the inversion of a fraction of spins less that $f(N)$, where $f(N)$ is an increasing function, divergent in the large N limit. We assume that such a function exists and that it allows a large number of LGS. This can be seen only in few cases, and proving this assumption in the general case would turn the cavity method into a full mathematical proof.

We consider a particular case where LGS can be characterized and enumerated, so that 1RSB solution can be applied and results can be checked versus confrontation done using completely different methods. We assume that, in the large N limit, the perturbations caused by changing the value of cavity spins only propagate to an infinitesimal fraction of the lattice. In this assumption, there is a one-to-one correspondence between LGS through the iteration. Still, their energy values may change, which means that the GGS could change after each iteration step. In order to find the GGS, a large number of LGS must be taken into account.

The assumptions can be formalized as follows:

- the cavity spins are *uncorrelated* within one LGS. The energy of the α-th LGS on a $G(N, q)$ is:

$$E(\{\sigma\})^\alpha = E_0^\alpha - \sum_{i=1}^{q} h_i^\alpha \sigma_i \tag{2.41}$$

  This equation cannot be applied to the GGS, since it may correspond to several LGS, depending on the cavity spins values.

- The E_0^α of low energy is an i.i.d. variable with Poisson distribution:

$$\rho(E_0) = \exp \mu(E_0 - E_{ref})$$

  where μ is a parameter, and E_{ref} is a reference energy close to the LGS energy.

- The local cavity fields on a given site h_i^α are i.i.d. variables distributed according to $P_i(h)$ which fluctuates from site to site. Therefore the order parameter is a functional $\mathcal{Q}(P(h))$ corresponding to the probability that a

random cavity field is distributed according to $P(h_i) = P(h)$. Moreover, the h_i^α and the LGS energies are not correlated.

An infinite order of RSB is expected to solve the problem, as it is well known for the large k case, which is equivalent to the Sherrington Kirkpatrick (SK) model. The 1RSB is thus an approximation which usually produces better results than the RS approach.

2.2.2 Limit for high connectivities

The Bethe lattice spin glass is expected to tend to the SK model in the $z \to \infty$ limit. This limit has been studied analytically by De Dominicis and Goldschmidt [86] using the $1/z$ expansion (at the 1RSB level), finding a divergence in the first order corrections to the free-energy density. In case of a $1/\sqrt{z}$ expansion at $T = 0$, the corrections are smaller at the second step of RSB.

In [87] Parisi and Tria have studied spin glasses with finite connectivity by considering the expansion around the high connectivity limit. In this case both the RRG and ER models have been studied within the first two steps of RSB, obtaining the free energy in inverse power of the average connectivity z. The results show that the divergent coefficient of the $1/z$ correction which appears at the 1RSB step at low temperatures becomes much smaller when computed at the 2RSB step, which suggests that the divergence is due to the finite number of RSB. Also, the expansion is possible in models with continuous J only if the entropy tends to zero at zero temperature, in the limit $z \to \infty$. The limits $z \to \infty$ and $T \to 0$ of [10] can be exchanged only in this case.

2.2.3 Sample-to-sample fluctuations in the Bethe lattice

We have seen that in the SK model, the sample-to-sample fluctuations of the order parameter are quantified by the Ghirlanda-Guerra relations [82, 88]. The simplest identity is:

$$\overline{P_J(q)P_J(q')} - \overline{P_J(q)P_J(q')} = \frac{1}{3}[\delta(q - q') - P(q)]P(q') \tag{2.42}$$

In the Bethe lattice the overlap distribution is not know analytically and must be computed numerically. The task is not easy, due to the large number of systems needed to observe the effects of atypical samples. A numerical study in this sense is presented in [89], where the sample-dependent overlap distributions are extracted along the critical AT line. The results show $P(q)$ distributions are skewed, with large left tails and a small deviation of the sample mean from the thermodynamic value q_0 of the overlap, which depends on the temperature T and external field H given by the AT line.

When the data are analyzed in terms of the single distributions $P_J(q)$, two types of contributions are observed. Arranging the samples on a scatter plot, according to the mean and variance of their sample overlap distribution, and integrating over regions of the scatter plot, one finds that:

- there is a large number of "typical" samples with roughly Gaussian $P_J(q)$ which contribute to the region close to the peak of $P(q)$;

- there is a small number of "atypical" samples which present (a) a second peak at an overlap value much smaller than q_0 or (b) a narrower distribution centered on a value greater than q_0.

The atypical samples can be described as systems with an effective external field different from H and that are therefore (a) below the critical line or (b) over the critical line. The main source of sample-to-sample fluctuations may be the presence of systems with different effective field and different critical temperature. The presence of atypical samples is not due to finite-size effects, since the fraction of atypical samples does not change much even in the thermodynamic limit.

Chapter 3

Finite-dimensional spin glasses

The validity of the RSB scenario in finite-dimensional spin glasses is still debated. Ironically, a simple model like the three-dimensional lattice with nearest neighbors interactions is also one of the most difficult models to approach analytically. Different theories have been suggested for describing the low-temperature phase, and the investigation relies mostly on numerical methods. This chapter is intended as a review of the concepts, of the methods and difficulties encountered in the descent to finite dimension.

3.1 The phase diagram of finite-dimensional models

Let us focus on the three-dimensional EA model. The existence of a glassy transition in this model has been debated for long. In this respect, two different models are considered: the random-bond Ising model with biased J distribution and the spin glass model with symmetric $P(J)$ and external magnetic field.

In the random-bond Ising model, the fraction of anti-ferromagnetic bonds is fixed to a value p. At low temperature, the model shows a complex behavior. If $p = 0$, there are only ferromagnetic bonds and the system resembles the ordinary ferromagnetic Ising model. If $p = 1$, there are only anti-ferromagnetic bonds and the phase can be considered again ordered. For intermediate concentrations of the anti-ferromagnetic bonds, neither ferromagnetic nor anti-ferromagnetic order exists, and the system is expected to be in the spin glass phase. The nature of the spin glass phase is however debated. Numerical studies on systems up to size $N = 16^3$ and $p = 0.5$ indicate the presence of a complex behavior in the spin glass phase in agreement with the mean-field scenario [90, 91].

The random-bond Ising model has been studied in the past using Monte-Carlo simulations [92], zero-temperature series expansions [93], high-temperature series expansions [94–96], Monte Carlo renormalization-group calculations [97], and renormalization-group theory [98]. All the studies agree qualitatively, predicting the existence of a critical line in the (T, p) plane which separates the spin glass phase and the ferromagnetic phase, but there is no agreement on the specific dependence on the temperature of the critical concentration p_c where the ferromagnetic order disappears.

The value of p_c has been obtained in the $T = 0$ phase by studying the scaling

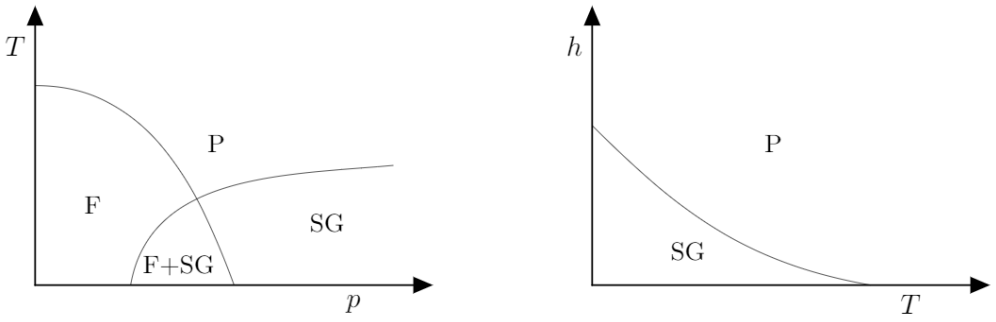

Figure 3.1. Phase diagram expected in the mean-field scenario at finite dimension. Left: the ferromagnetic phase (F) is expected to disappear above a first critical line $p_c(T)$, and the spin glass phase (SG) is expected to appear below the second critical line. In the mean-field scenario, a region with mixed behavior is supposed to appear below both the lines. Right: the AT line separates the disordered phase (P) from the spin glass phase (SG).

properties of the ground states. At $d = 2$, the only case in which exact ground states can be computed, the critical concentration is known to be $p_c = 0.10$ [99–101]. In the $d = 3$ case, the value found for the critical concentration is $p_c = 0.222$ [102].

Detecting the phase transition. Typical methods for detecting the phase transition include Finite Size Scaling methods [103]. These methods consist in deriving the behavior of certain observables of the system upon a change of the size, searching signs of critical behavior. Typical quantities involved are the site overlap q or the non-connected spin glass susceptibility χ_q.

Typically, a very useful descriptor is the *Binder cumulant*:

$$g_4 = \frac{3}{2} - \frac{1}{2}\frac{\overline{< q^4 >}}{\overline{< q^2 >}^2} \tag{3.1}$$

Other important parameters are the g_2 cumulant [104], which measures the lack of self-averageness of the spin glass susceptibility, and a combination of g_2 and g_4 [105]:

$$g_2 = \frac{\overline{< q^2 >^2} - \overline{< q^2 >}^2}{\overline{< q^2 >}^2}; \quad G = \frac{1}{2}\frac{g_2}{1 - g_4} \tag{3.2}$$

The Binder cumulant has been used to detect phase transitions in ordered systems, while g_2 has proved successful in diluted disordered models. Unfortunately, in Ising spin glasses they do not provide a clear signature of the phase transition since they require the evaluation of a four-point correlation function, which is statically noisier than the two-point one.

In this respect, it is more convenient to consider the *correlation-length*, which is defined in terms of the two-point correlation function. The correlation-length on a finite lattice [106] is defined by considering the overlap-overlap correlation function:

$$C(r) = \frac{1}{N}\sum_i \overline{< q_i, q_i + r >} \tag{3.3}$$

The correlation length ξ_L is found by a proper discretization of the momentum space for the Fourier transform $\hat{C}(k)$. In this respect, one can study the scaling behavior at the critical point, for $T > T_c$, where $C(r) \propto r^{-(d-2+\eta)}$. If ξ_∞ is the correlation-length of the infinite lattice, then:

- in the paramagnetic phase for $L \gg \xi_\infty$: $\xi/L = \mathcal{O}(1/L)$
- in the paramagnetic phase for $L \leq \xi_\infty$: $\xi/L = \mathcal{O}(1)$
- in the broken-symmetry phase for $L \leq \xi_\infty$: $\xi/L = \mathcal{O}(L^{d/2})$

In presence of a critical transition, the plot of the ξ/L cumulant should cross at the critical point. Numerical simulations [107] have shown the presence of a transition at finite temperature $T_c > 0$ for the $d = 3$ lattice, excluding the possibility of transition only at $T_c = 0$.

3.2 Low temperature

Once that the existence of a critical temperature $T_c > 0$ at finite dimension has been proven, one could wonder to what extent the mean-field theory is able to describe the low-temperature phase. It is known that the upper critical dimension is $d = 6$. This means that the mean-field (RSB) theory describes correctly the d-dimensional model for $d > 6$, but for lower dimensions a numerical approach is needed. We briefly review some of the numerical results obtained at low-temperature for the d-dimensional spin glass model in $d = 3, 4, 6$ dimensions, where evidence of RSB is found.

EA model in $d = 6$. The validity of RSB at $d = 6$ has been confirmed numerically in out-of-equilibrium simulations [108] by extracting the dynamic spin glass susceptibility $\chi(t)$. The expression for this function is derived from the overlap-overlap correlation function constraint to $q = 0$ $C_{RSB}(x)_{|q=0}$, computed in [77]. If the $d = 6$ spin glass phase behaves accordingly to the RSB scenario, then $\chi(t) \sim t^{h(T)}$ (if $q = 0$), where $h(T)$ is a discontinuous function of the temperature which is linear below the critical point. Numerical simulations [108] have confirmed these predictions.

EA model in $d = 3, 4$. At lower dimension, $d = \{3, 4\}$, the problem is handled by studying the decay of the dynamic overlap-overlap correlation function

$$C(x,t) = \frac{1}{L^3} \sum_i \overline{< \sigma_{i+x} \tau_{i+x} \sigma_i \tau_i >_t} \tag{3.4}$$

where σ, τ are two replicas evolving with the same disorder. In the $q = 0$ sector, which is obtained by controlling that the overlap is very small, the behavior of $C(x,t)$ was studied in numerical simulations in $d = 3$ [90, 109] and $d = 4$ [110, 111]. The numerical data show evidence a scaling behavior for the equilibrium value of the propagator:

$$C_{eq}(x) = \lim_{t \to \infty} C(x,t) \propto x^{-\alpha} \tag{3.5}$$

The exponent $\alpha \sim 0.5$ is independent of the temperature for $d = 3$ (in agreement with the value obtained in [112] at zero temperature) and strongly dependent on

the temperature in $d = 4$. The pure power behavior is supported by the mean-field theory, while it is in disagreement with the predictions from the DM, where $C_{eq}(x) \to q_{EA}$ as $x \to \infty$.

In [113, 114] Young and Katzgraber claim that there is no critical line in $d = 3$. However, it was argued by Parisi [115] that at finite volume there the results should be considered carefully, due to the effects coming from the cross-over region where there are configurations with negative magnetization which might affect the simulations. Moreover, using a different methodology, the transition has been detected in larger lattices in the presence of magnetic field [116, 117]. This analysis showed that the RSB effects decrease when the dimension is decreased, and detecting the dAT line would require very high sensitivity.

3.3 Zero temperature

In most cases, numerical simulations are able to thermalize the systems at temperatures $T_c/2 \lesssim T \lesssim T_c$. The investigation at lower temperatures is normally affected by critical slowdown, and even the best algorithms require a prohibitive computational time. On the other hand, many algorithms borrowed from computer science are very effective at computing spin glasses ground states. Searching the ground state of a magnetic system corresponds to the optimization problem of finding the set of variables - the Ising spins - which minimizes the cost function - the energy.

At this point, one should be careful when generalizing the results obtained for the zero temperature of finite volume systems to the mean-field description in the zero temperature limit of infinite volume systems. In fact, in the mean-field approach, the thermodynamic quantities are first computed in the infinite volume at finite temperature, and then the zero temperature results are obtained in the $T \to 0$ limit. In numerical simulations, instead, the ground states are computed at zero temperature for systems of finite-size and only after, the $N \to \infty$ results are inferred by looking at the scaling behavior of the quantities.

The two descriptions are equivalent only if is assumed that:

- exchanging the two limits would not affect the predictions;
- the transition from probability distributions which depend on the free-energy to the description in terms of energy is continuous.

3.4 Scaling behavior of local excitations

The advantage of studying finite-dimensional systems directly at zero temperature is that the ground state is unique, apart from degeneracy. In this case, it is interesting to consider the effects of a perturbation on the system. Depending on the nature of the problem, there are two possible types of perturbations:

- *surface* perturbations, typically produced by changing the boundary conditions from periodic (PBC) to antiperiodic (ABC), which induce a *domain wall* (DW) across the system;
- *bulk* perturbations, produced by coupling the system to a reference configuration, typically the ground state, by introducing a term of order ϵ into the

Hamiltonian.

Upon a perturbation, the equilibrium state of system deviates from its ground state, and an excited state is produced. Depending on the phase of the system, the geometrical properties and the energy of the excitation might be very different.

Stiffness exponent. Let us consider a d-dimensional lattice of linear size L and an *excitation* - the cluster of spins which are simultaneously reversed - of linear size ℓ. The *cost* of the excitation, the energy difference between the ground state and the excited state, typically scales as:

$$\Delta E \sim \ell^{\theta} \tag{3.6}$$

where θ is the *stiffness exponent*. The stiffness exponent is a fundamental quantity since it provides an insight into the properties of the excitation and it is important for the scaling corrections of different observables [118]. Moreover, it is essential for determining the nature of the spin glass phase of a model, since different theories predict different values for θ.

Depending on the type of cluster considered, different definitions of θ can be given[119]:

1. θ_g describes the energy of low-lying *global* excitations [120, 121] with $l \sim \mathcal{O}(L)$, whose energy is assumed to scale like L^{θ_g}

2. θ_l describes the energy of *local* excitations of finite volume called Minimum Energy Clusters (MEC). A MEC is defined as the cluster of minimum energy among the clusters of n spins which contain a given site i.

3. θ_{DM} describes the energy of the interface produced in domain wall experiments;

4. θ describes the energy of *droplets* defined as MEC which are *compact* and *size independent* [46, 122]. Typically this exponent is computed via domain-wall studies by assuming $\theta = \theta_{DW}$ [48, 123].

Changing the boundary conditions from periodic to antiperiodic in a ferromagnet with $J = +1$, at $T = 0$ and $d > 1$, for instance, causes the creation of an interface of cost $\Delta E \sim L^{\theta}_{DW}$. In a spin glass, the presence of frustrated bonds tends to decrease θ, which could also vanish. This is quite important for the stability of the system. If $\theta < 0$ the system is unstable with respect to spontaneous fluctuations which can grow at no cost. This is the case of the 1-dimensional chain, where $y = 0$ and there is no ordered state at any finite temperature. If $\theta > 0$, the system can sustain small fluctuations and the transition is at finite temperature. Moreover, the stiffness can be used to compute the lower critical dimension, since it vanishes at the lower critical dimension $\theta_{d_c} = 0$.

Scenarios in finite-dimensional systems. Regarding the nature of the spin glass phase, different theories have been formulated based on different arguments for describing finite-dimensional models. Differently from the mean-field theory, the *droplet model* (DP) is a renormalization group picture based on real-space properties and scaling laws [46, 122].

Mean-field scenario (RSB): In the mean-field scenario, the energy landscape is characterized by a large number of macroscopically different equilibrium states, corresponding to valleys with $\mathcal{O}(1)$ energy differences. One can assume that, upon a perturbation, the system must cross one of this states, and therefore the probability of finding a system-size excitation of $\mathcal{O}(1)$ energy must be finite, regardless of the size of the system. This is only possible if the probability of finding excitations of size L does not vanish in the thermodynamic limit, therefore $\theta_g = 0$. These excitations are supposed to be *space filling*, as the fractal dimension of their interface coincides with the topological dimension of the lattice ($d_s = d$).

Droplet Scaling Theory (DM): In the *droplet model* [46–48, 123] it is assumed that there is only one equilibrium state and that the excitations are droplets of energy ℓ^θ (see previous paragraph) which are compact and size independent. In other words, the perturbation produces a compact domain of inverted spins with a corrugated surface typically associated with a fractal dimension $d_s < d$. Since the energy cost for producing a droplet increases with the size (being infinite in the thermodynamic limit), the probability of finding excitations of size $\mathcal{O}(1)$ scales as $\ell^{-\theta}$ and the probability to find system-size excitations tends to zero, therefore $\theta_g > 0$. A natural realization of this picture is found in hierarchical lattices or in the Migdal-Kadanoff renormalization group, where it has been proven that $\theta_{DW} = \theta = \theta_l = \theta_g$[118].

Trivial-Non Trivial (TNT): The *Trivial-Non Trivial* model was suggested to account for a mixed behavior observed in numerical simulations on lattice in $d = 3$ and $d = 4$ [124, 125]. This model assumes that there are large size excitations like in the mean-field scenario, but their interface has fractal dimension $d_s < d$, like in the droplet picture. It has been shown that evidence of a TNT scenario is related to transient finite-volume effects [112, 126], and numerical experiments [127] have discarded the possibility that the TNT scenario is correct in these models.

Local excitations in mean-field systems The question of whether local excitations are present in mean-field glasses is still debated [119]. It is generally believed that the presence of droplet-like excitations would prevent the transition to the spin glass phase, based on the Bethe-Peierls argument, therefore the probability to find finite-volume excitations with energy $\mathcal{O}(1)$ should decrease as $\ell^{-\theta_l}$, with $\theta_l = \theta > 0$. In this case, the only difference between the RSB scenario and the DP would be the value of θ_g. This scenario is reproduced in the Random Energy Model (REM) [128, 129] where $\theta_g = 0$ and $\theta_l = \theta = \infty$[119].

On the other hand, it has been suggested [130, 131] that the energy of MEC might decrease with the size without affecting the presence of the RSB phase provided they are not size independent. In this case, it might be $\theta_l \neq \theta$ and $\theta_l < 0$. Negative values of θ_l, very close to zero, have been found in the $3d$ EA model [130, 131] while an asymptotic value $\theta_l = 0$ has been obtained for the Bethe lattice [119]. These results suggest that in mean-field systems low-energy excitations of all sizes are present and that they might be responsible for the replica symmetry breaking in the first place.

Stiffness exponent in d-dimensional models Many attempts have been made to calculate the stiffness at $d = 3$ [132–138] with transfer matrix, optimization, or renormalization group techniques.

In the beginning, it was argued that the stiffness would be negative at $d \leq 2$ and positive at $d \geq 3$. Numerical simulations have shown that at $d = 2$, $\theta_{DW} \sim -0.28$ and a fractal dimension of the interface $d_s \sim 1.3$, in agreement with the predictions of the droplet picture. [136, 139–142]. This value confirms that no phase transition is present in the square EA model and that the only ordered phase is at zero temperature.

Many attempts have been made to compute the stiffness at $d = 3$. The problem is that here the stiffness exponent is expected to be very small and positive, and it has been assumed to be $\theta \sim 0.19$. In $d = 4$, a computation provides $\theta \sim 0.64$.

3.4.1 Effects of a surface perturbation

Let us consider a d-dimensional model defined of the lattice $G(\mathcal{V}, \mathcal{E})$ with linear size L, volume $V = |\mathcal{V}| = L^3$ and $|\mathcal{E}| = 2dN$ edges. We consider here a change of boundary conditions from periodic (PBC) to antiperiodic (ABC), which induces a change of ground state from σ to τ. Given two interacting sites i, j connected by the edge $\nu = (i, j)$, the *local site overlap* and the local link overlap are defined as:

$$q(i) \equiv \sigma(i)\tau(i), \qquad q_l(\nu) \equiv q(i)q(j) \tag{3.7}$$

The local link overlap is $q_l(\nu) = -1$ if only one of the spins i, j is reverted in the excitation, while it is $q_l(\nu) = 1$ upon the inversion of both the spins (or none). In other words, the local link overlap is sensitive to a local change of configuration but not to a global change of configuration which would affect the local site overlap, for example in the total spin inversion.

For this reason, the link overlap is used for detecting the surface of the interface. Let us consider the averages:

$$q = \frac{1}{N}\sum_{i=1}^{N} q(i), \qquad q_l = \frac{2}{|\mathcal{E}|}\sum_{\nu\in\mathcal{E}} q_l(\nu) \tag{3.8}$$

While q is connected to the measure of the volume of the domain, the link overlap is connected to the *density* of its interface, defined as:

$$\rho = \frac{1}{2}(1 - q_l) \tag{3.9}$$

Let us assume that the density of the interface goes to zero with pure scaling law $\rho \sim L^{-\alpha}$. Following the arguments presented in [126], three possible scenarios are considered:

1. The interface is confined in a region of width L^z with *wandering* exponent $z < 1$, where the surface might have overhangs. The density can be roughly expressed as
$$\rho \sim L^z L^{d-1} L^{-d} \sim L^{-\alpha} \tag{3.10}$$
which results in $\alpha \geq 1 - z$.

2. The interface has fractal dimension d_s and wandering exponent $z = 1$. In this case one obtains for the density:

$$\rho \sim L^{d_s} L^{-d} \sim L^{\cdot \alpha} \tag{3.11}$$

which results in $\alpha = d - d_s$.

3. In the $L \to \infty$ limit the density does not tend to zero but to a constant value. In this case, the exponent α is zero, the interface is a dense set of measure 1 and it is space-filling: $d_s = d$.

The first case would be similar to what happens in the ferromagnetic model, where the ground states obtained with PBC and ABC are locally similar, apart from the domain wall. In this case, the interface is flat and its density is supposed to vanish in the thermodynamic limit, since it has measure zero, therefore $q_l \to 1$. In the droplet picture, the situation is similar but the interface is supposed to be corrugated, like in the second scenario. In the RSB picture, something very different happens. The ground state obtained with ABC is supposed to be locally similar to one of the low-lying minima of the energy landscape. In this case, the density does not vanish in the thermodynamic limit, therefore q_l does not tend to 1.

In [126], Marinari and Parisi have computed the link overlap of the 3d EA model using four different methods, obtaining a value $q_l = 0.79(7)$, which is three standard deviations different from the droplet prediction $q_l = 1$.

In [134] Hartmann has used a domain wall approach to compute the stiffness exponent of the three dimensional model from ground states, finding $\theta_{DW} \sim 0.19(2)$, which accounts for a non-zero transition temperature T_C for the $d = 3$ model.

3.4.2 Effects of a bulk perturbation

If $H_0(\sigma)$ is the Hamiltonian of the system, then one can consider the Hamiltonian:

$$\mathcal{H}_1(\sigma) = \mathcal{H}_0(\sigma) + \epsilon f(\sigma) \tag{3.12}$$

where the perturbation is a function which couples the configurations to the ground state σ_0 of $\mathcal{H}_0$, and is intended to be weak. A natural choice for the coupling term consists in considering a function of the overlap between the system and σ_0. The simplest choice is considering the *site overlap*:

$$f_(\sigma) = q(\sigma_0, \sigma) \equiv \frac{1}{N} \sum_i \sigma_0(i)\sigma(i) \tag{3.13}$$

This definition turns useful if the symmetry for global spin inversion is broken, for example by an external magnetic field. Another possible choice is considering the *link overlap*:

$$\mathcal{H}_{\sigma_0}(\sigma) = q_l(\sigma_0, \sigma) \equiv \frac{1}{ND} \sum_{<i,j>} q(i)q(j) \tag{3.14}$$

where $q(i) = \sigma_0(i)\sigma(i)$ is the local site overlap and the sum is over all the neighbors. This choice of perturbation is sensitive only to local changes of the configuration, giving a contribute only on the interface of a cluster of flipped spin.

This approach has been first used by Palassini and Young in [125] for studying short-range spin glasses in three and four dimensions, the Viana-Bray model and the SK model. In short ranged models they have found evidence for $\theta_g = 0$ and $d_s < d$, consistent with the TNT scenario suggested by Krzakala and Martin [124]. Further investigation has however discarded the possibility of such a scenario, suggesting that θ could be small, but different from zero. The results for the Viana-Bray and SK model, instead, confirm the presence of full RSB.

In [112], Marinari and Parisi have considered the ground state of 3D Ising spin glasses with Gaussian couplings, by studying the link overlap as a function of the square site overlap $q_l(q^2)$. The results have shown a strong correlation between the two quantities, and the behavior of $q_l(q^2)$ in the $L \to \infty$ limit is in agreement with the predictions of the RSB theory.

The ϵ-coupled Hamiltonian has been studied mostly numerically. However, an interesting analytical approach is found in [143], where the Bethe approximation of the coupled system is derived. A very interesting result concerns the instability of the RS solution at $h_{ext} = 0$, which yields a value $q = 0$ for $\epsilon = 0$, instead of the trivial value $q = 1$. This suggests a method for determining the AT line, based on the appearance of the RSB inconsistency in the calculations. The derivation of this result is quite interesting and is reproduced in Appendix D.

Part II

Simulation of ground states in spin glasses

Chapter 4

Cluster-Exact approximation of ground states

4.1 Introduction

From the arguments presented in the first part of the thesis, it is clear that the most interesting properties of spin glasses are observed far below the critical temperature, and that the discriminant between different theories consists mostly in the properties of the ground states and of the low-energy excitations. While there is no doubt about the correctness of the mean-field theory in describing infinite-range spin glasses like the SK model, it is not clear to which extent finite-dimensional models are described by a mean-field scenario. The study presented in the second part of this thesis is set within this context, as it focuses on the ground state properties of two models: the $J\pm$ Bethe lattice spin glass with coordination number $z = 3$ and the bond-diluted EA model in three dimensions, also in this case with constant connectivity $z = 3$. Despite the lack of a full RSB analytical solution, it is generally agreed that the first model is described by a mean-field scenario, a belief confirmed by numerical evidence (see Chapter 2.2). On the other hand, the numerical results on the three-dimensional EA model are more difficult to interpret and there is no consensus on the nature of its spin glass phase. The particular dilution introduced in the second model allows to push the computation to systems of larger size, and eliminate at the same time the fluctuations in the degree distribution typical of conventional bond dilution.

This chapter serves as an introduction to the results in the next two chapters, and it focuses on the computational aspects: we first introduce the most common techniques used for obtaining ground states; then we present the models under investigation (Section 4.3) and describe the computational setup, enter into the details of the algorithm used in the simulations, the Cluster-Exact Approximation [144, 145]. In 4.5 some preliminary results are presented, to verify the consistency of the algorithm. In 4.6 we present a computation of the overlap distribution of the ground states at zero temperature for detecting hints of ultrametricity in the system. In the final part, we provide a summary of our results and some conclusions.

4.2 Computation of ground states

The challenges presented by spin glasses are not limited to the analytical approach, as the computation of spin glasses exact ground states is considered an NP-hard problem [1] (see Section 1.2.3). In this respect, algorithms for finding ground states are divided into two classes: *exact* and *heuristic*. The first class includes algorithms which terminate and provide the minimum energy solution in a time which in the worst-case grows exponentially with the size N. The second class includes algorithms which provide good but not necessarily optimal solutions. Heuristic algorithms have the advantage of being fast and easy to program, allowing to study larger systems in a relatively short time, but it is important to test their *reliability*, in order to determine to which extent failed instances might undermine the study.

Exact algorithms. The most direct method for determining ground states would be the exhaustive search, which consists in exploring the whole configuration space and selecting the state with minimum energy. This solution is feasible only for very small systems infeasible, as the computational time required by this task grows exponentially with N for any instance. Commonly used exact algorithms include:

Branch-and-bound: This method finds the ground state by excluding large parts of the phase space which contain no low-lying configurations [146].

Branch-and-cut: This algorithm proceeds by writing the energy as a linear function with an additional set of inequalities which must hold for the solution [147, 148]. The method iteratively solves the linear problem, search for new inequalities which are violated and adds them to the set, until the solution is found. The exponential time grows exponentially with the size of the system, together with the number of inequalities, but the algorithm finds exact ground states.

Heuristics. In order to test the reliability of a heuristic method, one could ideally compare directly its results with the results provided by an exact algorithm, measuring the failure frequency and the associated error in the ground-state energy up to a certain size N, eventually extrapolating the behavior for larger systems. This method is not very reliable when the size of the systems studied with heuristics is much larger than $N \sim 10^2$, the maximum size which is possible to study with exact algorithms. A more reliable self-consistent test consists in extracting the frequency of identical solutions with minimum energy.obtained from random independent multiple starts of the algorithm. Generally, any heuristic becomes unreliable at large N, and an algorithm is considered reliable if it can postpone the failure threshold for as long as possible.

Many heuristic algorithms have been proposed in the literature. In the following we illustrate three algorithms which have been used for an extensive study of the Bethe lattice and the EA model:

Extremal Optimization [149] This method has been introduced by Böttcher

[1] The only case in which exact ground states can be found in polynomial time is for the 2D lattice with PBC in one direction

and Percus in [149] and has been used for studying the scaling properties of ground states in the SK model, in the Bethe lattice and in the bond-diluted EA model [138, 150–153]. In this algorithm, the local fields acting on the spins are sorted and ranked at every step. A particular site is then chosen and reversed, according to a scale-free probability distribution.

More specifically, every spin σ_i is assigned a *fitness* $\lambda_i = -$(num. violated bonds). If c_i is the degree of node i, and c_M is the maximum degree, then $|\lambda_i| \leq c_i \leq c_M$. The occurrencies of the spins with the same value are λ: $\{n_c\}_{0 \leq c \leq c_M}$, with $\sum_i n_i = N$. A *rank* l is drawn from the distribution $P(l) \sim l^{-\tau}$, where τ is a parameter that needs to be tuned, and an index is drawn such that $\sum_{i=j+1} n_j < l \leq \sum_{i=j} n_i$. A spin is chosen at random from the ones with $\lambda = n_j$, and its orientation is inverted unconditionally, then the fitness of its neighbors and $\{n_i\}$ are recalculated, and a new spin is chosen for an update.

Cluster Exact Approximation(CEA): This is the algorithm used in our simulations. The algorithm was developed by A.K. Hartmann [144] and has been used extensively for deriving the ground states of different models[91, 134, 135, 154–157]. This algorithm evolves towards the ground state by iteratively selecting clusters of non-frustrated spins which are then optimized by using graph-cut techniques. The details of the algorithm used in this thesis will be introduced in Section 4.4.

Genetic algorithms and genetic CEA: Genetic algorithms (GA) are optimization methods which take inspiration from the process of natural selection. A genetic algorithm is an iterative process which starts with a population of randomly chosen candidate solutions, called *individuals* or *phenotypes*, and evolves towards better solutions by mutating or altering part of the *genome* of the individuals. In the spin glass case, the individuals are binary codes corresponding to configurations of spins. For each iteration, the more fit individuals are stochastically selected from the current *generation*, and the genome of each individual is modified to form a new generation. Typical operations are:

- *mutation:* One or more randomly chosen *genes* (spins) are changed to maintain the genetic diversity of the population;
- *crossover:* the genetic information of two parents is combined by selecting one or more points in the genome, and the offsprings are generated by swapping the sequences between the points.

The algorithm usually terminates when either a maximum number of generations is reached, or a satisfactory fitness level is achieved for the population.

As an example, we describe a genetic algorithm introduced by Hartmann which is often used in combination with the CEA [158], called *genetic CEA*. The algorithm starts with an initial population of randomly chosen configurations. Two *parents* are selected from the population and two offsprings are created identical to the parents. Then, a mask is created using a small fraction of spins of a third individual and a two-points *crossover* of the parents is performed. The *masked* spins which have the same orientation of the spins of the parents are selected and swapped between the two offsprings. Finally, a random

mutation. Eventually, at this point, the energy is reduced by using the CEA algorithm.

4.3 The models

In our study, we consider two different spin glass models with bimodal distribution of couplings $J = \pm 1$:

1. Bethe lattice (BL) on random regular graphs (RRG);
2. 3-dimensional lattice with *"random regular bond dilution"* (RRBD);

The two models are similar in several aspects, as they both exhibit structural disorder, random interactions, and the same uniform degree distribution. However, they differ for their topology, the first being a subclass of random graphs, the second being a finite-dimensional lattice with short-range interactions.

Using the graph theory notation introduced in Chapter 1.1, each model is described by a graph of N elements in which each vertex i corresponds to an Ising spin variable σ_i and each edge (i, j) represents a pairwise interaction between the spins σ_i, σ_j. In the spin glass version, the coefficients J_{ij} of the interaction matrix are quenched, independent and identically distributed random variables sampled from the probability distribution $P(J) = \frac{1}{2}\delta(J+1) + \frac{1}{2}\delta(J-1)$. Each model is subject to a random field h with Gaussian distribution of zero mean and variance 1, rescaled by a factor H to study the systems in different regimes. The Hamiltonian of the systems is:

$$\mathcal{H}(\sigma) = -\sum_{<i,j>} J_{ij}\sigma_i\sigma_j - \sum_{i=1}^{N} h_i\sigma_i \tag{4.1}$$

where the sum runs over the edges (i, j) of the graph.

We recall hereafter the main properties of the two models and describe the procedure to generate the numerical samples.

Bethe Lattice spin glass: Bethe lattices spin glasses have been already introduced in Chapter 2. We recall that BLSG are defined on the random regular graph (RRG) ensemble $\mathcal{G}^{RRG}(N, z)$, the subset of the Erdos-Reyni random graphs with size N and uniform degree z (see Section 1.1). Every graph of $\mathcal{G}^{RRG}(N, z)$ has $M = zN$ edges, where M is an even number. In this thesis, we focus on the $J\pm$ model with minimum coordination number $z = 3$.

Due to the finite connectivity, the BL is expected to undergo an RSB transition at zero temperature and finite critical field $h = h_c$, where the AT line intercepts the $T = 0$ axis. The spin glass phase over the AT line is expected to be in the RS phase, while in the region below the critical line the replica symmetry is broken. In this region, the cavity method provides a solution approximated to the 1RSB level [10, 11]. The thermodynamic quantities obtained in this approximation are in good agreement with the numerical data. In particular, for the $J\pm, z = 3$ model, the values predicted for the energy density $e_3 = \lim_{N\to\infty} E_N/N$ are:

$$e_3^{RS} = -1.2777, \qquad e_3^{1RSB} = -1.2717 \tag{4.2}$$

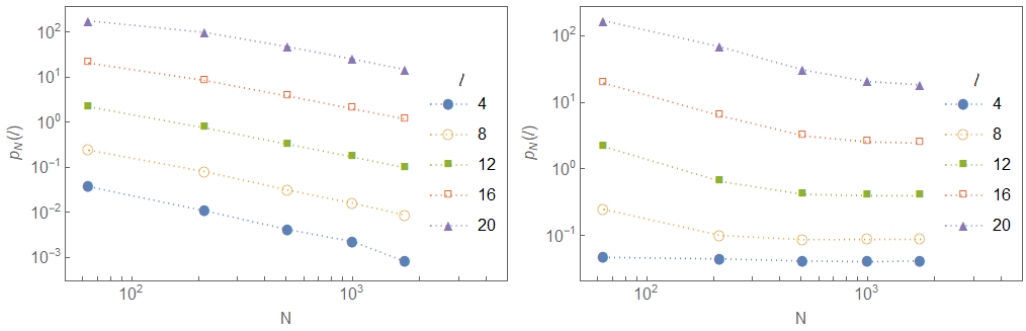

Figure 4.1. Scaling of the density of closed cycles of size ℓ in the two models, averaged over 30 samples. The density decreases constantly in the random regular graph phase (left), while it seems to saturate to a finite value in the three-dimensional regular lattice with regular bond-dilution (right).

The critical field can be calculated through the method suggested in [143] and described in Appendix D. For the $J\pm$ model with $z = 3$, the expected value is[159]:

$$h_c \sim 1.037 \tag{4.3}$$

Random Regular bond-diluted EA model in $d = 3$ The EA model, already introduced in the previous sections, is one of the most difficult models to study, both analytically and numerically. The upper critical dimension is $d = 6$, and the question of whether this model behaves similarly to mean-field models, or different theories should be taken into account, is still debated.

In order to push the computation to larger systems, it is often convenient to consider a diluted version of the model, which is supposed to belong to the same universality class. Normally, random dilution involves a certain amount of fluctuations in the thermodynamic quantities. We try to bypass the problem considering a random bond dilution where every node keeps the same number of neighbors $z = 3$. We shall refer to this model (improperly) as to the *random-regular bond-diluted* (RRBD) model. Compared to the cubic lattice, where $z = 2D = 6$, in the RRBD half of the bonds are randomly removed by keeping the local node degree constant.

It is important to remark that, even if the RRBD and the BL share the same degree distribution and a certain amount of structural disorder, the RRBD remains a short range model and maintains a spatial structure, features which are absent in the RRG. Moreover, differently from the Bethe lattice, where the average length of closed paths grows as $\sim \log N$, in this model the number of short cycles is not expected to vanish with the size (see Fig. 4.1), apart from effects due to the periodic boundary conditions.

We remark that the critical field for this model is not known *a priori*, and that even the existence of an RSB phase for this model is debated. This aspect will be treated more extensively in Chapter 6.

Generation of the samples Each graph $G(N, zN)$ is described by a set

σ, A, J, h, where:

- $\{\sigma_i\}$ is the array of the N Ising variables $\sigma_i = \pm 1$;
- $\{A_{ik}\}$ is the $N \times z$ adjacency list, each coefficient representing an outcoming edge (i, A_{ik});
- $\{J_{ik}\}$ is the $N \times z$ coupling list associated with the adjacency list. The coefficients J_{ij} are i.i.d. variables sampled over the symmetric distribution;

$$P(J) = \frac{1}{2}\delta(J-1) + \frac{1}{2}\delta(J+1) \tag{4.4}$$

- $\{h_i\}$, the external field, is an array of N i.i.d. random variables sampled with Gaussian probability $\mathcal{N}(0, 1)$.

One of the most delicate steps consists in generating graphs which are sampled uniformly over the ensemble, in order to avoid systematic errors.

The RRG graphs have been generated following the fast method described in Section 1.1.2. The RRBD samples have been generated using a matching algorithm. Starting from an edgeless 3D lattice with $N = L^3$ sites, where every node has degree $z = 0$:

1. a vertex i is chosen in a random sequence and coupled to a random neighbor with the same degree. After the matching both vertices have degree $z + 1$;
2. if no neighbors of i with same degree are found, then a random neighbor j is selected, an edge (i, j) is added, and a random edge (i, k) with $k \neq j$ is removed. After the matching i, j have degree $z + 1$, and k has degree z;
3. the procedure is repeated until all the nodes have degree $z + 1 = 1$, and then the procedure is repeated until every node has degree $z = 3$.

The algorithm converges in a reasonable time for $d = 3$ and for the values of L considered, but a further study of the matching problem has not been implemented in this analysis.

The parameters used for the generation of the samples are reported in Table 4.1. In general, the larger samples S_1, S_2 have been used mostly for the analysis presented in Chapter 6, while the smaller sets S_3, S_4 have been used for a preliminary analysis over the whole range of magnetic field, and also for studying the behavior at $H = 0$, where the large computational times set a limit to the size of the samples.

4.4 Cluster-Exact approximation

The CEA is a heuristic method introduced by A.K. Hartmann in [**hartmann1996cluster**] for obtaining the ground state of spin glasses. The algorithm is based on the iterative optimization of non-frustrated clusters extracted from the original graph. More precisely, the algorithm is divided into two phases:

- *Clustering*: in which a subgraph is generated randomly using a breadth-first search algorithm which selects a non-frustrated subgraph starting from a random root;

Set	S_1 RRG			S_2 RRBD	S_3 RRG	S_4 RRBD
N	# of samples	L	N	# of samples		
200	100000	4	64	32000	1000	1000
400	100000	6	216	16000	1000	1000
800	100000	8	512	8000	1000	1000
1600	$\lesssim$ 10000	10	1000	4000	1000	1000
3200	$\lesssim$ 5000	12	1728	2000	1000	1000
H	0.6 - 1.2			0.4 - 1.2	0.10 - 2.0	

Table 4.1. Table of the parameters used in the simulations

- *Optimization*: in which the cluster is optimized with respect to the boundary conditions imposed by the rest of the graph using a MIN-CUT method.

Since the clusters extracted in the first phase are free of frustration, they can be optimized exactly in just one step of the MIN-CUT algorithm.

The dynamics resulting from the iteration of this process is characterized by is a non-increasing energy function. Due to the possibility to optimize whole clusters of spins, the algorithm is able to avoid the local traps of the rough energy landscape which affect the dynamics of the basic steepest descent algorithm. Moreover, this algorithm is expected to be particularly effective on Bethe lattice spin glasses, where the effects of frustration are expected to appear only on large scale.

The algorithm was implemented by A.K. Hartmann [144, 145, 160] for simulating the ground states in the case of random field models [160] (for which the algorithm provides exact results in one step) and in the d-dimensional EA model with $d = 2, 3, 4$, with bimodal distribution of the couplings [91, 102, 134, 135, 144, 154–157], and Gaussian distribution [161]. The algorithm is often used in combination with the genetic algorithm described in the previous section. We used the CEA algorithm for obtaining the ground states in both the Bethe lattice and the d-dimensional model. In this respect, even if the RRBD model does not share the same scaling properties of the Bethe lattice concerning the density of cycles of finite-length, the average size of the clusters produced is comparable for the size considered (see Figure 4.3).

Hereafter, we describe more in detail the algorithm.

Clustering

A cluster is a subgraph $G'(V', E') \subset G(V, E)$ initially empty: $V' = E' = \emptyset$. The subgraphs are generated starting from a random root s_0 which is randomly selected from V and added to the cluster: $V' = \{s_0\}$, and proceeding to neighbor nodes in the breadth-first search order. More precisely, the neighbors of the root $s_{0j} \in \partial s_0$, are then tested in random order as potential candidates to be added to G'. The algorithm "visits" every neighbor $c_{ojk} \in \partial s_{0,j}$. If no neighbors have been visited yet by the algorithm, then c_{0i} is added to the cluster, and a new node is tested. If one of the neighbors c_{0jk} has been already visited by the algorithm, there are two possibilities:

- if the algorithm is set to produce *trees*, then c_{0jk} is immediately inserted in

the boundary B, and excluded by any further search;

- if closed paths are permitted, then c_{0j} is added to V' and (c_0, c_{0j}) is added to E' only if the gauge assigned to c_{0jk} does not contradict the one assigned on the previous "visit", otherwise is added to B.

When all the neighbors C_{0j} have been either added to G' or to B, the following element c_1 of the cluster is considered. The process stops when all of the elements of V' have been tested.

Gauge transformation

The coupling interactions are interpreted as *capacities* by the MIN-CUT algorithm. For this reason, no anti-ferromagnetic bonds must be present among the spins of the cluster. As new nodes are added to the cluster, a *gauge transformation* is performed to ensure all the spins inside the cluster have positive mutual couplings. For a cluster of n nodes, the gauge transformation is defined as a local inversion of the sign of the variables and of the couplings which leaves the local fields unchanged.

In particular, a vector $\mathbf{g} = g_1, ..., g_n$ with $g_i = \pm 1$ is defined. The root of the cluster s_0 is assigned an arbitrary coefficient $g_0 = 1$. Whenever a new node c_j is "visited" from c_i, it is assigned a gauge coefficient $g_j = \text{sign}(J_{ij})$. Due to the characteristics of the clustering algorithm, a new node is added to the cluster only if there are no contradictions in the assignment rules for g_i. At the end of the clustering phase, the matrix J' of the coefficients $J_{ij}g_ig_j$ is passed to the MIN CUT algorithm.

Optimization

The min-cut is a graph-partitioning algorithm which solves the problem of finding the minimum *cut* of the graph, a partition of the spin variables which minimizes the cost [12, 145]. The sub-graphs obtained from the clustering algorithm have a *regular* energy functional (see Section. C), in the sense that the coupling constants must be positive for the algorithm to converge. In the simulations, two different versions of MIN-CUT have been considered, the first based on the class provided by the LEMON library [2] , the second based on a 30% faster incremental breadth-first search algorithm [162, 163].

Iteration

The total energy of the system (or the number of unsatisfied bonds) is a monotonically decreasing function when the process is iterated for n_c steps. This corresponds to the iterative optimization of n_C different clusters. In general, two time scales are involved in the process. The first is the one required for the system to reach a low energy configuration, a 'valley' of the free energy landscape, which is usually very fast. The second is much slower since it involves the system exploring the metastable states, escaping the energy barriers, and proceeding towards local minima with

[2] Based on the `preflow.h` class included in the LEMON library (Library for Efficient Modeling and Optimization in Networks, https://lemon.cs.elte.hu). LEMON is an open-source C++ template library which provides tools for the implementation of combinatorial optimization tasks on networks.

increasingly lower energies, until the global ground state is eventually reached. This process requires usually a large number of steps, which increases with the size of the system. In order to be sure that the configuration provided is the true ground state, the algorithm is normally restarted n_S times from different random initial configurations.

In order to obtain reliable results, the following rule of thumb is adopted: the simulation terminates when for a given system and fixed n_c the same configuration is found 10 times. The probability of finding the true ground state energy, which is expected to decrease when N increases and $h \to 0$, is inversely proportional to n_s which is then expected to increase. The total computational time can be expressed in terms of the number of elementary optimizations $\mathcal{N} = n_c n_S$. Typically $\mathcal{N}$ is high if n_C is too low (not enough clusters to reach a minimum) or if n_C is too high. The minimum value $\mathcal{N}*$ is achieved by a preliminary analysis of the possible combinations.

Reproducing the correct probability distributions

In the $J\pm$ model, when $h = 0$, the ground state is typically degenerate. In this case, the CEA provides multiple solutions with the same energy and could be used for enumerating the ground states. From a comparison with the results obtained with simulated annealing (SA), it was argued by Sandvik [164] that in this case the results of the CEA might be affected by the parameters of the simulation, and that the CEA might not reproduce the correct probability distribution of the ground states, at least at $h = 0$. In fact, at zero magnetic field, the $J_\pm$ model has a large number of degenerate ground states and, depending on the context, one might need to consider only a part of them [91]. In this case, as reported in [165], one should be careful to select them with uniform probability and not according to the frequency they are found by the algorithm, which is biased [156].

4.5 Results

The algorithm is very fast at producing ground states of systems with $N \leq 1000$, and the performances are still acceptable for $N \leq 2000$, but they worsen as $N \sim 3200$. In the following, we measure the computational time in units of elementary 1-cluster optimizations, whose time complexity grows as $\mathcal{O}(N^2)$, as it can be seen in Fig.4.3. The number of clusters n_C generated per instance is optimized by sweeping the whole range of values in the range $[N/8, N]$. A good compromise is found using $n_C = N/8$, except for larger systems, where $n_C = N/4$ gives better results (Fig.4.2). The difference is negligible in small systems, but it becomes relevant at a larger size. For this reason, the value of n_c has been set to $N/4$ for all the systems.

A preliminary computation of the energies within a large range of values for H is shown in 4.5, where the SG models are compared with the RFIM version of the problem. While for $H > H_C$ the energy decreases almost linearly with H, for $H < 1$ the two models behave differently. Moreover, for $H \to zero$ the RRG energies are lower than the ones in the RRBD.

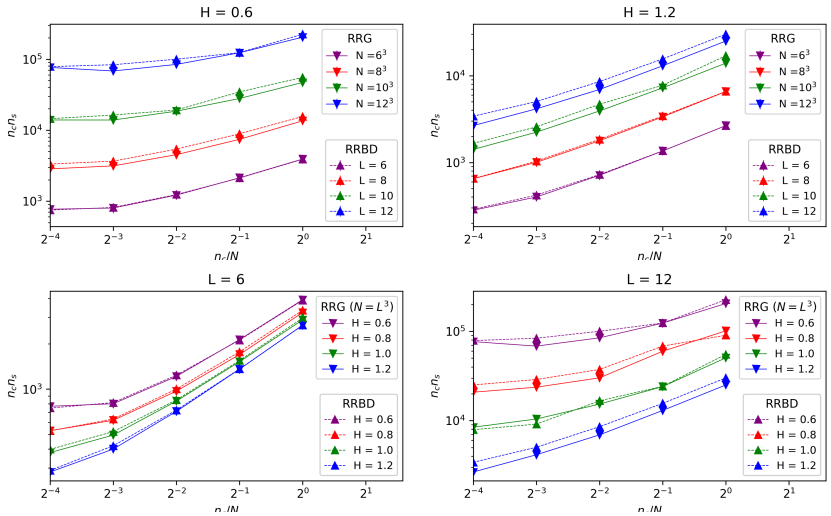

Figure 4.2. Dependence of the computational time $T = n_C n_S$ (in units of 1-cluster steps) on the number of clusters generated n_C (in units of n_C/N). Typically, the best performances are obtained for $n_C = N/8$ in small systems and $N/4$ in larger ones

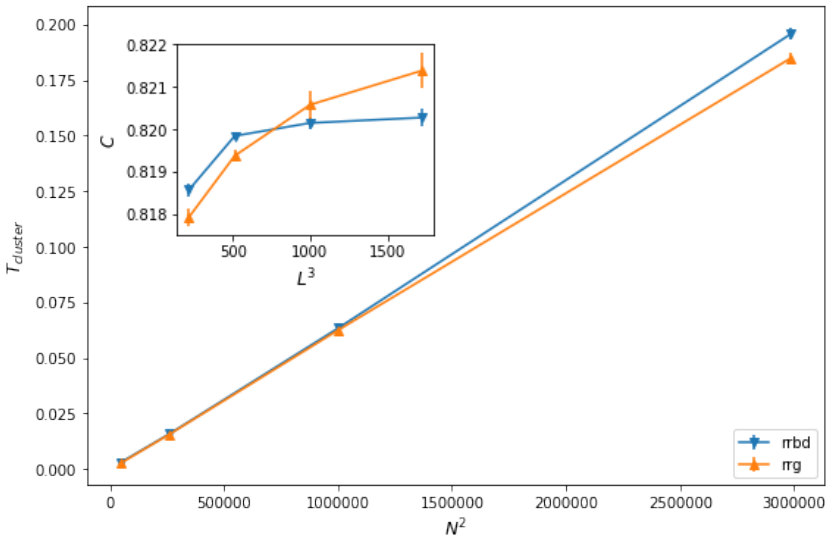

Figure 4.3. Main diagram: time complexity for the 1-cluster optimization, in CEA. The time grows as $\mathcal{O}(N^2)$. Inset: Average cluster size $< C >$ of the two models, as a fraction of the whole graph. At this stage the results do not depend on the magnetic field H.

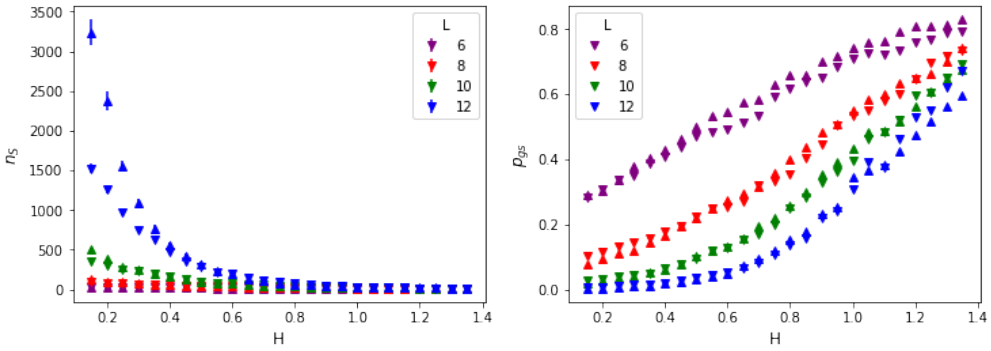

Figure 4.4. Reliability of the CEA algorithm. On the left, the dependence of the number of CEA iterations (number of starting conditions n_S) needed for finding ten times the same solution on the magnetic field H. On the right, the average probability of finding the correct ground state with a single iteration of the CEA algorithm. The duration of each iteration is fixed by the number of clusters generated $n_c = N/4$.

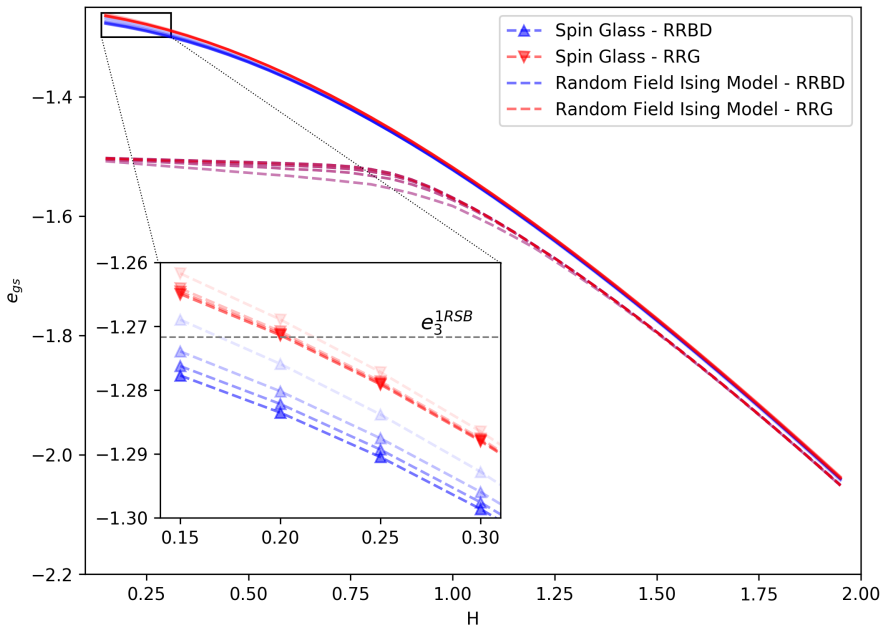

Figure 4.5. Dependence of the density of ground state energy $e_{GS} = E/N$ of the two graphic models on the random field H, in the spin glass and in the random field Ising model (RFIM) case. The curves with increasing opacity represent systems of increasing size $N = 6^3, 8^3, 10^3, 12^3$. In the inset the region close to $H = 0$ is magnified. The dashed horizontal line in the inset represents the asymptotic value of the energy density for the Bethe lattice with $z = 3$ obtained with the cavity method.

4.6 Ultrametricity

The presence of ultrametricity within the RSB scenario was derived first analytically [5, 6, 166, 167] and then confirmed numerically for the infinite-dimensional SK model [168, 169].

In finite-dimensional models, due to the lack of analytical solutions, ultrametricity can be detected only through numerical simulations, and it has been confirmed in three dimensions [170] and four dimensions [171, 172].

In [154], evidence of ultrametricity was detected in the 3D spin glass model with $J = \pm 1$ interactions, by direct examination of the distances between ground states. The method consists in analyzing triplets of ground states and comparing their mutual distances with the results expected in the two cases of ultrametricity and normal metric relations.

More precisely, given a triplet of states α, β, γ, whose mutual overlaps take increasing values $q_1 \leq q_2 \leq q_3$, one of the following relations is expected to hold:

- $q_1 > q_2 + q_3 - 1$ if the usual triangular inequalities hold;
- $q_1 \leq \min(q_2, q_3)$ if the system is ultrametric.

These relations might not hold rigorously for the ground states of finite-size systems, as a violation of ultrametricity is expected in small systems.

In [154], two different methods are used. The first method consists in measuring the difference $\delta q \equiv q_2 - q_1$ at fixed q_3. If the system is ultrametric, δq is expected to vanish for large N and the distribution $P(\delta q)$ is expected to be a Dirac delta centered in zero.

The second method consists in considering the distribution of one overlap $q_{\alpha\beta}$ when the other two are fixed at a certain value $q_{\alpha\gamma} = q_{\beta\gamma} = q_{fix}$. If the system is ultrametric, $q_{\alpha\beta}$ should fall within the interval $\{q_f ix, q_{EA}\}$, where q_{EA} is the self-overlap $P(q_1)$ distribution which falls out of the interval $[q_{fix}, q_{EA}]$. If the system is ultrametric, I_L should vanish for $N \to \infty$.

We looked for evidence of ultrametricity in the RRG and RRBD at zero temperature by using these methods at $H = 0$. A modified version of CEA was prepared, for searching and storing the configurations with ground state energy (due to the degeneracy of the $J\pm$ model ground states). The number of ground states for every sample was reduced by choosing a small number of configurations at random (disregarding their occurrence in the CEA), and for each system the set of all the couples and triplets of ground states was considered.

For each system three probability distributions were calculated:

1. $P(q) = \sum_\alpha \delta(q - q_\alpha)$;
2. $P(\delta q | q_3 = 0.5)$, where q_3 is the largest overlap;
3. $P(q | q_\alpha = q_\beta = 0.5)$, where the overlaps are not ordered.

The second and third distributions are computed at $q = 0.5$ for simplicity. The results are shown in 4.6. The presence of a peak of the $P(\delta q)$ distribution in zero is a sign of the abundance of isosceles triangles in the system. In the presence of ultrametricity the third distribution is expected to be null for $q < 0.5$, while according to the triangular inequality the region $q < 0.5$ should be populated.

The results, obtained for 1000 samples from the RRG and RRBD models with size $L = 6, 8, 10, 12$, are consistent with the hypothesis of ultrametricity up to a certain degree. The peaks are not perfect delta functions due to the finite-size effects, more evident in small systems, and to the fact that the constraints were not chosen rigorously, as the identities $q_3 = 0.5, q_\alpha = q_\beta = 0.5$ were implemented by choosing the values in a small interval $q \in [0.5, 0.6]$. The presence of two peaks on $q = 0.5$ and $q \sim 1$ in the third distribution are unexpected, and may be due to the fact that the ground states selected by the CEA are not sampled from the Boltzmann measure and might suffer from some systematic error. Nevertheless, the states selected by the CEA show hints of ultrametricity.

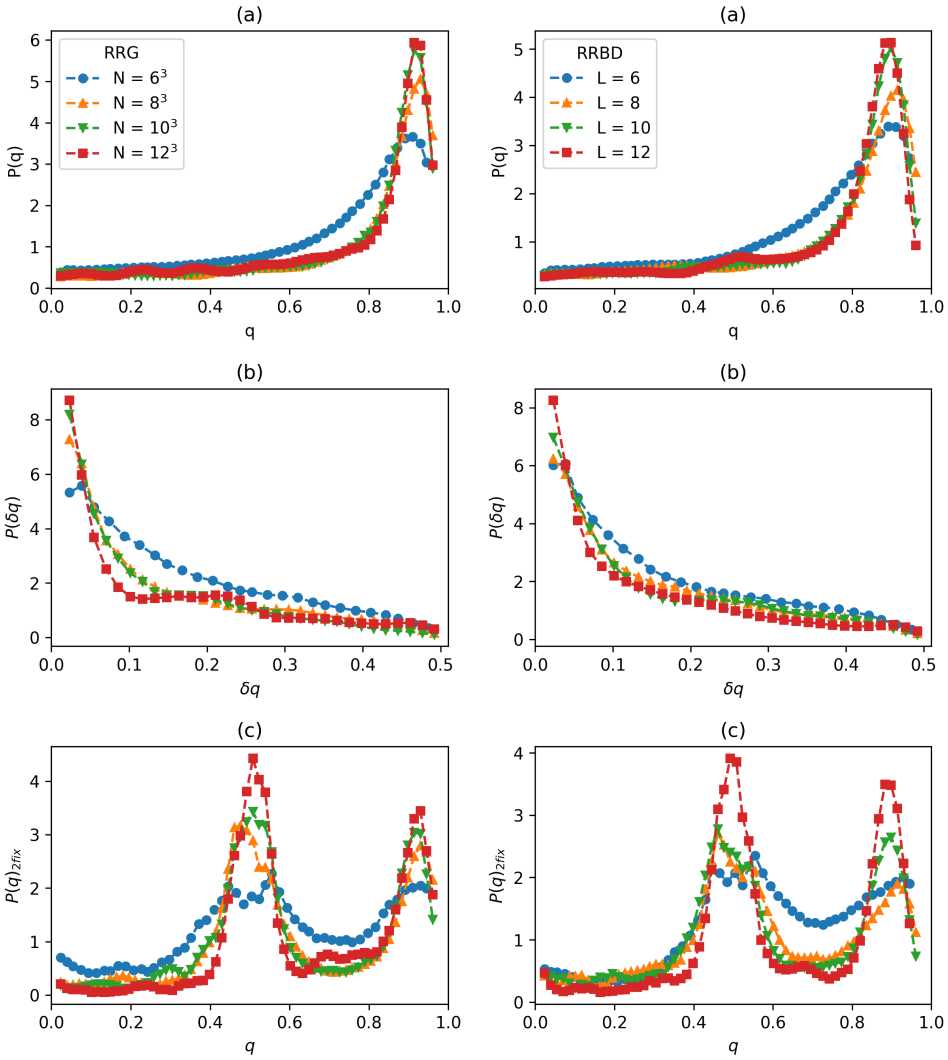

Figure 4.6. Measure of ultrametricity in RRG (left column) and RRBD (right column) spin glasses. The three distributions represent (a) the distribution $P(q)$ of the overlap between degenerate ground states; (b) the distribution of the variable $\delta q = q_2 - q_1$ when $q_3 \in [0.5, 0.6]$, where $q_1 < q_2 < q_3$ are the overlaps computed for all the possible triplets of states; (c) the distribution of the overlap $q_{\alpha\beta}$ when the other two overlaps are $q_{\alpha\gamma}, q_{\beta\gamma} \in [0.5, 0.6]$. The distributions are obtained by averaging over the single-sample distributions with equal weights.

Chapter 5

Finite-Size corrections

5.1 Introduction

In this chapter, we present a computation of the first order corrections to the ground state energy for the models defined in the previous chapter.

The computation of the scaling exponents provides useful information for classifying different models into universality classes. In this context, interesting features have been observed for the momenta of the ground state energy distribution in both finite-dimensional and mean-field models. Let us consider the mean value of the ground state energy density $e_0 = E_0/N$ and its standard deviation, for which we assume the following scaling forms:

$$< e_0 >_N = < e_0 >_\infty + AN^{-w} + \mathcal{O}(N^{-w_1}), w_1 > w \tag{5.1}$$

$$\sigma(e_0) = \sqrt{< e_0^2 > - < e_0 >^2} \sim AN^{-\rho} + \mathcal{O}(N^{-\rho_1}) \quad (\rho_1 > \rho) \tag{5.2}$$

One could consider different forms, eventually including higher orders, but in general, any asymptotic fit bares a certain amount of risk. In some cases, a presumed form might be insufficient, miss logarithmic corrections, or underestimate some range of values. The task is simplified when backed by a solid theory, which in finite-dimensional spin glasses is missing. In our case, due to the limited amount of points available for the extrapolation, we limit the study to the first order corrections.

Finite-size corrections to the average ground state energy

In order to set a paradigm, it is convenient to start with the SK model, which provides a comparison for the finite-dimensional results. Theoretical studies [173] and numerical simulations [138, 151, 174–176]agree in stating that finite-size corrections to the energy of the SK model behave for all $T \leq T_c$ according to Eq. (5.1) with $w = \frac{2}{3}$. In [177], the value is confirmed also adding a higher order correction equal to the square of the first order term, which improves the quality of the fit.

With respect to the Bethe lattice spin glass, numerical studies have been made on both the $J\pm$ [138, 178] and the Gaussian model. In [138, 177], the extrapolation of the data for $J\pm$ BLSG with $z = 3$ agrees very well with the asymptotic form (5.1) with exponent $w = \frac{2}{3}$. The asymptotic value found for the ground state energy is:

$$< e_3 >_\infty = -1.2715(1) \tag{5.3}$$

consistent with the 1RSB results reported in [11].

Ground state fluctuations The fluctuations of the ground state energy of the SK model exhibit an interesting behavior and show similarities with the values found for distributions describing the statistics of extreme-events [118, 151, 174, 179–181]. The energy fluctuations, normally studied in terms of the standard deviation defined in (5.2), provide important information on the structural properties of the ground states.

Two different conjectures have been made about the fist-order corrections: $\rho = \frac{3}{4}$ [118, 123] or $\rho = \frac{5}{6}$ [115, 182–186]. In both cases, the fluctuations decay faster than the ones expected in the assumption of negligible correlations between the terms of the spin glass Hamiltonian, for which the central limit theorem would provide $\rho = \frac{1}{2}$. For the SK model, a bound has been derived $\rho \geq \frac{3}{4}$ [187, 188], while a Gaussian behavior has been found for both finite-dimensional models [189] and sparse random graphs [118].

In this regard, the numerical results on the SK model do not provide a clear picture, as an initial value of $\rho = \frac{3}{4}$ was found initially [118, 151, 179], while evidence for $\rho = \frac{5}{6}$ [174] was found for larger systems, in agreement with recent theoretical predictions [175, 183, 184]

In the Bethe lattice spin glasses, the situation is similar. In [177], for instance, the value obtained for the fluctuations is consistent with $\rho = \frac{5}{6}$

5.2 Results

We have computed the FSC to the average ground state energy density for the two models defined in the previous chapter: the Bethe lattice spin glass (BL) and the random-regular bond diluted model (RRBD). The topic has already been introduced in Section5.1. The purpose of the finite-scaling analysis is to determine the asymptotic behavior of thermodynamic quantities measured at finite size. Different conjectures have been made in several theoretical and numerical studies, about the value of the exponents of the ground state energy. [178] Let us consider the asymptotic form

$$e_{GS}(N) = e_\infty + AN^{-w} \tag{5.4}$$

In the $J\pm$ model, the expected value for w is the same found in the SK model: $w = \frac{2}{3}$. Interestingly, the same exponent calculated on the Bethe lattice with Gaussian couplings has a different value: $w = \frac{4}{5}$.

In our case, the data were fitted using different values of w, assuming the asymptotic form (5.4), measuring the quality of the fit by a simple χ^2 test. We distinguish the two cases $H = 0$, $h > 0$.

The results at zero field for the BL spin glass, both for w and for the asymptotic value $< e_3 >_\infty$ are (see Fig. 5.1:

$$< e_3 >_\infty = -1.2715(6), \quad w \sim 0.66 \tag{5.5}$$

This result is consistent with other numerical results[138, 178] and with the value $e_3^{1RSB} = -1.2717$ obtained analytically with the cavity method [11].

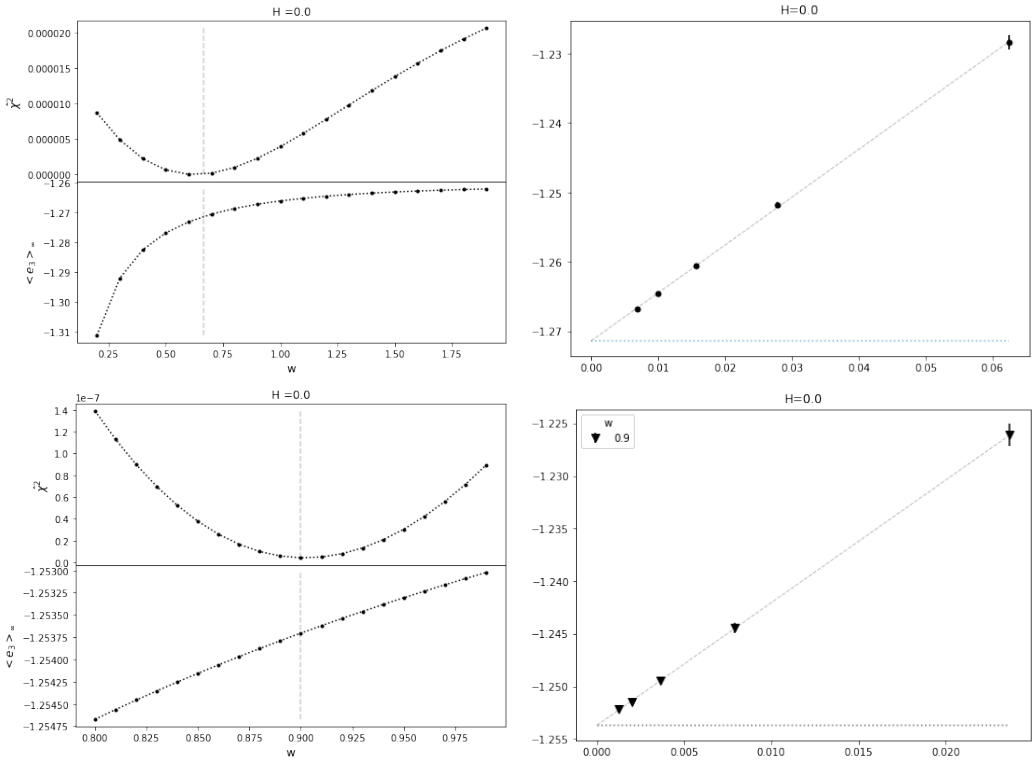

Figure 5.1. Finite-size corrections to the ground state energy at $H = 0$. On the left, the quality of the fits is measured for several values of w in terms of χ^2/dof, for the RRG (top) and the RRBD (bottom). On the right, the linear fit and extrapolation of the $< e_3 >_\infty$ asymptotic value for the two models, using $w = 2/3$ in the BL, and $w = 0.9$ for the RRBD. The values for the BL are in good agreement with the predictions. The situation is less clear in the RRBD, where two fits with different coefficients have been plotted.

For the RRBD the results are different:

$$< e_3 >_\infty = -1.2537(0), \quad w \sim 0.90 \tag{5.6}$$

The situation becomes less clear for the values calculated in field $H > 0$(Fig.5.2-5.3). In Table 5.1, the asymptotic values from the fit to the form (5.4) with $w = 2/3$ are reported. However, upon a χ^2 test, the best extrapolation is obtained with coefficients $w > 2/3$.

Besides, in the case of the RRBD the exponents are much larger, especially for $H > 0.8$. Here, we should consider the possibility that the transition point is $h_c^{RRBD} < h_c^{RRG}$. In this case, at $H = 1.0$, the RRBD systems might have already crossed the critical value and could be in the RS phase.

As a final qualitative analysis on the finite-size effects, let us consider the curves plotted in Fig.5.4. Here the deviation from the mean value is plotted in units of the standard deviation. The distribution of the standardized variables has a non-zero skewness, as it is clearly asymmetric, and finite-size effect can be seen on the tail of the distributions.

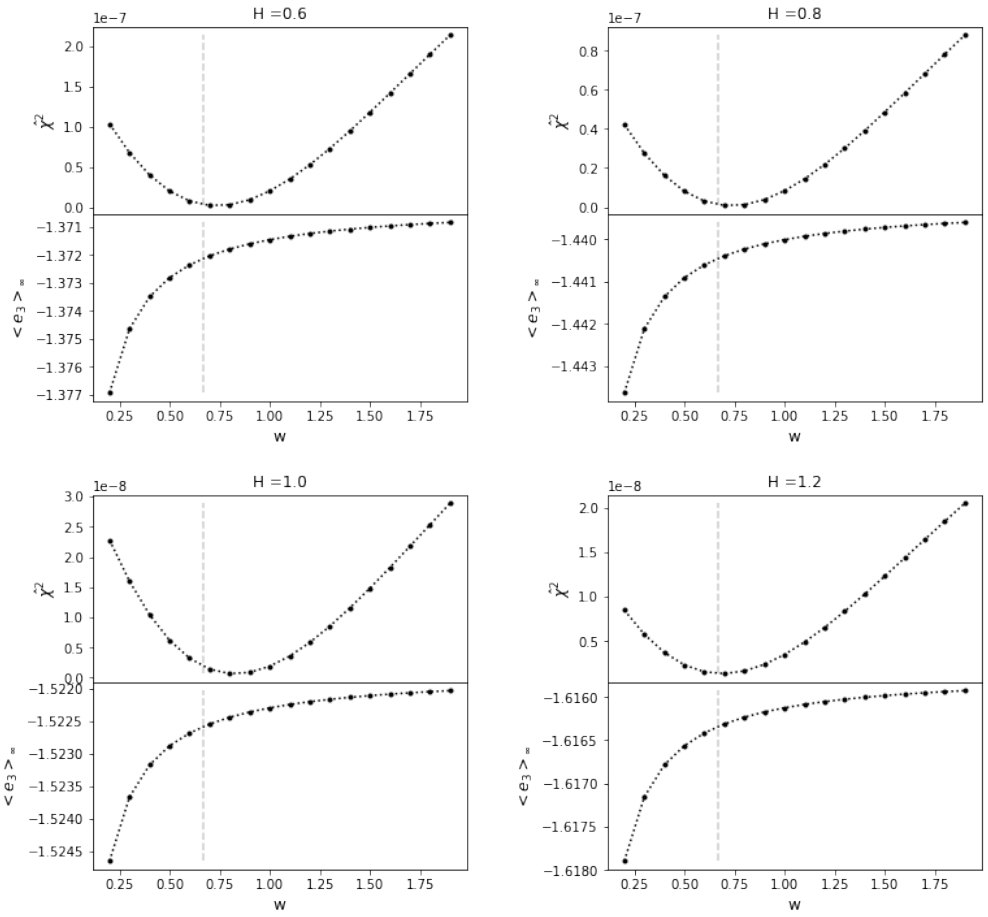

Figure 5.2. Finite-size corrections to the RRG for $H > 0$. Above, goodness of the fit to the asymptotic form (5.1) in terms of ξ^2/dof and asymptotic value of the density ground state energy $\langle e_3 \rangle_\infty$ as functions of the parameter w. The best fits are obtained for values larger than $w = 2/3$, the exponent computed in the $H = 0$ case. Below, linear fit and extrapolation of $< e_3^{RRG} >_\infty$, using $w = 2/3$.

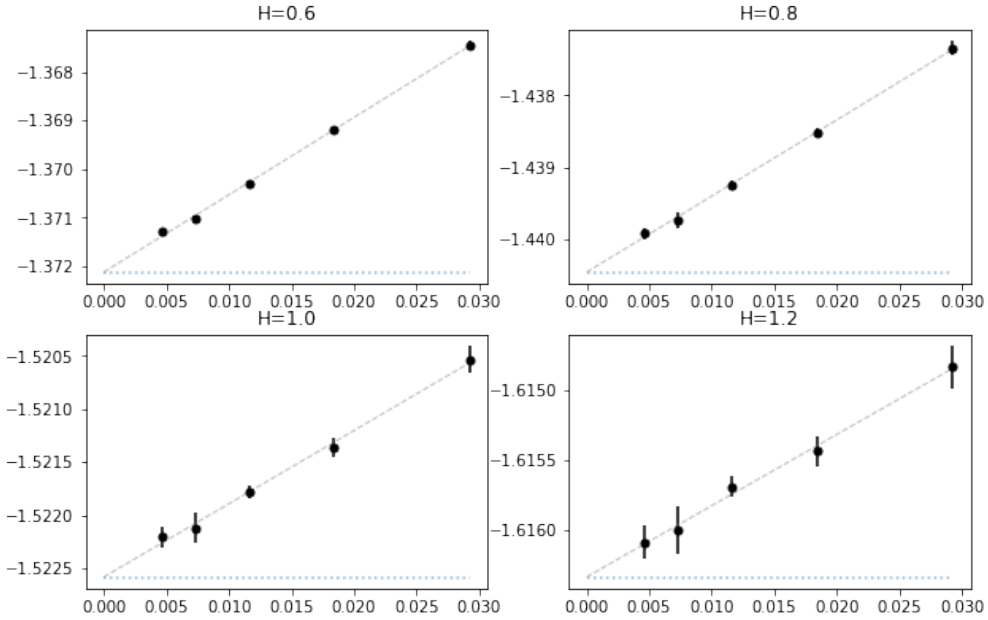

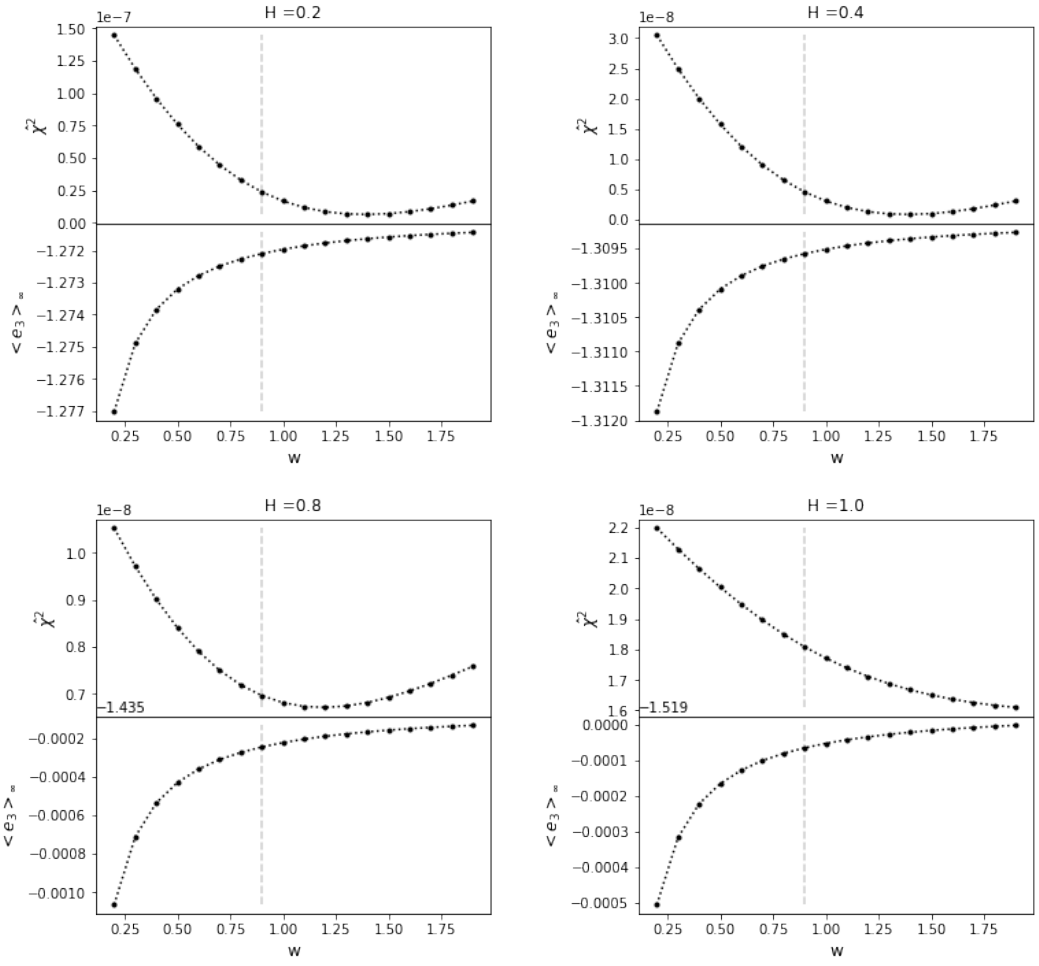

Figure 5.3. Finite-size corrections to the RRBD, $H > 0$. Above, goodness of the fit to the asymptotic form (5.1) in terms of ξ^2/dof and asymptotic value of the density of ground state energy $\langle e_3 \rangle_\infty$ as functions of the parameter w. The best fits are obtained for exponents w larger than in the $H = 0$ case, and second order corrections should be considered.

H	e_∞		
0.0	-1.27156	$\pm$	$5 \cdot 10^{-5}$
0.6	-1.37217	$\pm$	$6 \cdot 10^{-5}$
0.8	-1.44046	$\pm$	$3 \cdot 10^{-5}$
1.0	-1.52256	$\pm$	$6 \cdot 10^{-5}$
1.2	-1.61629	$\pm$	$3 \cdot 10^{-5}$
1.5	-1.77388	$\pm$	$9 \cdot 10^{-5}$

Table 5.1. Asymptotic values of the ground state energy for the Bethe lattice spin glass, in the large N limit

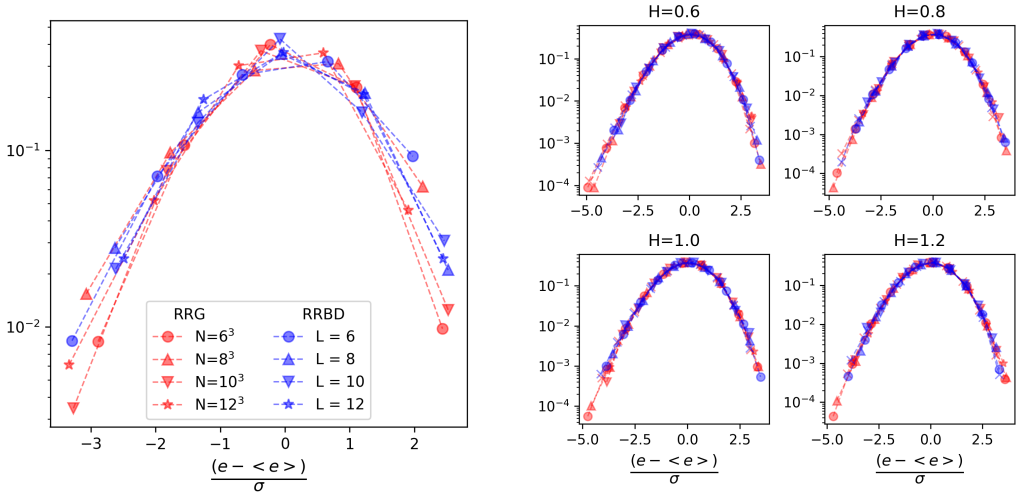

Figure 5.4. Distribution of the normalized variable $\frac{e-\langle e\rangle}{\sigma}$ for both the RRG and the RRBD model, at $H = 0$ (left) and $H > 0$ (right). It is evident how the distributions are skewed, with more values falling below the mean energy. Moreover, some finite size effects are visible on the tails.

5.3 Conclusions

In this chapter, we have computed the finite size-corrections to the ground state energy of the Bethe lattice and three-dimensional diluted EA model. At $H = 0$, the results for the Bethe lattice are consistent with the theoretical predictions and with previous numerical results. The results for the RRBD model are difficult to interpret since the type of dilution is quite different from the one used in previous works. The scaling exponent seems to be consistent with the values calculated in other works. At $H > 0$ the exponents are larger than expected, for both systems. In general, the analysis at $H \gtrsim 1$ suffers from the fluctuations of the field itself.

The study might be extended in the future to the fluctuations of ground state energy, which also present finite-size effects.

Chapter 6

Computation of the RSB order parameter

6.1 Introduction

In this chapter, we present some original results regarding the computation of the spin glass order parameter at zero temperature in two models with finite connectivity: the Bethe lattice spin glass, and the three-dimensional lattice with bond-dilution. The purpose of the investigation is to bring new numerical evidence into the debate about the nature of the spin glass phase of finite-dimensional models. In the previous chapters we have seen that there are several theories accounting for the behavior of finite-dimensional models, and the question whether the RSB scenario which characterizes the spin glass phase of infinite-range models [3, 4, 66, 190] can be extended to finite-dimensional models [46–48, 124–126] is still debated. The results presented in this chapter focus on the scaling properties of ground states, and in particular on the effects of the physical order parameter on the distribution of low-lying states of the energy landscape.

First of all, we would like to summarize the concepts presented in the previous chapters from the point of view of the *classification* of the ground states. The theory of spin glasses shows that in the low-temperature phase, even in the simplest form of mean-field approximation, the organization of the large number of equilibrium states is highly non-trivial. Classifying these states and their properties is a fundamental problem of equilibrium statistical mechanics. The task is typically simple when the phases are related by some symmetry. In ferromagnetic systems, for instance, the two states which constitute the low temperature phase in zero magnetic field can be classified by their opposite values of spontaneous magnetization and selected by a convenient small change of the external field or the boundary conditions.

In spin glasses, the situation is rather different. The rough free-energy landscape of the spin glass phase is fragmented in many disconnected regions which are not related by any simple transformation. In this scenario, the full classification of the pure states cannot be achieved by a simple choice of an order parameter, as the pure states are related in a more subtle way [66]. As already seen in Section 1, this task is carried out by introducing a notion of distance - the mutual overlap q between the states - and taking into account the full overlap distribution $P(q)$, which is the

physical order parameter.

In the case of the infinite-dimensional Sherrington-Kirkpatrick model, the order parameter is non-trivial, meaning that $P(q)$ is a continuous function which differs from a simple delta function. As a consequence, triplets of states form only isosceles triangles with respect to their overlap, as the mutual distances satisfy the ultrametric inequality. This is a much tighter constraint than the usual triangular inequalities (see Section 2.1.3). Ultrametricity has profound consequences on the structure of the space of the states, which are organized in clusters of elements with the same distance, which in turn are grouped in super-clusters at a larger scale, and so on.

One of the main questions is whether this structure is preserved when one descends to finite-dimensions. The mean-field approach does not provide exact solutions in this case, and the investigation relies mostly on numerical methods. In this respect, ultrametricity has been confirmed numerically at finite-dimension (see Section 4.6), even if some violations might be expected at finite-size. The derivation of the order parameter, on the other hand, is typically more difficult to achieve computationally.

The method adopted in this work is based on the results of Franz and Parisi [49] regarding the effects of Replica Symmetry Breaking on the structure of the energy landscape. We use the ϵ-coupling technique, based on the introduction of a coupling between a system and its ground state, to probe the energy landscape in terms of the energy gaps and overlap between the low-lying minima. The probability distribution of the excited states is thus exploited to compute the order parameter, using the formulas obtained in [49].
The numerical approach is not new, as the study of large-scale low-energy excitations has been described in different contexts , both numerically [125, 126, 161] and analytically[143]. However, to our knowledge, it is the first time that it is used for computing the order parameter directly from the computation of ground states.

We examine two different models: the Bethe lattice spin glass and the bond-diluted $d = 3$ lattice model with fixed $z < 2D$ neighbors per site. These are both examples of models with finite connectivity and homogeneous distribution of the node degree, but with a rather different topology.
In the first case, the lattice is a random regular graph (see. Section 1.1), and it lacks a spatial structure. We are interested in this model for at least two reasons. In the first place, a full RSB solution has not been derived yet for the Bethe lattice spin glass (see Section 2.2). Differently from the SK model, which exists only in the RSB phase at zero temperature, the Bethe lattice spin glass is known to undergo a phase transition at a critical value of the external field. Little is known about the region below the transition, as the study of the solutions breaks when the RS solution becomes unstable. The other reason is computational. The locally tree-like topology enables the exact computation of the ground states using efficient optimization algorithms. For the investigation, we used the Cluster-Exact Approximation algorithm (CEA) [144] developed originally by A.K.Hartmann (see Section 4).
The second model is obtained from the three-dimensional lattice by introducing a sort of *random regular bond dilution* (RRBD model). The resulting model is characterized by nearest-neighbors interaction with a constant number $z < 2D$ of neighbors. Here the effect of correlations due to short loops is still present, even at

large size, but the computation of ground states is easier than in the usual $z = 2d$ lattice. In this respect, it would be interesting to study how the properties of this model scale at different values of d, by keeping z constant. In both models, the order parameter is derived in the RSB and the RS phase, and the distributions are compared with the ones obtained for the ferromagnetic random field model (RFIM), where no RSB phase is present.

This chapter is organized in the following way: in Section 6.2 the general formalism is introduced, following the derivation presented in [49]. The numerical approach is described in Section 6.4, followed by the discussion of the results (Section 6.5). In the last section (Section 6.6) we present some conclusions and perspectives of this work.

6.2 Overlap distributions at zero temperature

The RSB order parameter. The physical spin glass order parameter is the probability distribution $P(q)$ of the mutual overlaps q among the large number of states. In this section, we recall the main concepts and formalism introduced in Section 2.1.2.

We consider a system of N spin variables σ_i, indicating with α, β two different states and with m_i^α, m_i^β the local magnetization at the site i in each state. The mutual overlap between the two states is defined as:

$$q_{\alpha\beta} = \frac{\sum_i m_i^\alpha m_i^\beta}{N} \tag{6.1}$$

At zero temperature, this definition coincides with the overlap between configurations. The distribution of the overlap is:

$$P(q) = \overline{P_J(q)} = \overline{\sum_{\alpha\beta} \delta(q - q_{\alpha\beta}) w_\alpha w_\beta} \tag{6.2}$$

where w_α, w_β are the weights associated with the Boltzmann decomposition and the overline indicates the average over the disorder. As $P_J(q)$ is not self-averaging, $P(q)$ differs from any single-sample distribution in the thermodynamic limit.
It is also convenient to define the integrated probability function

$$x(q) = \int_{-1}^{q} P(q')\, dq' \tag{6.3}$$

In the replica symmetric (RS) phase, $P(q)$ is expected to be a single delta function centered on a finite value of overlap:

$$P(q) = \delta(q - q_{EA}) \tag{6.4}$$

On the other hand, upon a transition to the full RSB phase, $P(q)$ is known to be a composition of two delta functions with a continuous function:

$$P(q) = x_m \delta(q - q_m) + x_M \delta(q - q_M) + \tilde{P}(q) \tag{6.5}$$

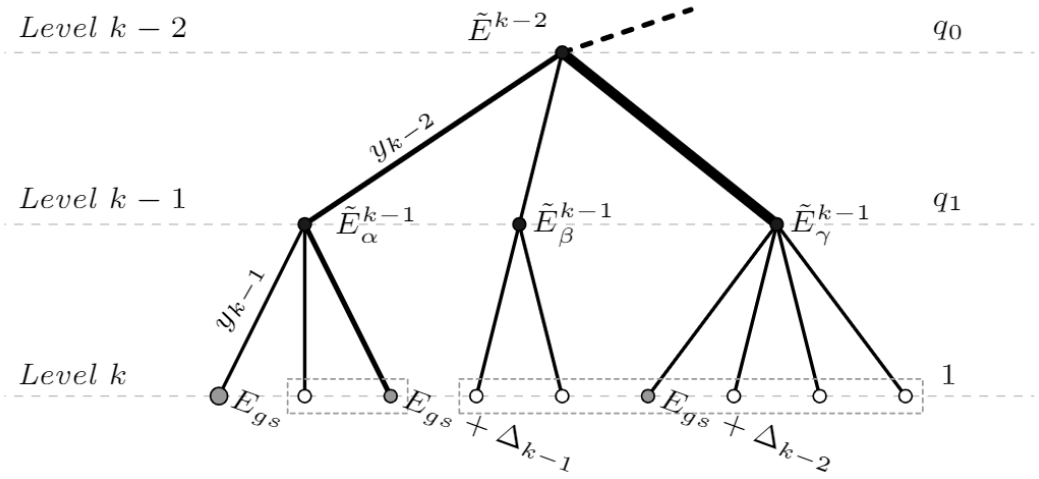

Figure 6.1. Ultrametric tree of depth k at $T = 0$. The leaves at the bottom (level k) represent the minima of the energy landscape with *real* energies, while the points at level $k-1(k-2)$ represent clusters of scale $q_{k-1}(q_{k-2})$, each characterized by *node* energy $\tilde{E}^{l+1}(\tilde{E}^{l+1})$. The ground state (larger grey point, bottom left) is the ground state with energy E_{gs}. The *first* $k-1$*-excited state* $(k-2)$ is the state with minimum energy $E_{gs}+\Delta_{k-1}$ $(E_{gs}+\Delta_{k-1})$ among all the minima within the same distance $q_{k-1}(q_{k-1})$ from the ground state (dashed rectangles).

where $\tilde{P}(q)$ is a smooth continuous function defined in the interval $[q_m, q_M]$. In general, in the low-temperature phase, q_m depends on the external field h and q_M depends on the temperature T. As $T \to 0$, $P(q,T)$ and $x(q,T)$ are assumed to be smooth functions of the temperature [66, 191–193]:

$$x(q,T) = Ty(q) + O(T^2) \tag{6.6}$$

where $y(q)$ may be singular at $q = 1$.

Although the approach here described is very general, and no model has been defined yet, it should be noticed that in our case the Hamiltonian will depend on an external magnetic field. As a consequence, the global spin inversion symmetry is broken, and the order parameter is expected to be defined only for non-negative values of overlap, at least in the thermodynamic limit.

Ultrametric tree at zero temperature The continuity of the overlap distribution over the interval $[q_{min}, 1]$ has profound physical consequences on the topology of the space of the configurations. Rather than being distributed randomly, the pure states have an ultrametric organization with respect to their overlap[5, 6, 194], forming a hierarchical structure of clusters of increasing scale which can be naturally represented in terms of a taxonomic tree. In this respect, a tree is a natural realization of an ultrametric system in which the distances between the leaves are measured according to their distance from their common parent. The construction of the tree at finite temperature has been already described in Section 2.1.4.
Here, we consider a a rooted tree of depth k describing a k-RSB system at zero temperature, with the following characteristics:

- each level l of the tree is assigned a scale q_l such that $q_0 < \ldots < q_k = 1$, the whole set of parameters representing a discretization of the interval $[q_{min}, 1]$;
- each node at level l is assigned a *node* energy $\tilde{E}^l$;
- the leaves of the tree at depth $l = k$ are the minima of the energy landscape, characterized by *real* energies $\tilde{E}^k = E$;
- the vertices at intermediate levels $l < k$ represent clusters of configurations (denoted *l-clusters*);
- at any fixed scale $q_l < 1$, the space of the configurations can be partitioned into disjoint l-clusters of elements with overlap $q \geq q_l$, the overlap being exactly q_l if they belong to different $l + 1$-clusters.

The tree is generated via an iterative stochastic process called *Derrida-Ruelle cascade*[84, 85]. Starting from the root, the branches stemming from each node are generated according to a Poisson point process level by level, until the leaves are reached. The process is described in detail in Appendix B. Here, we just observe that the tree depends on the parameters q_l through the function $y(q_l) = y_k$, the zero temperature order parameter defined in Eq. (6.6).

The *full*-RSB picture is recovered in the limit of infinite branching: $k \to \infty$. In this limit, the parameters y_l tend to a continuous increasing function $y(q)$ in the interval $[q_{min}, 1]$.

We would like to characterize the effects of ultrametricity on the energy landscape. Keeping in mind the structure of the ultrametric tree in Fig. 6.1, the first level of the tree (level $k-1$) consists of $(k-1)$-clusters whose elements have overlap q_{k-1}. We consider the $(k-1)$-cluster containing the ground state and the configuration with minimum energy in the same cluster, but different from the ground state. This is a *first* $(k-1)$*-excited state* with energy $E_{gs} + \Delta_{k-1}$. Following the same considerations, at the subsequent level we can identify a first $(k-2)$-excited state with energy $E_{gs} + \Delta_{k-2}$, and so on until the root is reached. The different $\Delta_0, \ldots, \Delta_{k-1}$ are random variables whose distribution is computed in [49] using a pure probabilistic computation over the ultrametric tree. The detailed computation is reproduced in Appendix B. The distribution depends on the scales q_l through the coefficients $y_0, \ldots, y_k$, and in the $k \to \infty$ limit is expressed by:

$$P(\{\Delta(q)\}) = e^{-\int_{q_{min}}^{1} dq\, y'(q)\Delta(q)} \prod_{q=q_{min}}^{1} y'(q)dq \tag{6.7}$$

where $\Delta(q)$ is a continuous decreasing function in $[q_{min}, 1]$.

The joint probability distribution $P(\Delta, q)$ In order to extract the order parameter from the formula in Eq. (6.7), few passages are still needed. The goal is to invert the formula and express $y(q)$ as a function of the joint probability distribution $P(\Delta, q)$.
The latter can be extracted from numerical simulations by sampling the energy landscape in terms of the overlap q and energy gap Δ between the different minima and the ground state.

We consider a system described by the Hamiltonian $\mathcal{H}_0$, with ground state σ_0. Let us denote $q(\sigma) = 1/N \sum_i \sigma^i \sigma_0^i$ the overlap between the ground state and a generic configuration σ. The energy landscape can be probed by introducing a perturbation in the system which is an increasing function of $f(q)$ and studying the new equilibrium state. Due to the presence of a magnetic field which breaks the symmetry for spin inversion, we consider the simplest case $f(q) = q$.
The perturbed Hamiltonian is:

$$\mathcal{H}_\epsilon(\sigma) = \mathcal{H}_0(\sigma) + \epsilon q(\sigma) \tag{6.8}$$

We remark that $\epsilon > 0$ is small, therefore the perturbation is a term of order $O(1)$ which is repulsive with respect to the ground state.

The new equilibrium state, the ground state of the perturbed system, has energy:

$$E_{GS}(\epsilon) = E_{GS}(0) + \min_{0 \le q \le 1} \{\Delta(q) + \epsilon q\} \tag{6.9}$$

Let q, Δ the parameters which correspond to the minimum of expression (6.9).
If the perturbation is not strong enough to destabilize the ground state, then $q = 1, \Delta = 0$ and $E_{GS}(\epsilon) = E_{GS}(0) + \epsilon$. This value is also an upper bound for the ground state energy $E_{gs}(\epsilon)$.
On the contrary, if there is a transition to an excited state, then the new energy of the perturbed system is:

$$E_{GS}(\epsilon) = E_{GS}(0) + \Delta + \epsilon q = E_{GS}(0) + \epsilon w \tag{6.10}$$

where $w = \Delta/\epsilon + q$. This situation is represented in Fig. 6.2.
Due to the previous considerations, the following inequalities must hold for Δ, q:

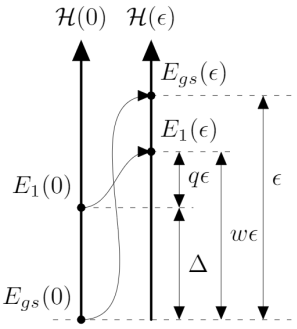

Figure 6.2. ϵ-coupling: first-excited state induced by a bulk perturbation

$$0 \le \Delta \le \epsilon(1 - q), \quad w < 1 \tag{6.11}$$

In general w could be negative at finite size, but in the limit $N \to \infty$ it is expected to be positive.

If the system is in the RSB phase, Δ, q are expected to be distributed according to Eq. (6.7). We derive an expression for the joint probability distribution $P(\Delta, q)$ by integrating Eq. (B.14) over all the $\Delta(q')$ with the condition $\Delta(q') \ge \min(0, \Delta + \epsilon(q - q'))$ and under the constraints (6.11):

$$P(\Delta, q) = \theta(1 - q - \Delta/\epsilon) y'(q)\, e^{-\epsilon \int_{q_{min}}^{q+\Delta/\epsilon} (y(q') - y(q_{min}))\, dq} + \delta(\Delta)\delta(q-1)\, e^{-\epsilon\chi} \tag{6.12}$$

where $\chi = y(q_{min}) + \int_{q_{min}}^{1} dq y(q)$.

Integrating Eq. (6.12) over Δ, one obtains:

$$P(q) = \epsilon y'(q) \int_q^1 dq' \, \exp\left(-\epsilon \int_{q_{min}}^{q'} dq'' \, (y(q'') - y(q_{min}))\right) + \delta(q-1)\exp(-\epsilon\chi) \tag{6.13}$$

It is complicated to extract the order parameter from this formula, as it depends at the same time on the derivative of $y(q)$ and on its integral function.
A simpler expression can be obtained noticing that Eq. (6.13) depends on Δ only in the combination $w = q + \Delta/\epsilon$. Integrating over Δ, q for fixed w with the condition $0 < q < w$, one finds:

$$P(w) = \theta(1-w)\,(y(w) - y(q_{min}))\,\epsilon \exp\left(-\epsilon Y(w)\right) + \delta(w-1)\exp(-\chi) \tag{6.14}$$

where

$$Y(w) \equiv \int_{-\infty}^{w} y(q) - y(q_{min})\, dq \tag{6.15}$$

Finally, integrating between w and 1 this function, the following simple expression is found:

$$Q(w) \equiv \int_w^1 P(w')\, dq \; = \exp -(\epsilon Y(w)) \tag{6.16}$$

Inverting the formula, one finds the expression for $Y(w)$:

$$Y(w) = -\frac{\log Q(w)}{\epsilon} \tag{6.17}$$

This formula shall be used for deriving $Y(w)$ from $Q(w)$, which can extracted from numerical simulations.

Before introducing the numerical approach, few more observations are needed. The first is about the expected results. Due to the lack of a general analytic solution, the order parameter at zero temperature $y(q)$ has been derived analytically only in few cases. In [49], $Y(w)$ is plotted in the cases of the SK model, where $y(q) \sim q(1-q)^{-1/2}$ in the PaT approximation [191], and the spherical model (see Fig. 6.3).
Moreover, the predictions of the analysis are valid in the assumption that the system is ultrametric. In general, a violation of the relations (6.12-6.14) should be expected if ultrametricity does not hold.

Another important observation regards the exact function which will be computed. Since the different distributions are derived by integrating over the interval $[q_{min}, 1]$, only the difference $y(q) - y(q_{min})$ can be extracted from the simulations. Moreover, due to the fluctuations present at finite-size and to the limitations imposed by the long computational times for obtaining exact ground states, we will derive the function $Y(w)$ rather than $y(q)$, as it is statistically more stable.

6.3 The models

We consider the models already defined in Chapter 4, in both the spin glass version (SG) with $J = \pm 1$, and the ferromagnetic version (RFIM):

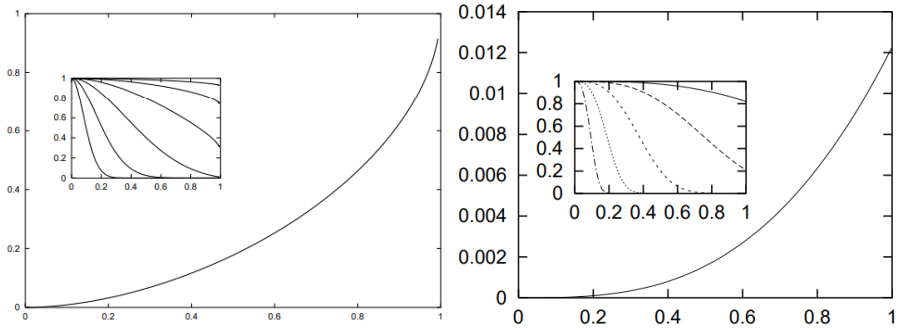

Figure 6.3. Example: $Y(w)$ function at $h = 0$ for the SK model (left) and the spherical model (right). In the insets, $Q(w)$ functions computed for several values of ϵ (reproduced from [49]).

1. Bethe lattice (BL) on random regular graphs (RRG);

2. 3-dimensional lattice with *"random regular bond dilution"* (RRBD);

We recall that each model is described by a graph of N elements in which each vertex i corresponds to a Ising spin variable σ_i and each edge (i, j) represents a pairwise interaction between the spins σ_i, σ_j. In the spin glass version, the coefficients J_{ij} of the interaction matrix are quenched, independent and identically distributed random variables sampled from the probability distribution $P(J) = \frac{1}{2}\delta(J + 1) + \frac{1}{2}\delta(J - 1)$. Moreover, in order to study the RSB transition at zero temperature, a gaussian external field h with zero mean is applied. The gaussian field is generated once for each sample with variance $\sigma_h^2 = 1$, and then is rescaled by a factor H to study the transition.

The Hamiltonian of the systems is:

$$\mathcal{H}(\sigma) = -\sum_{<i,j>} J_{ij}\sigma_i\sigma_j - \sum_{i=1}^{N} h_i\sigma_i \tag{6.18}$$

where the sum runs over the edges (i, j) of the graph.

The two models are studied in both the spin glass ($J = \pm 1$) and ferromagnetic ($J = 1$) version. In the first case, the object of the investigation is the transition from the RS to the RSB phase at the critical value of the field h_c. The second case corresponds to a random field Ising model, which undergoes a phase transition from the ferromagnetic phase to the paramagnetic phase for $H = 1$ but exhibit no RSB phase. This model is used for comparison with a system in the RS phase.

6.4 Numerical approach

The numerical approach is based on the computation of exact ground states of a large sample of spin glasses. In computational science, this task is equivalent to a hard optimization problem and requires approximated algorithms. In our case, graph-cut based algorithms are expected to be particularly effective, due to the topology of the systems.

Generating the samples. Each graph $G(N, zN)$ is described by σ, A, J, h, where:

- $\{\sigma_i\}$ is the array of the N Ising variables which need to be optimized;
- $\{A_{ik}\}$ is the $N \times z$ adjacency list, each coefficient representing an outcoming edge (i, A_{ik});
- $\{J_{ik}\}$ is the $N \times z$ coupling list associated to the matrix A_{ik};
- $\{h_i\}$, the external field, is an array of N random variables extracted from the normal distribution $\mathcal{N}(0, 1)$.

The RRG samples are generated by means of the fast algorithm [62] described in Section 4.3. The RRBD samples are generated starting from a 3D lattice with $N = L^3$ sites and no edges. Then, for each value of degree $d = 0, \ldots, z-1$, every site i with degree d_i is randomly coupled to a nearest neighbor by adding and edge (i, j), until no more sites with degree d are present. In the last step, if $d_j > z$ then one of the old edges (i, j) is replaced. The procedure continues until $d = z$ for every site. The algorithm converges in a reasonable time for $D = 3$ and for the values of L considered.

The J matrix is generated with random coefficients $J = \pm 1$ in the SG problem. The transition is driven by rescaling the external field by a factor H. The parameters used for the main analysis of the overlap distribution are reported in Table 6.1. The cases in which different values of the parameters are used for the computation of other quantities, usually on smaller samples, will be mentioned further in the data analysis. **Computation of ground states** For the computation of the ground

Random regular graph	
N	# of samples
200	100000
400	100000
800	100000
1600	10000
3200	10000
H	0.6, 0.8, 1.0, 1.2
ϵ	1.0, 2.0

Diluted 3D lattice		
L	N	# of samples
6	196	32000
8	512	16000
10	1000	8000
12	1728	4000
H	0.2, 0.4, 0.6, 0.8, 1.0, 1.2	
ϵ	1.0, 2.0	

Table 6.1. Table of the parameters used in the simulations for both the RRG and the RRBD model

states we use the CEA algorithm [144, 160] described in Section 4.2. This algorithm is based on the iterative optimization of non-frustrated subgraphs (clusters) of maximum size extracted from the system. Since in the Bethe lattice short cycles are expected to be rare for large N, frustration is expected to occur only on large scale. This suggests that large clusters can be optimized at once very rapidly utilizing min-cut techniques until a minimum is eventually reached.
The algorithm can reach deep states in a relatively short time, but it does not converge automatically to the exact ground state. For this reason, the procedure is repeated for each sample starting from for different initial random configurations

until the same state is reached 10 times. This is considered the exact ground state of the system.

The computational time depends on both the size of the systems and the rescaling factor. The algorithm converges quickly to the ground state in the RS phase (few starting conditions), and in a reasonable time for $H \lesssim H_c$. As $\mathcal{H} \to 0$ the computational time for the worst instances increases rapidly.

We observe that other efficient algorithms are used in literature for the computation of exact states, including genetic algorithms [], extreme optimization [], and BP-based algorithms []. Despite min-cut being computationally more expensive on large graphs, after an initial comparison with other techniques [ADD REF GA/EO] the CEA algorithm was found to be more efficient, possibly due to the topology of the systems.

The algorithm consists of the following steps for each element of the sample:

1. computation of the ground state σ^0 of the unperturbed system with Hamiltonian $\mathcal{H}(0)$;
2. computation of the ground state σ^ϵ of the coupled system with Hamiltonian $\mathcal{H}(\epsilon)$ for different values of ϵ;
3. extraction of $E_{gs}(0), E_{gs}(\epsilon)$, and $q = 1/N \sum_i \sigma_i^0 \sigma_i^\epsilon$;
4. computation of the quantities Δ, w:

$$\Delta = E_{GS}(\epsilon) - E_{GS}(0) - \epsilon q, \quad w = q + \Delta/\epsilon$$

Data analysis The data extracted from the simulations have been first filtered and resampled.

Data filtering: Before proceeding, data have been cleared from the *outliers* falling out of the boundaries imposed by inequalities (6.11). Samples have been discarded in two cases:

1. $\Delta < 0$
2. $w > 1$

The first case results from $\mathcal{H}_0(\sigma_\epsilon) < E_{gs}(0)$, impossible if σ_0 is the ground state of the unperturbed system. This is due to a wrong computation of σ_0. The second case results from $E_{gs}(\epsilon) > E_{gs}(0) + \epsilon$, which implies that σ_ϵ is not the ground state of the perturbed system, since there is at least one configuration (σ_0) with lower energy.
The amount of data discarded is less than the 1% of the whole sample, the number of occurrences slightly increasing in larger systems.

Resampling: A *jackknife* resampling is used for estimating the fluctuations of the extracted distributions. The jackknife is a resampling method normally used to

reduce the bias affecting the estimation of higher moments, for example in the case of distributions of variables obtained from some non-linear combination of other averages. Rather than performing a complicated analysis on the original set of data, the jackknife proceeds by averaging over a large number of random samples extracted from the original. For a single set of $\mathcal{N}$ observations, $\mathcal{N}$ samples of $\mathcal{N}-1$ elements are extracted by discarding one element per time. The moments computed over the resampled sets are unbiased.

In our case, the technique is used differently. The distributions are first computed over 1000 samples of size $\mathcal{N}/2$ obtained discarding half of the observations at random. The final results are thus obtained by averaging over the resampled distributions.

Once the data have been filtered and resampled, the order parameter has been extracted in two different ways.

METHOD 1: *Computation from the $P(w)$ distribution*

First, the distribution of the variable w $P_{H,N}(w)$ is extracted for each value of N, H (6.15-6.17). Then, $Q_{H,N}(w)$ and $Y_{H,N}(w)$ are extracted. At this step $Q_{H,N}(w)$ is expected to depend on ϵ, but $Y_{H,N}(w)$ is expected to be independent of the perturbation, if ϵ is order $O(1)$.
The asymptotic distribution $Y_H(w)$ is then computed by fitting the functions $Y_{N,H}(w)$ at fixed values of w to the asymptotic form:

$$Y_{H,N}(w) = Y_H(w) + g_H(w)N^{-\alpha} \tag{6.19}$$

with α to be evaluated from the data.

METHOD 2: *Computation from the $P(\Delta, q)$ distribution*

This method is used for checking the consistency of Eq. (6.12) and the extent of validity of the assumptions made in Section 6.2.
The relation (6.12) suggests that in the RSB phase, the $P(\Delta, q)$ depends on the product of a function of $Y(q + \Delta/\epsilon)$ and on its second derivative $y'(q)$:

$$P(\delta, q) \sim y'(q)Q(q + \Delta/\epsilon), \quad for q < 1 - \Delta/\epsilon, \Delta > 0 \tag{6.20}$$

Due to the particular form of the rhs of the equation, we consider the transformation $\Delta \to w = q - \Delta/\epsilon$:

$$P(\Delta, q)d\Delta dq \to \frac{1}{\epsilon}P(w, q)dwdq \tag{6.21}$$

The derivative of the order parameter can thus be expressed as:

$$y'(q) = \frac{P(w, q)}{\epsilon Q(w)} \tag{6.22}$$

This implies that the rhs of the equation must be constant with respect to w, at fixed q, apart from the cut-off introduced by the Θ function. Moreover, $y'(q)$ can be computed by considering the constant values taken at different q.

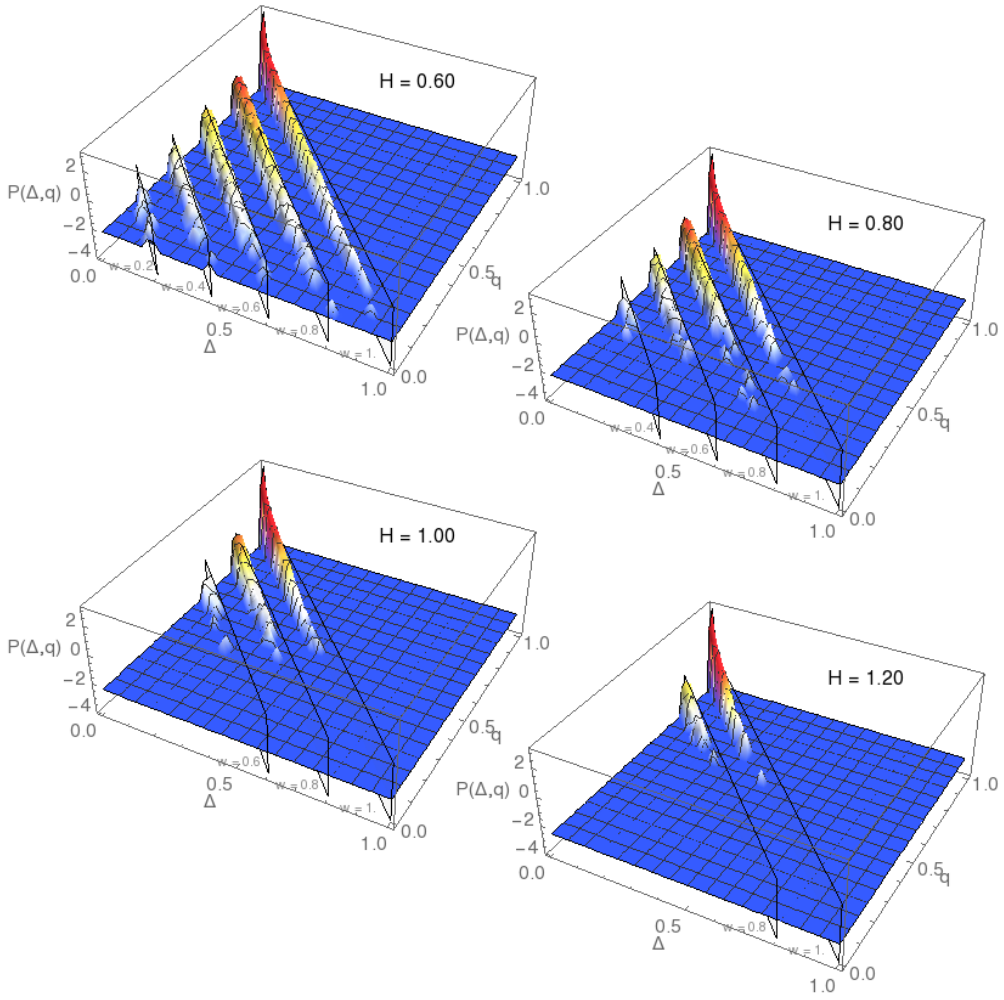

Figure 6.4. Joint distribution $P_{H,N}(\Delta, q)$ of the $N = 800$ BLSG at different values of the rescaling factor H, for $\epsilon = 1$. The data are plotted for a set of fixed values of the variable $w = q + \Delta/\epsilon$.

6.5 Results

Method 1

The distributions $P_{H,N}(\Delta, q)$ show a clear dependence on the size N and present a peak in $\Delta = 0, q = 1$ which becomes sharper as H increases (see Fig. 6.4). The functions $Y_{N,H}(w)$ are computed from the distributions $P_{N,H}(w)$ for each of the resampled datasets, and then averaged.

In the SG case, $Y_{H,N}(w)$ is a size-dependent, increasing function of w, singular in $w = 1$. The distribution is defined for positive values of q, except for small systems, where the left tail is extended to small negative values of q in the RSB phase. This is reasonable at finite size, where ultrametricity does not hold strictly. The curves show only a weak dependence on ϵ, in agreement with Eq. (6.17)), according to

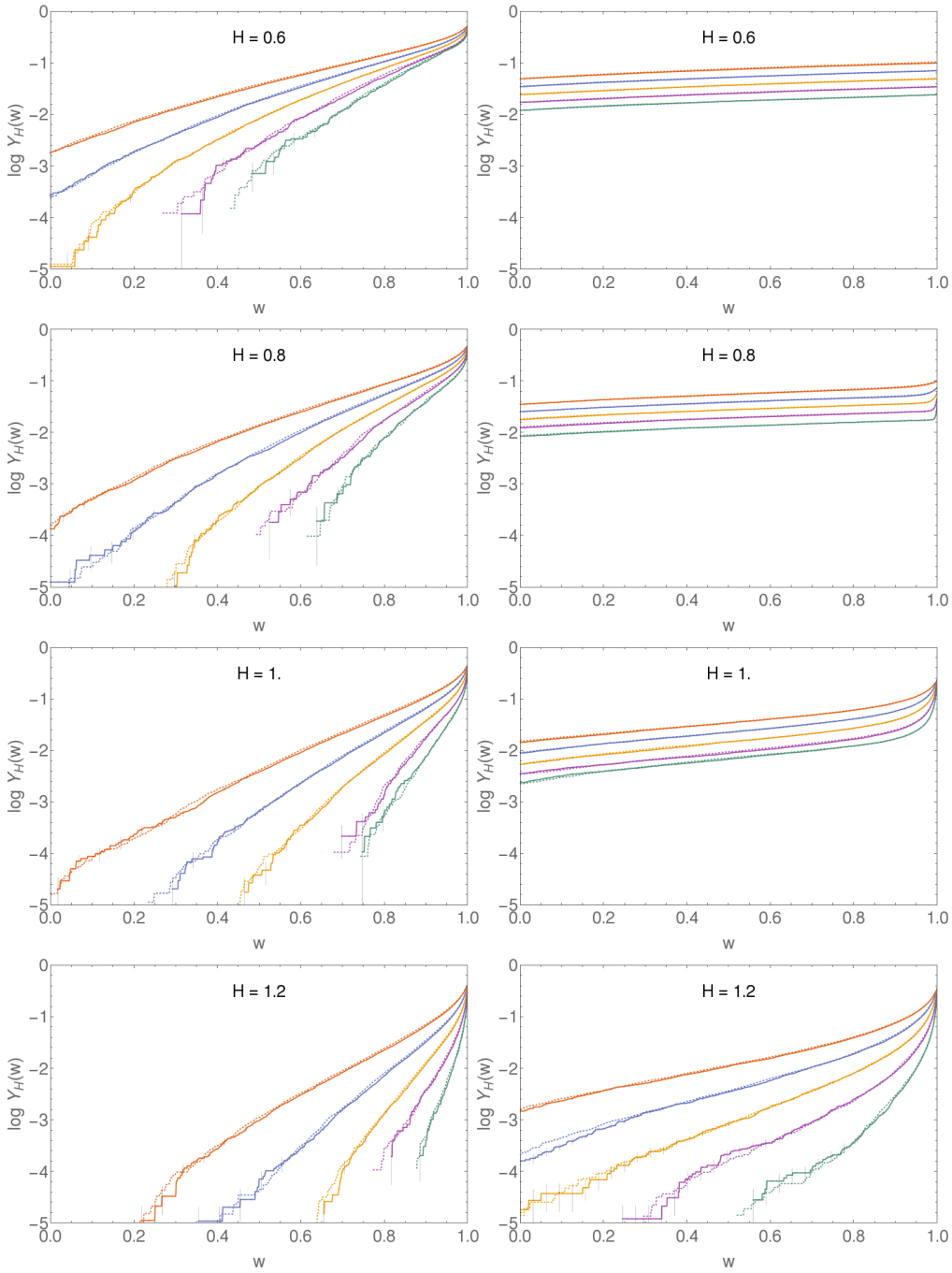

Figure 6.5. Bethe lattice overlap distribution $Y_{H,N}(w)$ in the spin glass case (SG, left column) and RFIM case (right column), at different values of the rescaling factor H. In each box, every line represent a different system size ($N = 200, 400, 800, 1600, 3200$, from top to bottom). There are no significative differences between the curves computed for $\epsilon = 1$ (solid) and $\epsilon = 2$ (dashed).

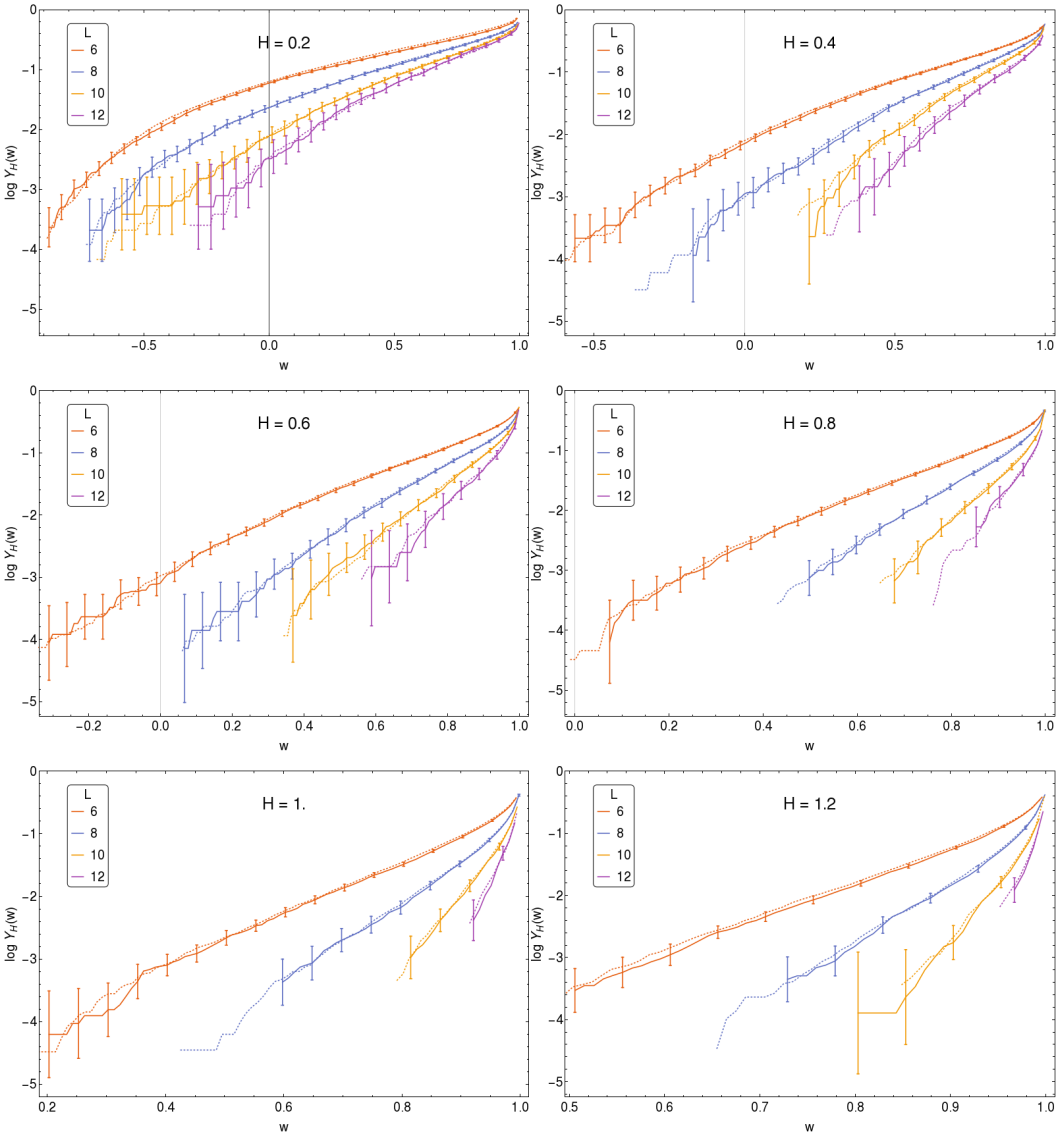

Figure 6.6. Overlap distribution $Y_{H,N}(w)$ of the RRBD model in the spin glass case (SG, left column) and in the RFIM case (right column), for different values of the rescaling factor H. In each box, every line represent a different system size ($L = 6, 8, 10, 12$, from top to bottom). There are no significative differences between the curves computed for $\epsilon = 1$ (solid) and $\epsilon = 2$ (dashed).

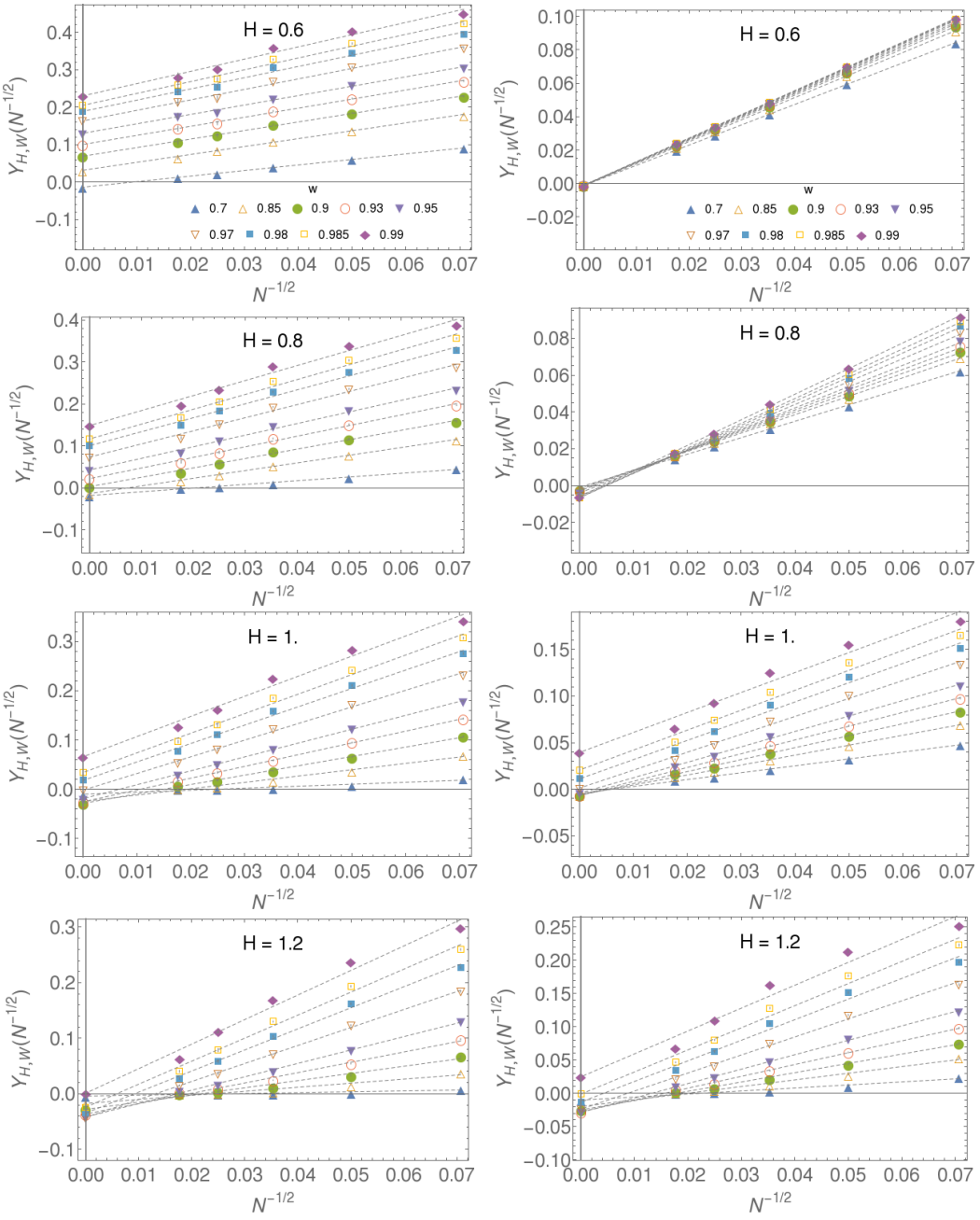

Figure 6.7. Best fit and extrapolation of $Y_H(w)$ for the Bethe lattice, in the SG (left column) and RFIM case (right column). The curves are plotted at fixed values of w versus $N^{-1/2}$, and fitted to the form ((6.23)). The quality of the fit decreases for $w \to 1$. The lines with negative y-intercept are assumed to scale exponentially and extrapolate to $Y_H(w) = 0$.

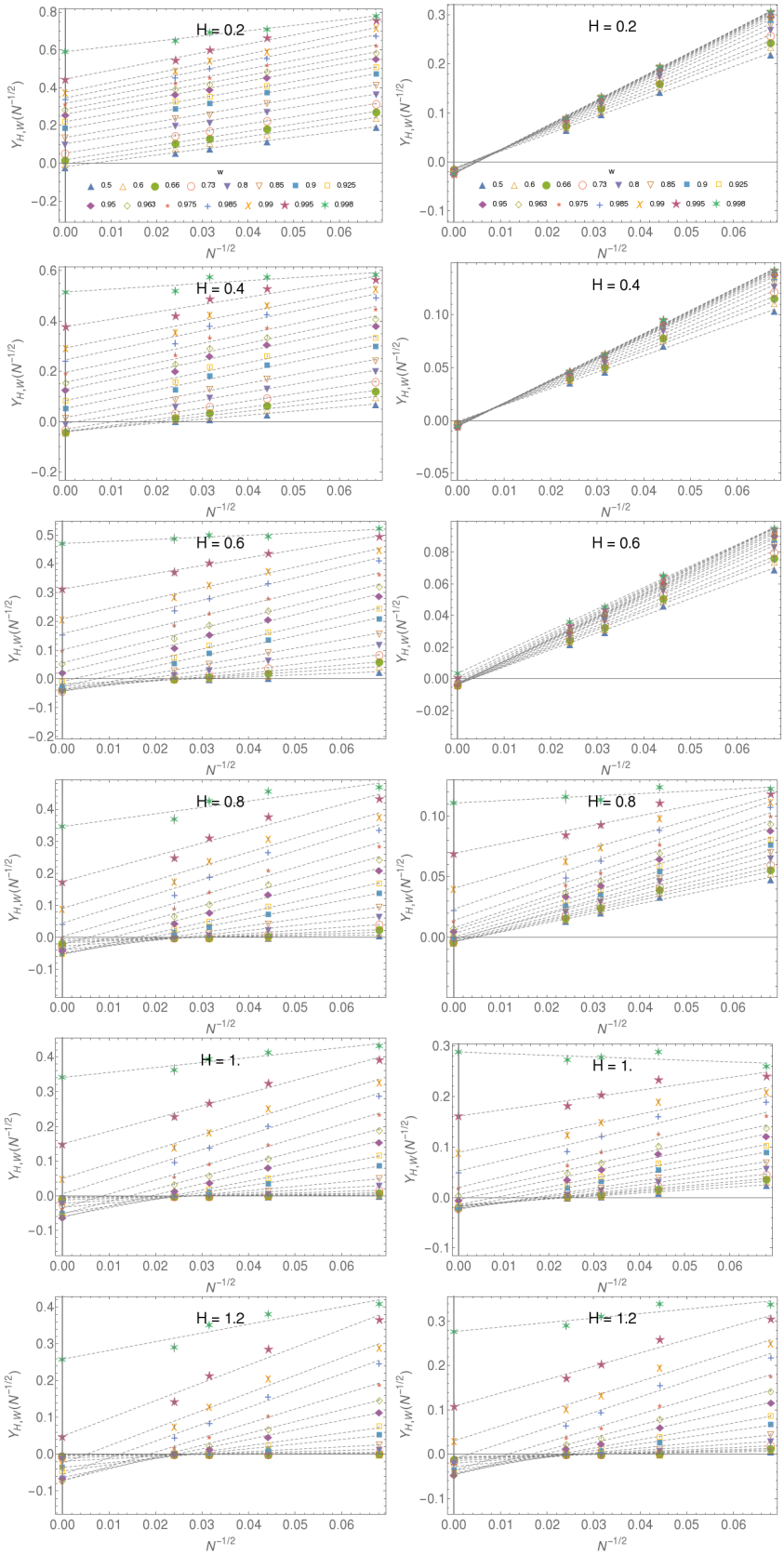

Figure 6.8. Best fit and extrapolation of $Y_H(w)$ for the RRBD model, in the SG (left column) and RFIM case (right column). The curves are plotted at fixed values of w versus $N^{-1/2}$, and fitted to the form ((6.23)).

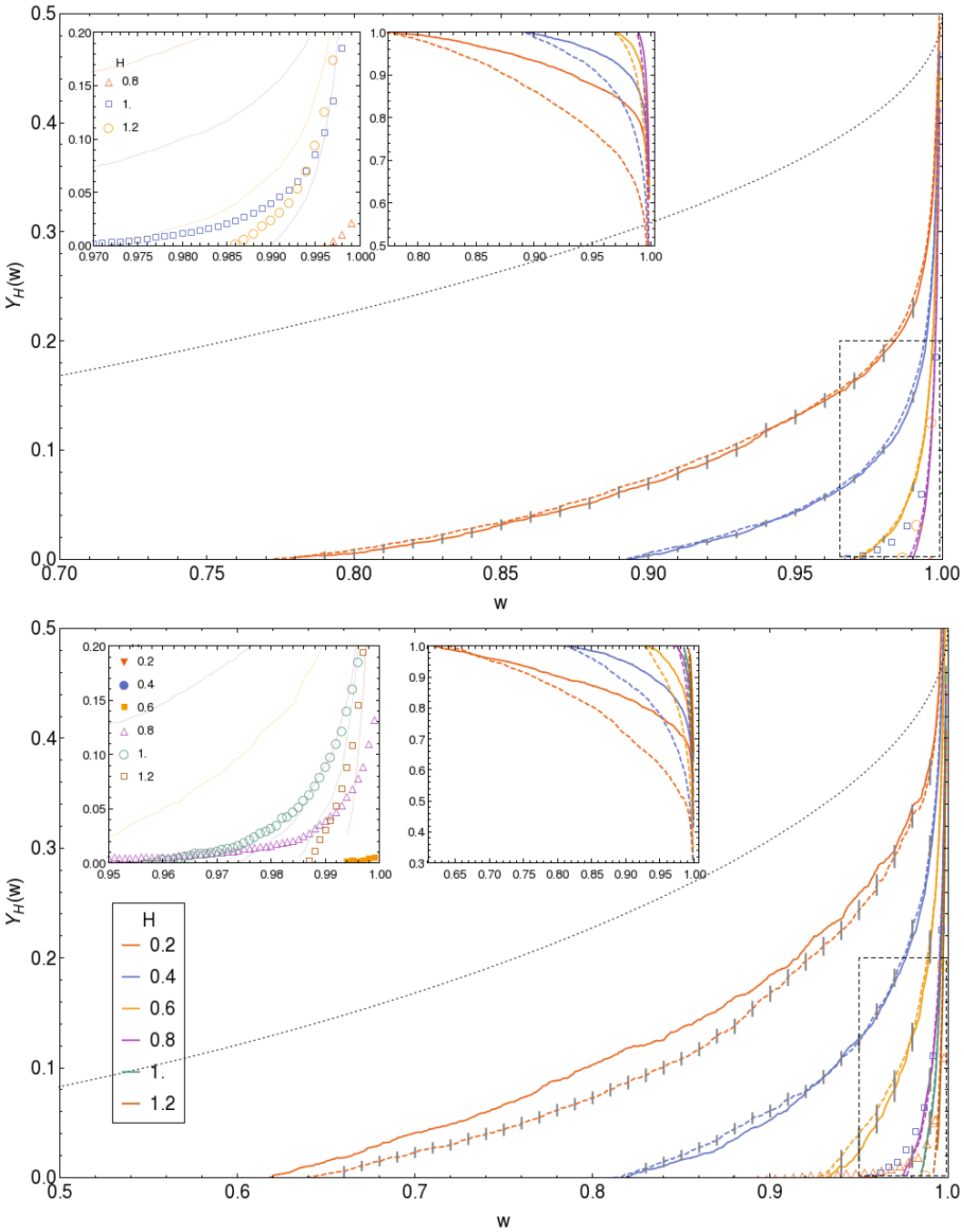

Figure 6.9. Asymptotic functions $Y_H(w)$ derived for the Bethe lattice (top) and for the RRBD model (bottom), in the spin glass case (lines) and in the RFIM case (markers). The curves are plotted for different values of H and ϵ ($\epsilon = 1$ (solid lines) and $\epsilon = 2$ (dashed lines)). The dotted isolated line represents the $Y(w)$ function of the SK model calculated at $H = 0$ (PaT approximation). In each figure, the left inset shows a zoom on the small dashed region, where the RFIM points are concentrated. In the right inset, the $Q_H(w)$ distributions are plotted for increasing values of H (from bottom to top), and different values of ϵ (solid and dashed lines). It is evident that $Y(w)$ does not depend on ϵ, differently from $Q(w)$.

which $Y(w)$ must not depend on ϵ if the perturbation is of order $O(1)$.

We are interested in the asymptotic value of $Y_{H,N}(w)$ in the $N \to \infty$ limit. For this purpose, we extracted the *section* of the distributions at fixed w as a function of N, and fitted the curves to the scaling form:

$$Y(N, w) = Y(w) + g(w)N^{-\alpha} \tag{6.23}$$

Using an exponent $\alpha = 0.5$, the fitted curves are in good agreement with the data in the region not too close to the singularity ($w \lesssim 0.98$) for $\alpha = 0.5$ (see Fig. 6.7).

The results show that below a critical value $w_c = w_c(H)$, the asymptotic value $Y_H(w)$ corresponding to the y-intercept of the regression line is negative. We assumed that for $w < w_c(H)$ the functions scale exponentially. These values are discarded, since they involve non-physical values for the order parameter, and are set to zero.

The asymptotic values obtained for $w > w_c$ were used to plot the $Y_H(w)$. We comment separately the results for the SG and the RFIM models shown in Fig. 6.7 - 6.9:

Spin glass model : In the RRG, the critical value $w_c(H) \to 1$ as $H \to H_c = 1.037$, and the $Y(w)$ are increasing functions, singular in $w = 1$. For $H \gtrsim 1$, $Y_H(w) = \delta(w - 1)$, apart from a small discrepancy due to the non perfect fit to the form 6.23.
These results agree with the RSB scenario: the zero-temperature order parameter is trivial for $H > H_c$ (RS phase) and it becomes continuous in the interval $[w_c(H), 1]$ upon a RSB transition, in the region where the RS solution becomes unstable.

We observed similar behavior in the RRBD model, where $Y_H(w)$ was derived up to a value of $H = 0.2$. For small values of the field, the computational time is longer, especially in the diluted lattice where the density of short cycles is higher and the higher frustration prevents from finding the exact ground state. In this case, we used smaller samples, and the results are less precise. Moreover, we do not know exactly the value of H_C for this model. Looking at the results, we could assume that the transition happens near $H_C \sim 0.8$, since this is the value were $Y_H(w) \sim \delta(w - 1)$.

Ferromagnetic model : For the RFIM in the ferromagnetic phase ($H < 1$), we extrapolate an asymptotic value for the order parameter $Y_H(w) = \delta(w - 1)$. The peak in this region is very sharp, as all the regression lines converge to 0. In the paramagnetic phase, the function is smoother, but it can still be considered a delta function.
These results confirm the assumption that $Y_H(w)$ is trivial in the RS phase, and that the SG and the RFIM order parameters are similar in the RS phase.

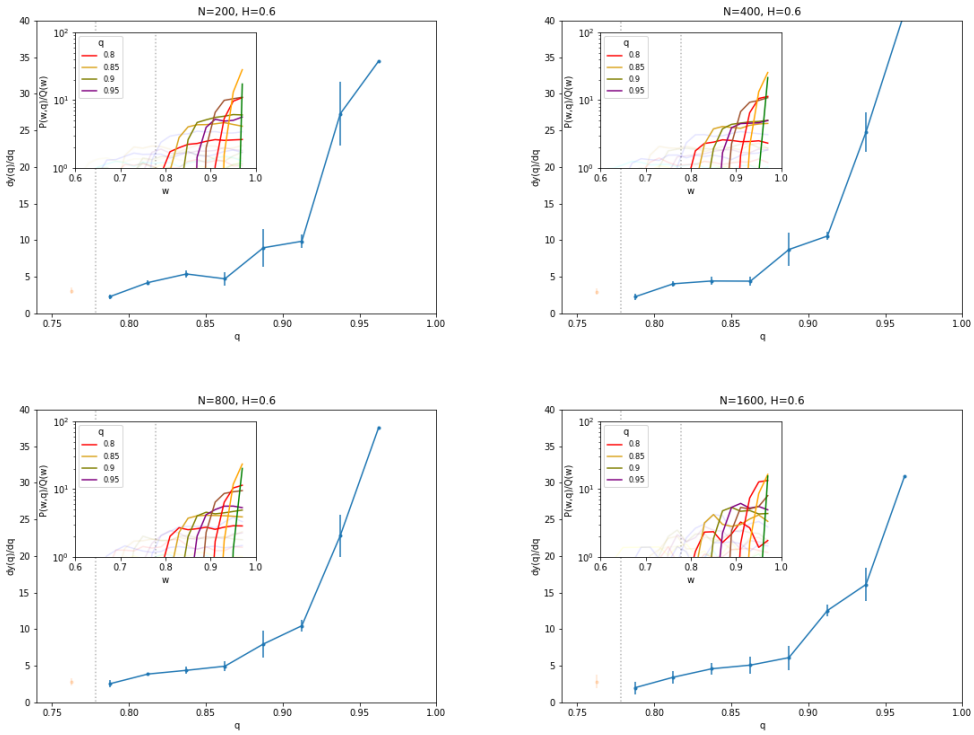

Figure 6.10. Alternative derivation of the order parameter (Method 2) in the BL spin glass ($H = 0.6$). In the main diagram: $y'(q) = \frac{P(w,q)}{\epsilon Q(w)}$ for $q \in [w_c, 1]$. In the inset: plot of $\frac{P(w,q)}{\epsilon Q(w)}$ vs w at fixed q. The curves present an immediate plateau after an initial step due to the constraints on the variables w, q.

Method 2

In order to test the consistency of the approach, the ratio $R_q(w) = P_{N,H}(w,q)/Q_{N,H}(w)$ is plotted at fixed values of q. If Eq. (6.12) is correct, this function is expected to be constant (apart from the effects of the step function), being a function of q only, Moreover, this function corresponds to the derivative of the order parameter according to formula (6.22).

The results for the RRG at $H = 0.6$ are shown in Fig. 6.10. Each curve $R_q(w)$ is plotted by fixing selecting only a small fraction of the data in the interval $[q, q + dq]$, therefore the distributions present higher fluctuations. Still, the function $y'(q)$ can be estimated by considering the average value of the plateau for each value of q (see Fig. 6.10).

In order to compare these results to the previous ones, $y'(q)$ was integrated twice to produce the $Y(w)$ distribution. The results, shown in Fig. 6.11 only for the Bethe lattice at $H = 0.6$, are in good agreement with the $Y_{N,H}(w)$ computed with the first method, apart from a factor $\sim 1/3$. Due to the minor precision of the method, we consider this result acceptable, and in agreement with the expectations.

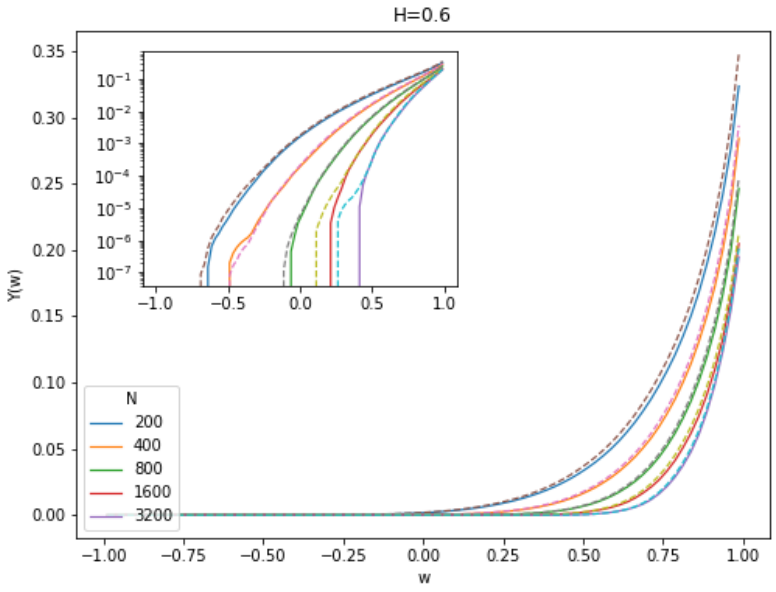

Figure 6.11. $Y_{N,H}(w)$ of the Bethe lattice spin glass model at $H = 0.6$ for $\epsilon = 1$ (solid lines) and $\epsilon = 2$(dashed lines), computed with the second method. The functions are similar to the ones computed with the first method, apart from a rescaling factor ~ 0.3

6.6 Conclusions

The $Y(w)$ distribution, defined as the integral function of the zero-temperature order parameter of the RSB transition, was derived numerically for the Bethe lattice spin glass and for the diluted lattice with fixed connectivity in $d = 3$. The distributions were computed near the critical field h_c, and the results are consistent with the RSB description, which prescribes that $Y(w)$ should be continuous in the interval $[w_c, 1]$ at zero temperature.

In the Bethe lattice, where the RS solution becomes unstable at $H = H_C$, $Y(w)$ is a continuous function in the RSB phase, and tends to a delta function $\delta(w - w_C)$ for $H \to H_C$. In the second case, where H_C is not known *a priori*, the critical field is approximately $H \sim 0.8$, but the method is not precise enough to determine the exact value. We compared the spin glass model and the random field Ising model in the RS phase, observing a similar behavior in the two models. $Y(w)$ is a sharp δ in the ferromagnetic case and behaves similarly to the spin glass model in the paramagnetic phase, where the random field is expected to be dominant.

Finally, we checked the consistency of the whole approach by deriving $Y(w)$ with an alternative method. These results present a similar behavior but a little numerical discrepancy with the previous ones. Nevertheless, given the lack of precision due to the less significant statistical sample, the results prove the consistency of the approach and the validity of the theoretical assumptions.

In this respect, we remark that the whole approach relies on the assumption of ultrametric space of configurations. In [49], a violation of the scaling form of $Y(w)$,

is observed for large values of the perturbation, in systems where ultrametricity does not hold. The fact that in our simulations $Y(w)$ does not depend on ϵ, seems to confirm that ultrametricity holds in the BLSG. A comparison of our results with a future analytic derivation of $y(q)$ might provide information on possible deviations from the full RSB description in our model.

The method could be extended to larger systems and higher connectivity. However, there is a computational limit set by the increasing algorithmic complexity with the coordination number. Despite the CEA algorithm being particularly effective on systems with tree-like topology, the number of starting conditions needed for obtaining the exact ground states grows quickly with the size of the systems, and the algorithm is not reliable for $N > 3200$. The performance is expected to be worse for higher connectivity, as short cycles are more frequent. Nevertheless, more efficient algorithms for the computation of spin glass ground states could improve the effectiveness of this method.

Chapter 7

Conclusions

Three aspects concerning the ground states of finite-dimensional models have been considered in this thesis, for the $J\pm$ Bethe lattice spin glass with $z = 3$, and the $J\pm$ EA diluted model with bond dilution and $d = 3$:

Spin glass order parameter The distributions of the overlap have been derived from the energy landscape low-lying excitations. The results for the BL model are consistent with the mean-field description, and a transition to the RSB phase is observed at $H \sim 1$. Even more interesting is that the same kind of transition is observed in the RRBD model at $H \sim 0.8$. Also in this case, for $H < 0.8$ the $Y(w)$ distribution is continuous and it can be assumed that the system undergoes an RSB transition. Moreover, the consistency of the Franz-Parisi formula which relates the order parameter and the experimental distributions have been proved in our model.

Finite-size corrections to the energy The finite-size corrections to the average ground state energy density have been computed in the range $0 \leq H < 2$. The results at $H = 0$ are consistent with the 1RSB theory in the case of the Bethe lattice, and in general they are consistent with results found in other works. The results at $H > 0$ present higher exponents with respect to the first-order corrections and higher-order corrections should probably be considered.

Ultrametricity The presence of ultrametricity has been studied by considering the overlap between triplets of degenerate ground states at zero temperature. Triangular inequalities are excluded, but a certain violation of ultrametricity is observed, probably due to the finite-size effects. Also, it is not granted that the CEA algorithm samples the degenerate ground states with the correct Boltzmann distribution.

This work opens perspectives about future developments. In the first place, deriving the overlap distribution is a powerful tool to detect hints of RSB scenario in a system, and a more extended analysis of finite-dimensional models needs to be implemented. A possible course of action might consist in determining first the transition point for the RRBD, then running a systematic analysis for

$H \to 0$. Moreover, it would be interesting to extend the whole analysis to the finite temperature regime, in higher dimension $d = 4$, and higher connectivity $z > 3$.

For the finite-size corrections, only the first-order corrections to the energy were computed. An attempt was made to compute the corrections to the susceptibility by measuring the size of the excitations caused by 1-flip perturbations, but the results were too noisy to derive the corrections. Thus, an interesting development would be the computation of the finite-size corrections to the susceptivity and the fluctuations of the ground state energy.

Appendices

Appendix A

Random free energies

In this section we give a justification for the assumption of random free energies made in section 2.1.4, by following the arguments of Mezard and Virasoro presented in Ref. [5].

Let us define the *free energy of a pure state* in such a way that:

$$P_\alpha = \frac{e^{-\beta f_\alpha}}{\sum_\gamma e^{-\beta f_\gamma}} \tag{A.1}$$

Our purpose is to explore the consequences of assumin that the free energies of the pure states are random variables drawn from the probability distribution:

$$\mathcal{P}_\rho(f_\alpha) = \rho \exp \rho(f_\alpha - f_c)\theta(f_c - f_\alpha) \tag{A.2}$$

where f_c is a cut-off, $\rho = \rho(\beta, H) = \beta(1-y)$ (y is the right plateau in the $q(x)$ function). This is a very important point, since it allows a derivation of the RSB solution from probabilistic arguments.

Pure states. Let us consider M states with free energies distributed as $\mathcal{P}_\rho(f_\alpha)$. The moments M_k can be computed as follows:

$$\begin{aligned}
M_k = \quad & \overline{\textstyle\sum_\alpha P_\alpha^k} = \textstyle\int \prod_{\alpha=1}^M d\mathcal{P}(f^\alpha) \sum_{\alpha=1}^M (\frac{e^{-\beta f_\alpha}}{\sum_\gamma e^{-\beta f_\gamma}})^k = \\
& = M \textstyle\int \prod_{\alpha=1}^M d\mathcal{P}(f^\alpha) \frac{e^{-\beta k f_1 \alpha}}{(\sum_\gamma e^{-\beta f_\gamma})^k} \\
Z^{-k} = \quad & (\textstyle\sum_\gamma e^- \beta f_\gamma)^{-k} = \frac{1}{\Gamma(k)} \int_0^\infty d\lambda \lambda \grave{\imath}^{k-1} e^{-\lambda Z} \\
M_k = \quad & M \textstyle\int_0^\infty d\lambda \frac{\lambda k-1}{\Gamma(k)} \int d\mathcal{P}(f_1) e^{-\beta k f_1 - \lambda e^{-\beta f_1}} \times \\
& \times \textstyle\int d\mathcal{P}(f_2) e^{-\lambda e^{-\beta f_2}} \int ... \int d\mathcal{P}(f_M) e^{-\lambda e^{-\beta f_M}} = \\
& = M \textstyle\int_0^\infty d\lambda \frac{\lambda k-1}{\Gamma(k)} \underbrace{\int d\mathcal{P}(f) e^{-\beta k f - \lambda e^{-\beta f}}}_{g(\lambda,k)} (\underbrace{\int d\mathcal{P}(f) e^{-\lambda e^{-\beta f}}}_{g(\lambda,0)})^{M-1} = \\
& = M \textstyle\int_0^\infty d\lambda \, \Gamma(k)^{-1} \, \lambda^{k-1} \, g(\lambda, k) \, g(\lambda, 0)^{M-1}
\end{aligned} \tag{A.3}$$

The cut-off f_c in $\mathcal{P}_\rho(f)$ and the number of pure states M should be sent to infinity by keeping the density of levels at given free-energy fixed:

$$M \to \infty, \quad f_c \to \infty, \quad v = M e^{-\rho f_c} = \text{const.} \tag{A.4}$$

Computing the functions $g(\lambda, k),\ g(\lambda, 0)^M$ in this limit, one finds:

$$M_k = \frac{\Gamma(k - \rho/\beta)}{\Gamma(k)\Gamma(1 - \rho/\beta)} \tag{A.5}$$

This is exactly the result found with the replica computation for the $k - th$ moment of $f_J(W, y)$ identifying $y = 1 - \rho/\beta$. The inclusive distribution $f^{(k)}(P_1, ..., P_k)$ is found in the same way.

Clusters of pure states. The results can be generalized to the probability distribution of cluster of states. Because of ultrametricity, given a scale of length q, the pure states can be grouped in clusters I such that:

$$W_I = \frac{e^{-\beta f_I}}{\sum_K e^{-\beta f_K}}$$

where the f_I represents the free energy of the I cluster. Again we assume that these variables are distributed exponentially, but with a parameter $\rho(q) = \beta(1 - y(q))$:

$$\mathcal{P}_{\rho(q)}(f_\alpha) = \rho(q) e^{\rho(q)(f_\alpha - f_c)} \theta(f_c - f_\alpha) \tag{A.6}$$

Considering one cluster at scale q_1 and its M subclusters at scale $q_2 > q_1$, the distribution of the free energies $f_1, ..., f_M$ is:

$$\mathcal{P}_{q_1,q_2}(f_1, ..., f_M) \propto \prod_{\alpha=1}^{M} \mathcal{P}_{\rho(q_2)}(f_\alpha) \left(\sum_{\alpha=1}^{M} e^{-\beta f_\alpha} \right)^{\frac{\rho(q_1)}{\beta}} \tag{A.7}$$

The relation can be generalized to n scales of clusters. From the exclusive distribution $f^E(P_1, ..., P_M)$ it is possible to obtain the $\Pi(Y)$ distribution, deriving the same results found in the previous sections.

Appendix B

Joint probability distribution of the energy gaps

In this section we present the detailed calculation of the joint probability distribution of the energy gaps for a *full*-RSB system (see Section 6.2), following the derivation presented in [49].

The ultrametric organization of k-RSB systems can be naturally represented in terms of the branching process of a tree. We consider a rooted tree of depth k (see Section 1.1) whose leaves represent the pure states of the system and whose intermediate vertexes represent cluster of states. In the $T = 0$ case, the leaves at the last level represent minima of the energy landscape.
Each level of the tree,starting from the root at $l = 0$, is assigned a scale q_l. These parameters are defined in the interval $[0, 1]$ and are chosen in increasing order $0 \leq q_0 < \ldots < q_k = 1$. The portion of the tree which stems from a node at level l is denoted *l-cluster*. States which belong to the same l-cluster but in different $l+1$-clusters have the same mutual overlap $q = q_l$.

The tree is generated following a Derrida-Ruelle branching process[5, 66, 84, 85, 166, 194]. At each level, the l-clusters are assigned a *generalized energy* $\tilde{E}^l$, which at the last level corresponds to the real energy of the minima $\tilde{E}^k = E$. The root is assigned a sample-dependent reference energy $\tilde{E}^0$. Starting from the root, the branches of every node are generated via a Poisson point process. The number of different $l+1$-clusters with energy in the interval $(\tilde{E}^{l+1}, E^{l+1} + d\tilde{E}^{l+1})$ contained in a l-cluster of energy $\tilde{E}^l$ (corresponding to the fraction of branches with energy in the specified interval stemming from the same node), is a Poisson variable with expected value:

$$d\mathcal{N}^{l+1}(\tilde{E}^{l+1}) = p_l(\tilde{E}^{l+1}|\tilde{E}^l)d\tilde{E}^{l+1} = e^{y_l(\tilde{E}^{l+1}-\tilde{E}^l)}d\tilde{E}^{l+1} \tag{B.1}$$

The tree depends on the parameters q_l only through the coefficients $y_l = y(q_l)$, where $y(q)$ is an increasing function defined in the interval $[0, 1]$ corresponding to the overlap distribution at zero temperature defined in Section (6.15).

Let us consider the l-cluster which contains the ground state of the system with energy E_{gs}. We consider, among all the states that belong to the same l-cluster but are in a different $l+1$-cluster, the one with minimum energy. This state is defined *first l-excited state* and has energy $E_{gs} + \Delta_l$.

In the following sections we show how to derive the joint probability distribution of the energy gaps $P(\Delta_0, \dots, \Delta_{k-1})$ following a pure probabilistic computation based on the properties of the tree.

1RSB

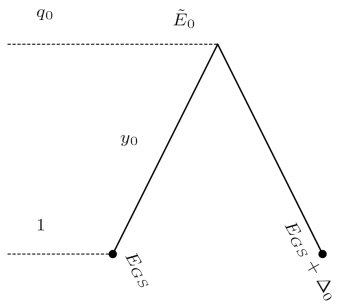

In the 1RSB phase, only two values of overlap are allowed at zero temperature: $q_0, 1$. All the minima of the system belong to the same 0-cluster and have overlap q_0. The average number of configurations with energy in the interval $(E, E + dE)$ is:

$$d\mathcal{N}^1(E) = \nu_0(E|\tilde{E}^0)dE = e^{y_0(E-\tilde{E}^0)}dE \tag{B.2}$$

We remark that in our description configurations which differ for a number finite number of spin, are identified in the thermodynamic limit.

The probability that $E = E_{gs}$ is the ground state energy follows the extreme values distribution of the minima, given by the Gumbel law [181]:

$$\mu_0(E_{gs}|\tilde{E}^0) = e^{y_0(E_{gs}-\tilde{E}^0)}e^{-A_0 e^{y_0(E_{gs}-\tilde{E}^0)}} \tag{B.3}$$

where $A_0 = y_0^{-1}$. The joint probability to have a ground state energy E_{gs} and a first 0-excited state of energy E_1 corresponds to the event to have a ground state of energy E_{gs} and no configurations in the interval (E_{gs}, E_1):

$$P_1(E_{gs}, E_1|\tilde{E}^0) = \nu_1(E_{gs}|\tilde{E}^0)\mu_1(E_1|\tilde{E}^0) = e^{y_0(E_{gs}-\tilde{E}^0)}e^{y_0(E_1-\tilde{E}^0)}e^{-y_0^{-1}e^{y_0(E_1-\tilde{E}^0)}} \tag{B.4}$$

Defining $\Delta_0 = E_1 - E - 0$ and integrating over E_{gs}, E_1, one finds the probability distribution of the energy gap:

$$P(\Delta_0) = \frac{1}{y_1}e^{-y_1\Delta_0} \tag{B.5}$$

k-RSB

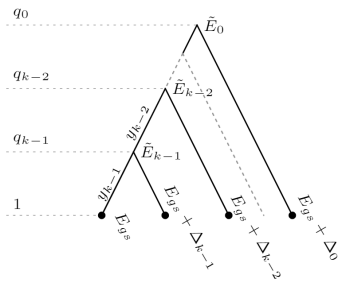

In the k-RSB phase, the joint probability of the energy gaps is derived by iteration, starting from the last levels. Let us consider the set of $l+1$-clusters branching from the same l-cluster. We proceed by induction assuming that Eq. (B.3) holds at the level $l+1$ and proving that it holds at level l:

$$\mu_{l+1}(E|\tilde{E}^{l+1}) = e^{y_{l+1}(E-\tilde{E}^{l+1})}e^{A_{l+1}e^{y_{l+1}(E-\tilde{E}^{l+1})}} \tag{B.6}$$

This represents the probability to have a ground state of an $l+1$-cluster ($l+1$-*ground state*) with energy E. The probability to find an

$l+1$-ground state with energy E in an l-cluster with energy $\tilde{E}^l$ is:

$$\begin{aligned}\nu_l(E|\tilde{E}^l) &= \int d\mathcal{N}^{l+1}(E^{l+1})\ \mu_{l+1}(E|\tilde{E}^{l+1}) = \\ &= \int d\tilde{E}^{l+1} p_l(\tilde{E}^{l+1}|\tilde{E}^l)\mu_{l+1}(E|\tilde{E}^{l+1}) = \\ &= const \times e^{y_l(E-\tilde{E}_l)}\end{aligned} \tag{B.7}$$

Following the asme reasoning as in the 1RSB case, the probability of an l-ground state of energy E is:

$$\mu_l(E|\tilde{E}^l) = e^{y_l(E-\tilde{E}^l)} e^{A_l e^{y_l(E-\tilde{E}^l)}} \tag{B.8}$$

The joint probability of finding a ground state energy E_{gs} and l-excited states with energy gaps $\Delta_0, ..., \Delta_{k-1}$ with respect to fixed values of $\tilde{E}^0, \ldots, \tilde{E}^{k-1}$ is:

$$\begin{aligned}P_k(&E_{gs},E_{gs}+\Delta_{k-1}, ..., E_{gs}+\Delta_0|\tilde{E}^{k-1}, ..., \tilde{E}^0) = \\ &=\nu_{k-1}(E_{gs}|\tilde{E}^{k-1})\mu_{k-1}(E_{gs}+\Delta_{k-1}|\tilde{E}_{k-1}) \times ... \times \mu_0(E_{gs}+\Delta_0|\tilde{E}_0) = \\ &=\nu_{k-1}k(E_{gs}|\tilde{E}^{k-1}) \prod_{l=0}^{k-1} \mu_l(E_{gs}+\Delta_l|\tilde{E}^l)\end{aligned} \tag{B.9}$$

Marginalizing this conditional probability with respect to $\tilde{E}_1, \ldots, \tilde{E}_{k-1}$ one finds:

$$\begin{aligned}&P_k(E_{gs}, E_{gs}+\Delta_{k-1}, ..., E_{gs}+\Delta_0|\tilde{E}_0) = \\ &= \int \left(\prod_{l=0}^{k-2} p_l(\tilde{E}^{l+1}|\tilde{E}^l)\mu_l(E_{gs}+\Delta_l|E^l)d\tilde{E}^{l+1} \right) \nu_{k-1}(E_{gs}|\tilde{E}^{k-1})\mu_{k-1}(E_{gs}+\Delta_{k-1}|\tilde{E}^{k-1}) = \\ &= \int \left(\prod_{l=0}^{k-2} d\tilde{E}^{l+1} \right) e^{y_0(\tilde{E}^1-\tilde{E}^0)} e^{y_1(\tilde{E}^2-\tilde{E}^1)} \ldots e^{y_0(\tilde{E}^{k-1}-\tilde{E}^{k-2})} \times \\ &\quad \times \mu_0(E_{gs}+\Delta_0|\tilde{E}^1) \ldots \mu_{k-1}(E_{gs}+\Delta_{k-1}\tilde{E}^{k-1})\nu_{k-1}(E_{gs}|\tilde{E}^{k-1}) = \\ &= \prod_{l=2}^{k} \left(\Delta y_l e^{-\Delta y_l \Delta_l} \right) \nu_1(E_{gs}|E_0)\mu_1(E_{gs}+\Delta_1|E_0)\end{aligned} \tag{B.10}$$

In order to solve the formula let us just consider the last integration:

$$\begin{aligned}\int \tilde{d}E^{k-1} e^{y_{k-2}(E_{k-1}-E_{k-2})} \mu_{k-1}(E_{gs}+\Delta_{k-1}\tilde{E}_{k-1})\nu_{k-1}(E_{gs}|\tilde{E}_{k-1}) = \\ = (y_{k-1}-y_{k-2}) e^{(y_{k-1}-y_{k-2})\Delta_{k-1}} \nu_{k-1}(E_{gs}|\tilde{E}_{k-1})\end{aligned} \tag{B.11}$$

Integrating telescopically over the rest of the variables $d\tilde{E}^1 ... d\tilde{E}^{k-2}$ one obtains:

$$P_k(E_{gs}, E_{gs}+\Delta_{k-1}, ..., E_{gs}+\Delta_0|\tilde{E}_0) = \prod_{l=1}^{k-1} \left(\Delta y_k e^{-\Delta y_k \Delta_k} \right) \mu_0(E_{gs}+\Delta_0|\tilde{E}^0)\nu_0(E_{gs}|\tilde{E}^0) \tag{B.12}$$

where $\Delta y_l \equiv y_l - y_{l-1}$.
The final formula is found by integrating over E_{gs}:

$$P(\Delta_0, ..., \Delta_{k-1}) = \prod_{l=0}^{k-1} e^{-\Delta_l \Delta y_l} \Delta y_l \tag{B.13}$$

full RSB

Finally we consider a tree of infinite depth for describing *full* RSB system. In the limit of continuous branching the discrete parameters become continuous functions of the variable q in the interval $[q_{min}, 1]$: $\Delta_l \to \Delta(q),\ y_l \to y(q),\ \Delta y_l \to y'(q)dy$. Differently from the original derivation in [49], where $q_{min} = 0$ due to the zero magnetic, we assume here that $y(q)$ is null for $q < q_m in$ and that if $y_0 \to y(q_{min}) \neq 0$ then $y'(q_{min}) = y(q_{min})\delta(q - q_{min})$. Under these assumptions, the joint probability distribution is:

$$P(\{\Delta\}) = e^{-\int_{q_{min}}^{1} dq\, y'(q)\Delta(q)} \prod_{q=q_{min}}^{1} y'(q)dq \tag{B.14}$$

Appendix C

Maximum-Flow and Minimum-Cut

Minimum cut. The computation of the exact ground states of a spin glass is a hard optimization problem, mostly due to the presence of a certain degree of frustration. On the other hand, in systems with unfrustrated interactions, a solution can be found in polynomial time by means of *graph cut* methods[12].

In graph theory, a cut $C = (S, T)$ is partition of the nodes set $\mathcal{V}$ of a graph $G = (\mathcal{V}, \mathcal{E})$ into two subsets S, T. The *cut-set* of C is the set of edges that are *crossed* by the cut. The *cost* of a cut is either the cardinality of the cut-set (the number of broken edges) in unweighted graphs, or the sum of the weights of the cut-set in weighted graphs. The MIN-CUT problem consists in finding the cut with minimum cost. In the case of an Ising spin glass with J_{ij} coupling interactions, the cost is the energy which must be spent to assign to any spin an up or down state. In general not every energy functional can be minimized by using this method. In order to prove the equivalence between Ising spins energy minimization and graph cut methods there must be an equivalence also between the energy functionals.

Equivalence between spin glass problem and MIN-CUT Let us consider a model on a graph $G_{\mathcal{V},\mathcal{E}}$ with boolean variables $s = 0, 1$ The total energy of the system is:

$$E_{tot} = \sum_{i \in \mathcal{V}} D_i(s_i) + \sum_{(i,j) \in \mathcal{E}} V_{ij}(s_i, s_j) \tag{C.1}$$

The graph cut method moves towards the ground state only if the functional V is *regular*:

$$V_{ij}(0,0) + V_{ij}(1,1) \leq V_{ij}(1,0) + V_{ij}(0,1) \tag{C.2}$$

Applying a transformation $s_i = 2\sigma_i - 1$, it can be proved that the Hamiltonian of a magnetic system satisfies the regularity condition as long as all J_ij are positive.

In the spin glass case, the condition (C.2) is satisfied only locally upon a local gauge transformation $J_{ij}\sigma_i \to J'_{ij}\sigma'_i$. This condition is the core of the CEA algorithm used throughout the thesis.

In spin glasses, the graph cut problem consists in partitioning the spins two sets *spin-up* V_+ and *spin-down* V_-. Let us denote by $\Delta \subset \mathcal{E}$ the cut-set and by Γ_+ (Γ_-) the set of edges with both end points in V_+ (V_-). The Hamiltonian can thus be

decomposed as:

$$\begin{aligned} H &= -\sum_{(i,j)\in\Gamma_+} J_{ij}\sigma_i\sigma_j - \sum_{(i,j)\in\Gamma_-} J_{ij}\sigma_i\sigma_j - \sum_{(i,j)\in\Delta} J_{ij}\sigma_i\sigma_j = \\ &= -\sum_{(i,j)\in\Gamma_+} J_{ij} - \sum_{(i,j)\in\Gamma_-} J_{ij} + \sum_{(i,j)\in\Delta} J_{ij} = \\ &= -C + 2\sum_{(i,j)\in\Delta} c_{ij} \end{aligned} \tag{C.3}$$

where $C = \sum_{(i,j)\in E} J_{ij}$ is a constant and c_{ij} is the *cut weight* for the ij-th edge. It follows that minimizing the energy is equivalent to choosing a cut in such a way that the second term is maximum. Therefore there is a strict correspondence between minimizing the energy of the magnetic system and finding a *max-cut* (or min-cun) of the graph representation of the lattice.

The MAX-FLOW MIN-CUT theorem. Let us consider a ferromagnetic system with $J_{ij} > 0$ in an external field $\{h_i\}_{i=1...N}$. The exact ground state can be found by means of the following algorithm. First, the magnetic system is mapped on the network $G = (\mathcal{V}, \mathcal{E})$, so that every spin corresponds to a vertex $i = 1...N$. In addition, two more special vertices are defined: the *source* ($i = 0$) and the *sink* ($i = N + 1$).

The lattice is divided into two subgraphs A, B, characterized by the values of the variable $t(i) = 1$, if $i \in A$, $t(i) = -1$ otherwise.

The undirected couplings of the system are mapped onto edges which are directed as $i \to j, i < j$. Moreover, for each site, there is an ingoing edge from the source, and an outgoing edge to the sink. An additional 'phantom' edge $(0, n + 1)$ is added, connecting the source to the sink. Each edge is provided with a non-negative capacity:

$$\forall i, j \in \{1, ..., N\} \quad c(i,j) = \begin{cases} 4J_{ij} & j \in \partial i, i < j \\ 0 & \text{otherwise} \end{cases} \tag{C.4}$$

Moreover:

$$\forall i: \quad w(i) = 2\sum_{j\in\partial i} J_{ij} - 2h_i t(i) - \sum_{j\in\partial i}$$

$$\text{if } w(i) \geq 0: \begin{cases} c(i, N+1) = w(i) \\ c(0,i) = 0 \end{cases}$$

$$\text{if } w(i) < 0: \begin{cases} c(i, N+1) = 0 \\ c(0,i) = -w(i) \end{cases}$$

In this way all the capacities are non-negative, except for the source-sink capacity:

$$c(0, n+1) = -\sum_{ij} J_{ij} + \sum_{i=1}^{N} h_i t(i) - \sum_{j=1}^{N} c(0,j) \tag{C.5}$$

A *cut* separating 0 and $n + 1$ is a partition $S, \overline{S}$ ($S \cup \overline{S} = V$, $S \cap \overline{S} = \emptyset$), such that $0 \in S$ and $n + 1 \in \overline{S}$. The cut can be specified by defining a vector

$X = \{1, x_1, ..., x_N, 0\}$ with $x_i = 1$ if $i \in S$, $x_i = 0$ otherwise. The capacity of the cut is the sum of the capacities of the edges directed from S to $\overline{S}$:

$$C(S, \overline{S}) = \sum_{i \in S, j \in \overline{S}} c(i,j) = \sum_{i,j=0}^{N+1} c(i,j) x_i (1 - x_j)$$

The last expression is a quadratic form which results in the hamiltonian of the system with the previous choice of $c(i,j)$, and $\sigma_i = (2x_i - 1)t(i)$.

In order to determine the capacity of the minimum cut, the max-flow min-cut theorem is used: the maximum flow through the network is equal to the capacity of the minimum cut. There are several algorithms which calculate the maximum flow. The *Ford-Fulkerson algorithm (FFA)* [195] works assigning flow values $f(i,j)$ to each edge and imposing the conservation of the flow at each edge. All the flows are initially set to zero. The flow through the network is then augmented stepwise starting from the sink, repeating the process until no more increment is possible. The value of $c(0, n+1)$ is only considered in a second moment, when is added to the result, being part of the edges connecting S to $\overline{S}$. The capacities are usually expressed as integer or rational numbers, in order to avoid convergence problems. The output of the FFA is a set of flows $\{f(i,j)\}$ and $(S, \overline{S})$ is a mincut if the edges connecting the two partitions fulfill the condition $f(i,j) < c(i,j)$. In systems with degeneracy, only one ground state can be found with this algorithm.

A more effective variation of the FFA algorithm is often used, the Edmonds–Karp algorithm, which runs in a time $O(VE^2)$.

Appendix D

Stability analysis via ϵ-coupling

The effects of the introduction of a bulk perturbation have been studied in literature mostly numerically. However, in [143], Pagnani and Parisi have approached the problem analytically, deriving the cavity equations in the case of Gaussian Bethe lattice spin glass with connectivity $k+1$, in presence of external field h_{ext}. The derivation is instructive because, beside the theoretical interest, it provides a method for detecting the AT line. We follow here the main arguments of the Pagnani-Parisi derivation and present some of the aspects which concern the topics exposed in this thesis.

We consider an Ising Bethe lattice spin glass, described by Hamiltonian:

$$\mathcal{H}[\sigma] = -\sum_{<i,j>} J_{ij}\sigma_i\sigma_j - h_{ext}\sum_i \sigma_i \tag{D.1}$$

Wefirst recall the Bethe approximation of the model, and then obtain the cavity equations for the ϵ-coupled model. We show that the instability of the 1RSB solution can be easily detected from the inconsistency of the solution at $q = 0$.

Bethe approximation Let us consider the merging process of k branches rooted at spins $i = 0, \ldots, k$ onto a new spin R. Before the merging, we leave the spin at the i root undetermined. The ground state energy is conditioned by the value of σ_i:

$$E(\sigma_i) = A_i - h_i\sigma_i \tag{D.2}$$

where A is a constant and h_i is an *effective* field. Note that h_i contains the effect of the external field. The energy of the system of k branches *before* the merging is the sum of the $E(\sigma_i)$ terms conditioned by the value of the spins $1, \ldots, k$.
The energy *after* the merging is

$$E'(\sigma_1, \ldots, \sigma_k, \sigma_R) = \sum_{i=1}^{k}(E_i(\sigma_i) - J_{Ri}\sigma_R\sigma_i) - h_{ext}\sigma_R \tag{D.3}$$

The ground state energy is found by minimizing E' with respect to $\sigma_1, \ldots, \sigma_R$ at fixed σ_R. This corresponds to choosing independently the sign of each σ_i such that $(h_i + J_{Ri}\sigma_R)\sigma_i = |h_i + J_{Ri}\sigma_R|$. The last term can be written as:

$$h_i + J_{Ri}\sigma_R = w(h_i, J_{Ri}) + \lambda(h_i, J_{Ri})\sigma_R \tag{D.4}$$

where

$$\begin{aligned} w(h_i, J_{Ri}) &= \frac{|h+J| + |h-J|}{2} \\ \lambda(h_i, J_{Ri}) &= \frac{|h+J| - |h-J|}{2} \end{aligned} \tag{D.5}$$

which results in

$$E'(\sigma_R) = \sum_{i=1}^{k} A_i - w(h_i, J_{Ri}) - (\lambda(h_i, J_{Ri} + h_{ext})\sigma_R \tag{D.6}$$

By comparing this formula with Eq.(D.2), one finds the recursion relation:

$$h_R = \sum_{i=1}^{k} \lambda(h_i, J_{Ri}) + h_{ext} \tag{D.7}$$

Cavity equations for the ϵ-coupled system We consider two systems described by two different set of variables. The first system, which depends on the variables σ_i, is described by the usual Hamiltonian:

$$\mathcal{H}_0[\sigma] = -\sum_{<i,j>} J_{ij}\sigma_i\sigma_j - h_{ext}\sum_i \sigma_i \tag{D.8}$$

where the coupling costants J_{ij} are i.i.d. variables with Gaussian distribution of mean 0 and variance 1. Let σ^0 be the ground state of $\mathcal{H}_0$, and let us consider a second system defined on the same Bethe lattice and depending on the variables τ (but also on the ground state $sigma^0$ which is fixed), with Hamiltonian:

$$\mathcal{H}_\epsilon[\tau] = -\sum_{<i,j>} J_{ij}\tau_i\tau_j - h_{ext}\sum_i \tau_i - \epsilon\sum_i \sigma_i^0\tau_i \tag{D.9}$$

The perturbation is repulsive if $\epsilon < 0$ (it increases the energy of σ^0), repulsive if $\epsilon > 0$. The ground state of $H_\epsilon[\tau]$ is τ^ϵ. We are interested in studying the overlap

$$q \equiv \overline{q_J} = \frac{1}{N}\sum_i \overline{\sigma_i^0\tau_i^\epsilon} \tag{D.10}$$

Let us consider the process of *iteration* (See 2.2, i.e. the merging of k branches onto the $k+1$-th site R described by an effective field (D.11):

$$h_R = \sum_{i=1}^{k} \lambda(h_i, J_{Ri}) + h_{ext} \tag{D.11}$$

The value of the effective field acting on τ_R in the second system depends on the value σ_R value in the first system. As a result, one needs to take into account three quantities related to merging of the branches onto the root R: the effective field h_R acting onto σ_R and the effective fields $h_R^\pm$ acting on τ_R under the condition $\sigma_R = \pm 1$.

The equation for h_R is exactly the same as Eq.(D.7) in the first system. The value of $\sigma_i^0 = \text{sign}(h_i + J_{Ri}\sigma_R^0)$ is determined by assuming in turn that $\sigma_R = \pm 1$. The effective field acting onto τ_R is thus:

$$h_R^{\sigma_R^0} = \sum_{i=1}^{k} \lambda(h_i^{\sigma_i^0}, J_i) + \epsilon\sigma_R^0 + h_{ext} \tag{D.12}$$

In order to measure the overlap, we can consider a new meging of $k+1$ branches onto a new node S. One obtains for the value of the effective fields of the two systems:

$$H_S = \sum_{i=1}^{k+1} \lambda(h_i, J_{S,i}) + h_{ext}; \quad H_S = \sum_{i=1}^{k+1} \lambda(h_i^{\sigma^0}, J_{S,i}) + \epsilon\sigma^0 + h_{ext} \tag{D.13}$$

The spins σ_S and τ_S take the orientation of the local field and the contribution to the overlap is $\sigma_S^0\tau_S^0$.

Results. The numerical results at $h_{ext} = 0$ show that for $\epsilon > 0$ the overlap is $q = -1$, as expected, and that for negative values the overlap decreases slowly from 1. The interesting part is that at $\epsilon = 0$, the overlap is $q = 0$, while one would expect that $q = 1$. This is a proof of the inconsistency of the RS solution, but it is not a problem. On the opposite, it is possible to perform the computation at $T > 0$ and find the value of h_{ext} where the $\epsilon = 0$ is inconsistent. In this way it possible to trace the AT line. This method gives for the critical field at zero temperature of the $J_\pm$ model the value $h_c \sim 1.037$ used in Chapter 6 as critical field.

Bibliography

[1] S. F. Edwards and P. W. Anderson. "Theory of spin glasses". *Journal of Physics F: Metal Physics* **5**: p. 965, 1975.

[2] D. Sherrington and S. Kirkpatrick. "Solvable model of a spin-glass". *Physical Review Letters* **35**: p. 1792, 1975.

[3] G. Parisi. "Infinite number of order parameters for spin-glasses". *Physical Review Letters* **43**: p. 1754, 1979.

[4] G. Parisi. "The order parameter for spin glasses: a function on the interval 0-1". *Journal of Physics A: Mathematical and General* **13**: p. 1101, 1980.

[5] M. Mézard and M. A. Virasoro. "The microstructure of ultrametricity". *Journal de Physique* **46**: pp. 1293–1307, 1985.

[6] M. Mézard et al. "Nature of the spin-glass phase". *Physical Review Letters* **52**: p. 1156, 1984.

[7] R. Rammal, G. Toulouse, and M. A. Virasoro. "Ultrametricity for physicists". *Reviews of Modern Physics* **58**: p. 765, 1986.

[8] F. Guerra. "Broken replica symmetry bounds in the mean field spin glass model". *Communications in mathematical physics* **233**: pp. 1–12, 2003.

[9] M. Talagrand. "The parisi formula". *Annals of mathematics*, pp. 221–263, 2006.

[10] M. Mézard and G. Parisi. "The Bethe lattice spin glass revisited". *The European Physical Journal B-Condensed Matter and Complex Systems* **20**: pp. 217–233, 2001.

[11] M. Mézard and G. Parisi. "The cavity method at zero temperature". *Journal of Statistical Physics* **111**: pp. 1–34, 2003.

[12] M. Mezard and A. Montanari. *Information, physics, and computation*. Oxford University Press, 2009.

[13] M. Mézard and G. Parisi. "Replicas and optimization". *Journal de Physique Lettres* **46**: pp. 771–778, 1985.

[14] M. Mézard and G. Parisi. "Mean-field equations for the matching and the travelling salesman problems". *EPL (Europhysics Letters)* **2**: p. 913, 1986.

[15] M. Mézard, G. Parisi, and R. Zecchina. "Analytic and algorithmic solution of random satisfiability problems". *Science* **297**: pp. 812–815, 2002.

[16] F. Krzakała et al. "Gibbs states and the set of solutions of random constraint satisfaction problems". *Proceedings of the National Academy of Sciences* **104**: pp. 10318–10323, 2007.

[17] T. R. Kirkpatrick, D. Thirumalai, and P. G. Wolynes. "Scaling concepts for the dynamics of viscous liquids near an ideal glassy state". *Physical Review A* **40**: p. 1045, 1989.

[18] A. Cavagna. "Supercooled liquids for pedestrians". *Physics Reports* **476**: pp. 51–124, 2009.

[19] G. Parisi and F. Zamponi. "Mean-field theory of hard sphere glasses and jamming". *Reviews of Modern Physics* **82**: p. 789, 2010.

[20] L. Leuzzi et al. "Phase diagram and complexity of mode-locked lasers: from order to disorder". *Physical Review Letters* **102**: p. 083901, 2009.

[21] C. Conti and L. Leuzzi. "Complexity of waves in nonlinear disordered media". *Physical Review B* **83**: p. 134204, 2011.

[22] M. Mézard, G. Parisi, and A. Zee. "Spectra of Euclidean random matrices". *Nuclear Physics B* **559**: pp. 689–701, 1999.

[23] R. Kühn. "Spectra of sparse random matrices". *Journal of Physics A: Mathematical and Theoretical* **41**: p. 295002, 2008.

[24] T. Rogers et al. "Cavity approach to the spectral density of sparse symmetric random matrices". *Physical Review E* **78**: p. 031116, 2008.

[25] M. Mezard and G. Parisi. "Replica field theory for random manifolds". *Journal de Physique I* **1**: pp. 809–836, 1991.

[26] F. Morcos et al. "Direct-coupling analysis of residue coevolution captures native contacts across many protein families". *Proceedings of the National Academy of Sciences* **108**: E1293–E1301, 2011.

[27] A. Decelle et al. "Asymptotic analysis of the stochastic block model for modular networks and its algorithmic applications". *Physical Review E* **84**: p. 066106, 2011.

[28] A. Decelle and F. Ricci-Tersenghi. "Pseudolikelihood decimation algorithm improving the inference of the interaction network in a general class of ising models". *Physical Review Letters* **112**: p. 070603, 2014.

[29] F. Krzakala et al. "Statistical-physics-based reconstruction in compressed sensing". *Physical Review X* **2**: p. 021005, 2012.

[30] J. J. Hopfield. "Neural networks and physical systems with emergent collective computational abilities". *Proceedings of the national academy of sciences* **79**: pp. 2554–2558, 1982.

[31] D. J. Amit, H. Gutfreund, and H. Sompolinsky. "Spin-glass models of neural networks". *Physical Review A* **32**: p. 1007, 1985.

[32] R. Monasson and R. Zecchina. "Weight space structure and internal representations: a direct approach to learning and generalization in multilayer neural networks". *Physical Review Letters* **75**: p. 2432, 1995.

[33] S. Franz, S. Hwang, and P. Urbani. "Jamming in multilayer supervised learning models". *arXiv preprint arXiv:1809.09945*, 2018.

[34] G. Parisi. "A simple model for the immune network". *Proceedings of the National Academy of Sciences* **87**: pp. 429–433, 1990.

[35] E. Agliari et al. "Multitasking associative networks". *Physical Review Letters* **109**: p. 268101, 2012.

[36] F. Altarelli et al. "Bayesian inference of epidemics on networks via belief propagation". *Physical Review Letters* **112**: p. 118701, 2014.

[37] F. Morone and H. A. Makse. "Influence maximization in complex networks through optimal percolation". *Nature* **524**: p. 65, 2015.

[38] J.-P. Bouchaud and M. Potters. *Theory of financial risk and derivative pricing: from statistical physics to risk management*. Cambridge university press, 2003.

[39] D. Challet, M. Marsili, and R. Zecchina. "Statistical mechanics of systems with heterogeneous agents: Minority games". *Physical Review Letters* **84**: p. 1824, 2000.

[40] L. Dall'Asta, M. Marsili, and P. Pin. "Collaboration in social networks". *Proceedings of the National Academy of Sciences* **109**: pp. 4395–4400, 2012.

[41] V. Bapst et al. "The quantum adiabatic algorithm applied to random optimization problems: The quantum spin glass perspective". *Physics Reports* **523**: pp. 127–205, 2013.

[42] M. Ballerini et al. "Interaction ruling animal collective behavior depends on topological rather than metric distance: Evidence from a field study". *Proceedings of the national academy of sciences* **105**: pp. 1232–1237, 2008.

[43] W. Bialek et al. "Social interactions dominate speed control in poising natural flocks near criticality". *Proceedings of the National Academy of Sciences* **111**: pp. 7212–7217, 2014.

[44] U. Bastolla and G. Parisi. "The modular structure of Kauffman networks". *Physica D: Nonlinear Phenomena* **115**: pp. 219–233, 1998.

[45] C. De Dominicis, I. Kondor, and T. Temesvári. "Beyond the sherrington-kirkpatrick model". In: *Spin glasses and random fields*. World Scientific, 1998. Pp. 119–160.

[46] D. S. Fisher and D. A. Huse. "Ordered phase of short-range Ising spin-glasses". *Physical Review Letters* **56**: p. 1601, 1986.

[47] D. S. Fisher and D. A. Huse. "Equilibrium behavior of the spin-glass ordered phase". *Physical Review B* **38**: p. 386, 1988.

[48] W. McMillan. "Scaling theory of Ising spin glasses". *Journal of Physics C: Solid State Physics* **17**: p. 3179, 1984.

[49] S. Franz and G. Parisi. "Non trivial overlap distributions at zero temperature". *The European Physical Journal B-Condensed Matter and Complex Systems* **18**: pp. 485–491, 2000.

[50] N. Biggs, E. K. Lloyd, and R. J. Wilson. *Graph Theory, 1736-1936*. Oxford University Press, 1986.

[51] B. Bollobás and B. Béla. *Random graphs*. 73. Cambridge university press, 2001.

[52] B. Bollobás. *Modern graph theory*. Vol. 184. Springer Science & Business Media, 2013.

[53] P. Erdös and A. Rényi. "On random graphs Publ". *Math. debrecen* **6**: pp. 290–297, 1959.

[54] S. Bornholdt and H. G. Schuster. *Handbook of graphs and networks: from the genome to the internet*. John Wiley & Sons, 2006.

[55] R. Pastor-Satorras and A. Vespignani. *Evolution and structure of the Internet: A statistical physics approach*. Cambridge University Press, 2007.

[56] J. Garcia-Ojalvo. "Physical approaches to the dynamics of genetic circuits: a tutorial". *Contemporary Physics* **52**: pp. 439–464, 2011.

[57] S. Boccaletti et al. "Complex networks: Structure and dynamics". *Physics reports* **424**: pp. 175–308, 2006.

[58] D. B. West et al. *Introduction to graph theory*. Vol. 2. Prentice hall Upper Saddle River, NJ, 1996.

[59] J. Park and M. E. Newman. "Statistical mechanics of networks". *Physical Review E* **70**: p. 066117, 2004.

[60] B. Bollobás. "A probabilistic proof of an asymptotic formula for the number of labelled regular graphs". *European Journal of Combinatorics* **1**: pp. 311–316, 1980.

[61] B. D. McKay and N. C. Wormald. "Uniform generation of random regular graphs of moderate degree". *Journal of Algorithms* **11**: pp. 52–67, 1990.

[62] A. Steger and N. C. Wormald. "Generating random regular graphs quickly". *Combinatorics, Probability and Computing* **8**: pp. 377–396, 1999.

[63] E. A. Bender and E. R. Canfield. "The asymptotic number of labeled graphs with given degree sequences". *Journal of Combinatorial Theory, Series A* **24**: pp. 296–307, 1978.

[64] N. C. Wormald. "The asymptotic distribution of short cycles in random regular graphs". *Journal of Combinatorial Theory, Series B* **31**: pp. 168–182, 1981.

[65] K. H. Fischer and J. A. Hertz. *Spin glasses*. Vol. 1. Cambridge university press, 1993.

[66] M. Mézard, G. Parisi, and M. Virasoro. *Spin glass theory and beyond: An Introduction to the Replica Method and Its Applications*. Vol. 9. World Scientific Publishing Company, 1987.

[67] S. Franz and M. Leone. "Replica bounds for optimization problems and diluted spin systems". *Journal of Statistical Physics* **111**: pp. 535–564, 2003.

[68] F. Zamponi. "Mean field theory of spin glasses". *arXiv preprint arXiv:1008.4844*, 2010.

[69] S. Edwards and P. Anderson. "Theory of spin glasses. II". *Journal of Physics F: Metal Physics* **6**: p. 1927, 1976.

[70] S. Franz, G. Parisi, and M. A. Virasoro. "Interfaces and louver critical dimension in a spin glass model". *Journal de Physique I* **4**: pp. 1657–1667, 1994.

[71] M. Mézard and G. Parisi. "On the solution of the random link matching problems". *Journal de Physique* **48**: pp. 1451–1459, 1987.

[72] G. Parisi and M. Ratiéville. "On the finite size corrections to some random matching problems". *The European Physical Journal B-Condensed Matter and Complex Systems* **29**: pp. 457–468, 2002.

[73] R. Brunetti et al. "Extensive numerical simulations of weighted matchings: Total length and distribution of links in the optimal solution". *EPL (Europhysics Letters)* **14**: p. 295, 1991.

[74] J. Houdayer, J. B. De Monvel, and O. Martin. "Comparing mean field and Euclidean matching problems". *The European Physical Journal B-Condensed Matter and Complex Systems* **6**: pp. 383–393, 1998.

[75] M. Talagrand. "The Sherrington–Kirkpatrick model: A challenge for mathematicians". *Probability Theory and Related Fields* **110**: pp. 109–176, 1998.

[76] M. Talagrand. *Spin glasses: a challenge for mathematicians: cavity and mean field models*. Vol. 46. Springer Science & Business Media, 2003.

[77] J. De Almeida and D. J. Thouless. "Stability of the Sherrington-Kirkpatrick solution of a spin glass model". *Journal of Physics A: Mathematical and General* **11**: p. 983, 1978.

[78] G. Parisi. "A sequence of approximated solutions to the SK model for spin glasses". *Journal of Physics A: Mathematical and General* **13**: p. L115, 1980.

[79] D. J. Thouless, P. W. Anderson, and R. G. Palmer. "Solution of'solvable model of a spin glass'". *Philosophical Magazine* **35**: pp. 593–601, 1977.

[80] G. Parisi. "Facing complexity". *Physica Scripta* **35**: p. 123, 1987.

[81] F. Guerra. "About the overlap distribution in mean field spin glass models". *International Journal of Modern Physics B* **10**: pp. 1675–1684, 1996.

[82] M. Aizenman and P. Contucci. "On the stability of the quenched state in mean-field spin-glass models". *Journal of statistical physics* **92**: pp. 765–783, 1998.

[83] G. Parisi. "On the probability distribution of the overlap in spin glasses". *International Journal of Modern Physics B* **18**: pp. 733–743, 2004.

[84] D. Ruelle. "A mathematical reformulation of Derrida's REM and GREM". *Communications in Mathematical Physics* **108**: pp. 225–239, 1987.

[85] L.-P. Arguin. "Spin glass computations and Ruelle's probability cascades". *Journal of Statistical Physics* **126**: pp. 951–976, 2007.

[86] C. De Dominicis and Y. Goldschmidt. "Replica symmetry breaking in finite connectivity systems: a large connectivity expansion at finite and zero temperature". *Journal of Physics A: Mathematical and General* **22**: p. L775, 1989.

[87] G. Parisi and F. Tria. "Spin glasses on Bethe lattices for large coordination number". *The European Physical Journal B-Condensed Matter and Complex Systems* **30**: pp. 533–541, 2002.

[88] S. Ghirlanda and F. Guerra. "General properties of overlap probability distributions in disordered spin systems. Towards Parisi ultrametricity". *Journal of Physics A: Mathematical and General* **31**: p. 9149, 1998.

[89] G. Parisi and F. Ricci-Tersenghi. "A numerical study of the overlap probability distribution and its sample-to-sample fluctuations in a mean-field model". *Philosophical Magazine* **92**: pp. 341–352, 2012.

[90] E. Marinari et al. "Numerical evidence for spontaneously broken replica symmetry in 3D spin glasses". *Physical Review Letters* **76**: p. 843, 1996.

[91] A. K. Hartmann. "Evidence for nontrivial ground-state structure of 3d±J spin glasses". *EPL (Europhysics Letters)* **40**: p. 429, 1997.

[92] S. Kirkpatrick. "Frustration and ground-state degeneracy in spin glasses". *Physical Review B* **16**: p. 4630, 1977.

[93] G. Grinstein, C. Jayaprakash, and M. Wortis. "Ising magnets with frustration: Zero-temperature properties from series expansions". *Physical Review B* **19**: p. 260, 1979.

[94] J. Reger and A. Zippelius. "Three-dimensional random-bond Ising model: Phase diagram and critical properties". *Physical Review Letters* **57**: p. 3225, 1986.

[95] R. Fisch. "High-temperature series for the±J random-bond Ising model". *Physical Review B* **44**: p. 652, 1991.

[96] R. R. Singh. "Spin-glass–ferromagnetic–paramagnetic multicritical point". *Physical Review Letters* **67**: p. 899, 1991.

[97] Y. Ozeki and H. Nishimori. "Phase diagram and critical exponents of the±J ising model in finite dimensions by Monte Carlo renormalization group". *Journal of the Physical Society of Japan* **56**: pp. 1568–1576, 1987.

[98] G. Migliorini and A. N. Berker. "Global random-field spin-glass phase diagrams in two and three dimensions". *Physical Review B* **57**: p. 426, 1998.

[99] J. Bendisch. "On the ground-state threshold in random two-dimensional Ising±J models". *Journal of statistical physics* **67**: pp. 1209–1217, 1992.

[100] J. Bendisch. "Groundstate threshold p_c in Ising frustration systems on 2D regular lattices". *Physica A: Statistical Mechanics and its Applications* **202**: pp. 48–67, 1994.

[101] N. Kawashima and H. Rieger. "Finite-size scaling analysis of exact ground states for±J spin glass models in two dimensions". *EPL (Europhysics Letters)* **39**: p. 85, 1997.

[102] A. K. Hartmann. "Ground-state behavior of the three-dimensional±J random-bond Ising model". *Physical Review B* **59**: p. 3617, 1999.

[103] J. Cardy. *Scaling and renormalization in statistical physics*. Vol. 5. Cambridge university press, 1996.

[104] H. Ballesteros et al. "Measures of critical exponents in the four-dimensional site percolation". *Physics Letters B* **400**: pp. 346–351, 1997.

[105] F. Ritort and M. Sales. "A conjectured scenario for order-parameter fluctuations in spin glasses". *Journal of Physics A: Mathematical and General* **33**: p. 6505, 2000.

[106] F. Cooper, B. Freedman, and D. Preston. "Solving $\varphi^4_{1,2}$ field theory with Monte Carlo". *Nuclear Physics B* **210**: pp. 210–228, 1982.

[107] H. Ballesteros et al. "Critical behavior of the three-dimensional Ising spin glass". *Physical Review B* **62**: p. 14237, 2000.

[108] G. Parisi et al. "Mean field dynamical exponents in finite-dimensional Ising spin glass". *Journal of Physics A: Mathematical and General* **30**: p. 7115, 1997.

[109] E. Marinari et al. "Off-equilibrium dynamics at very low temperatures in three-dimensional spin glasses". *Journal of Physics A: Mathematical and General* **33**: p. 2373, 2000.

[110] G. Parisi, F. Ricci-Tersenghi, and J. J. Ruiz-Lorenzo. "Equilibrium and off-equilibrium simulations of the Gaussian spin glass". *Journal of Physics A: Mathematical and General* **29**: p. 7943, 1996.

[111] L. Berthier and J. P. Bouchaud. "Geometrical aspects of aging and rejuvenation in the Ising spin glass: A numerical study". *Physical Review B* **66**: p. 054404, 2002.

[112] E. Marinari and G. Parisi. "Effects of a bulk perturbation on the ground state of 3D Ising spin glasses". *Physical Review Letters* **86**: p. 3887, 2001.

[113] H. G. Katzgraber and A. P. Young. "Probing the Almeida-Thouless line away from the mean-field model". *Physical Review B* **72**: p. 184416, 2005.

[114] A. Young and H. G. Katzgraber. "Absence of an Almeida-Thouless line in three-dimensional spin glasses". *Physical Review Letters* **93**: p. 207203, 2004.

[115] G. Parisi. "Some considerations of finite-dimensional spin glasses". *Journal of Physics A: Mathematical and Theoretical* **41**: p. 324002, 2008.

[116] E. Marinari et al. "Small window overlaps are effective probes of replica symmetry breaking in three-dimensional spin glasses". *Journal of Physics A: Mathematical and General* **31**: p. L481, 1998.

[117] F. Krzakala et al. "Zero-temperature responses of a 3D spin glass in a magnetic field". *Physical Review Letters* **87**: p. 197204, 2001.

[118] J.-P. Bouchaud, F. Krzakala, and O. Martin. "Energy exponents and corrections to scaling in Ising spin glasses". *Physical Review B* **68**: p. 224404, 2003.

[119] F. Krzakała and G. Parisi. "Local excitations in mean-field spin glasses". *EPL (Europhysics Letters)* **66**: p. 729, 2004.

[120] J. Houdayer and O. Martin. "A geometrical picture for finite-dimensional spin glasses". *EPL (Europhysics Letters)* **49**: p. 794, 2000.

[121] J. Houdayer, F. Krzakala, and O. Martin. "Large-scale low-energy excitations in 3-d spin glasses". *The European Physical Journal B-Condensed Matter and Complex Systems* **18**: pp. 467–477, 2000.

[122] A. Bray and M. Moore. "Scaling theory of the ordered phase of spin glasses". In: *Heidelberg Colloquium on glassy dynamics*. Springer. 1987. Pp. 121–153.

[123] T. Aspelmeier, M. Moore, and A. Young. "Interface energies in Ising spin glasses". *Physical Review Letters* **90**: p. 127202, 2003.

[124] F. Krzakala and O. Martin. "Spin and link overlaps in three-dimensional spin glasses". *Physical Review Letters* **85**: p. 3013, 2000.

[125] M. Palassini and A. Young. "Nature of the spin glass state". *Physical Review Letters* **85**: p. 3017, 2000.

[126] E. Marinari and G. Parisi. "Effects of changing the boundary conditions on the ground state of Ising spin glasses". *Physical Review B* **62**: p. 11677, 2000.

[127] P. Contucci et al. "Ultrametricity in the Edwards-Anderson model". *Physical Review Letters* **99**: p. 057206, 2007.

[128] B. Derrida. "Random-energy model: Limit of a family of disordered models". *Physical Review Letters* **45**: p. 79, 1980.

[129] B. Derrida. "Random-energy model: An exactly solvable model of disordered systems". *Physical Review B* **24**: p. 2613, 1981.

[130] J. Lamarcq et al. "Non-compact local excitations in spin-glasses". *EPL (Europhysics Letters)* **58**: p. 321, 2002.

[131] J. Lamarcq, J.-P. Bouchaud, and O. Martin. "Local excitations of a spin glass in a magnetic field". *Physical Review B* **68**: p. 012404, 2003.

[132] M. Palassini and A. Young. "Triviality of the ground state structure in Ising spin glasses". *Physical Review Letters* **83**: p. 5126, 1999.

[133] M. Cieplak and J. Banavar. "Scaling of stiffness in Ising spin glasses". *Journal of Physics A: Mathematical and General* **23**: p. 4385, 1990.

[134] A. K. Hartmann. "Scaling of stiffness energy for three-dimensional±J Ising spin glasses". *Physical Review E* **59**: p. 84, 1999.

[135] A. K. Hartmann. "Calculation of ground states of four-dimensional±J Ising spin glasses". *Physical Review E* **60**: p. 5135, 1999.

[136] A. Carter, A. Bray, and M. Moore. "Aspect-ratio scaling and the stiffness exponent θ for Ising spin glasses". *Physical Review Letters* **88**: p. 077201, 2002.

[137] A. K. Hartmann et al. "Stiffness exponent of two-dimensional Ising spin glasses for nonperiodic boundary conditions using aspect-ratio scaling". *Physical Review B* **66**: p. 224401, 2002.

[138] S. Boettcher. "Numerical results for ground states of spin glasses on Bethe lattices". *The European Physical Journal B-Condensed Matter and Complex Systems* **31**: pp. 29–39, 2003.

[139] A. Bray and M. Moore. "Lower critical dimension of Ising spin glasses: a numerical study". *Journal of Physics C: Solid State Physics* **17**: p. L463, 1984.

[140] W. McMillan. "Domain-wall renormalization-group study of the three-dimensional random Ising model". *Physical Review B* **30**: p. 476, 1984.

[141] M. Palassini and A. Young. "Evidence for a trivial ground-state structure in the two-dimensional Ising spin glass". *Physical Review B* **60**: R9919, 1999.

[142] A. K. Hartmann and A. Young. "Lower critical dimension of Ising spin glasses". *Physical Review B* **64**: p. 180404, 2001.

[143] A. Pagnani, G. Parisi, and M. Ratieville. "Near-optimal configurations in mean-field disordered systems". *Physical Review E* **68**: p. 046706, 2003.

[144] A. K. Hartmann. "Cluster-exact approximation of spin glass groundstates". *Physica A: Statistical Mechanics and its Applications* **224**: pp. 480–488, 1996.

[145] A. K. Hartmann and H. Rieger. "New optimization algorithms in physics". 2004.

[146] A. Hartwig, F. Daske, and S. Kobe. "A recursive branch-and-bound algorithm for the exact ground state of Ising spin-glass models". *Computer Physics Communications* **32**: pp. 133–138, 1984.

[147] C. De Simone et al. "Exact ground states of Ising spin glasses: New experimental results with a branch-and-cut algorithm". *Journal of Statistical Physics* **80**: pp. 487–496, 1995.

[148] C. De Simone et al. "Exact ground states of two-dimensional±J Ising spin glasses". *Journal of Statistical Physics* **84**: pp. 1363–1371, 1996.

[149] S. Boettcher and A. Percus. "Nature's way of optimizing". *Artificial Intelligence* **119**: pp. 275–286, 2000.

[150] S. Boettcher and A. G. Percus. "Optimization with extremal dynamics". *complexity* **8**: pp. 57–62, 2002.

[151] S. Boettcher. "Extremal optimization for Sherrington-Kirkpatrick spin glasses". *The European Physical Journal B-Condensed Matter and Complex Systems* **46**: pp. 501–505, 2005.

[152] S. Boettcher. "Stiffness exponents for lattice spin glasses in dimensions $d = 3, \ldots, 6$". *The European Physical Journal B-Condensed Matter and Complex Systems* **38**: pp. 83–91, 2004.

[153] S. Boettcher. "Numerical results for spin glass ground states on Bethe lattices: Gaussian bonds". *The European Physical Journal B* **74**: pp. 363–371, 2010.

[154] A. K. Hartmann. "Are ground states of 3D±J spin glasses ultrametric?" *EPL (Europhysics Letters)* **44**: p. 249, 1998.

[155] A. K. Hartmann. "Ground-state clusters of two-, three-, and four-dimensional±J Ising spin glasses". *Physical Review E* **63**: p. 016106, 2000.

[156] A. Hartmann. "How to evaluate ground-state landscapes of spin glasses thermodynamical correctly". *The European Physical Journal B-Condensed Matter and Complex Systems* **13**: pp. 539–545, 2000.

[157] G. Hed et al. "Spin domains generate hierarchical ground state structure in J=±1 spin glasses". *Physical Review Letters* **86**: p. 3148, 2001.

[158] A. K. Hartmann. "Analysis of the statistical behavior of the genetic cluster-exact approximation". *Physica A: Statistical Mechanics and its Applications* **275**: pp. 1–14, 2000.

[159] C. Lucibello, T. Rizzo, and M. Angelini. Private communication.

[160] A. Hartmann and K. Usadel. "Exact determination of all ground states of random field systems in polynomial time". *Physica A: Statistical Mechanics and its Applications* **214**: pp. 141–152, 1995.

[161] A. Hartmann and A. Young. "Large-scale low-energy excitations in the two-dimensional Ising spin glass". *Physical Review B* **66**: p. 094419, 2002.

[162] A. V. Goldberg et al. "Maximum Flows by Incremental Breadth-First Search". In: *Algorithms – ESA 2011*. Springer Berlin Heidelberg, 2011. Pp. 457–468.

[163] A. V. Goldberg et al. "Faster and More Dynamic Maximum Flow by Incremental Breadth-First Search". In: *Algorithms - ESA 2015*. Springer Berlin Heidelberg, 2015. Pp. 619–630.

[164] A. Sandvik. "Comment on" Evidence for nontrivial ground-state structure of 3d ±J spin glasses"". *EPL (Europhysics Letters)* **45**:

[165] A. K. Hartmann. "Reply to comment on "Evidence for nontrivial ground-state structure of 3d ±Jspin glasses"". *Europhysics Letters (EPL)* **45**: pp. 747–748, 1999. DOI: 10.1209/epl/i1999-00232-4.

[166] M. Mézard et al. "Replica symmetry breaking and the nature of the spin glass phase". *Journal de Physique* **45**: pp. 843–854, 1984.

[167] S. Franz, G. Parisi, and M. Virasoro. "Ultrametricity in an inhomogeneous simplest spin glass model". *EPL (Europhysics Letters)* **17**: p. 5, 1992.

[168] N. Parga, G. Parisi, and M. A. Virasoro. "A numerical investigation of the overlap distribution among pure states in the spin glass phase". *Journal de Physique Lettres* **45**: pp. 1063–1069, 1984.

[169] R. N. Bhatt and A. Young. "Long range Ising spin glasses: critical behavior and ultrametricity". *Journal of Magnetism and Magnetic Materials* **54**: pp. 191–193, 1986.

[170] S. Caracciolo et al. "Low temperature behaviour of 3-D spin glasses in a magnetic field". *Journal de Physique* **51**: pp. 1877–1895, 1990.

[171] A. Cacciuto, E. Marinari, and G. Parisi. "A numerical study of ultrametricity in finite-dimensional spin glasses". *Journal of Physics A: Mathematical and General* **30**: p. L263, 1997.

[172] E. Marinari, G. Parisi, and J. Ruiz-Lorenzo. "Numerical simulations of spin glass systems". In: *Spin Glasses and Random Fields*. World Scientific, 1998. Pp. 59–98.

[173] G. Parisi, F. Ritort, and F. Slanina. "Several results on the finite-size corrections in the Sherrington-Kirkpatrick spin-glass model". *Journal of Physics A: Mathematical and General* **26**: p. 3775, 1993.

[174] M. Palassini. "Ground-state energy fluctuations in the Sherrington–Kirkpatrick model". *Journal of Statistical Mechanics: Theory and Experiment* **2008**: P10005, 2008.

[175] T. Aspelmeier et al. "Finite-size corrections in the sherrington–kirkpatrick model". *Journal of Physics A: Mathematical and Theoretical* **41**: p. 324008, 2008.

[176] H. G. Katzgraber et al. "Universality-class dependence of energy distributions in spin glasses". *Physical Review B* **72**: p. 094421, 2005.

[177] S. Boettcher. "Simulations of ground state fluctuations in mean-field Ising spin glasses". *Journal of Statistical Mechanics: Theory and Experiment* **2010**: P07002, 2010.

[178] S. Boettcher. "Numerical results for ground states of mean-field spin glasses at low connectivities". *Physical Review B* **67**: p. 060403, 2003.

[179] A. Andreanov, F. Barbieri, and O. Martin. "Large deviations in spin-glass ground-state energies". *The European Physical Journal B-Condensed Matter and Complex Systems* **41**: pp. 365–375, 2004.

[180] C. Monthus and T. Garel. "Matching between typical fluctuations and large deviations in disordered systems: application to the statistics of the ground state energy in the SK spin-glass model". *Journal of Statistical Mechanics: Theory and Experiment* **2010**: P02023, 2010.

[181] J. P. Bouchaud and M. Mézard. "Universality classes for extreme-value statistics". *Journal of Physics A: Mathematical and General* **30**: p. 7997, 1997.

[182] A. Crisanti et al. "Replica trick and fluctuations in disordered systems". *Journal de Physique I* **2**: pp. 1325–1332, 1992.

[183] G. Parisi and T. Rizzo. "Large deviations in the free energy of mean-field spin glasses". *Physical Review Letters* **101**: p. 117205, 2008.

[184] G. Parisi and T. Rizzo. "Phase diagram and large deviations in the free energy of mean-field spin glasses". *Physical Review B* **79**: p. 134205, 2009.

[185] G. Parisi and T. Rizzo. "Large deviations of the free energy in diluted mean-field spin-glass". *Journal of Physics A: Mathematical and Theoretical* **43**: p. 045001, 2009.

[186] G. Parisi and T. Rizzo. "Universality and deviations in disordered systems". *Physical Review B* **81**: p. 094201, 2010.

[187] T. Aspelmeier. "An exact relation between free energy fluctuations and bond chaos in the Sherrington–Kirkpatrick model". *Journal of Statistical Mechanics: Theory and Experiment* **2008**: P04018, 2008.

[188] T. Aspelmeier. "Free-energy fluctuations and chaos in the Sherrington-Kirkpatrick model". *Physical Review Letters* **100**: p. 117205, 2008.

[189] J. Wehr and M. Aizenman. "Fluctuations of extensive functions of quenched random couplings". *Journal of Statistical Physics* **60**: pp. 287–306, 1990.

[190] G. Parisi. "Order parameter for spin-glasses". *Physical Review Letters* **50**: p. 1946, 1983.

[191] E. Marinari et al. "Replica symmetry breaking in short-range spin glasses: Theoretical foundations and numerical evidences". *Journal of Statistical Physics* **98**: pp. 973–1074, 2000.

[192] G. Parisi and G. Toulouse. "A Simple hypothesis for the spin glass phase of the infinite-ranged SK model". *Journal de Physique Lettres* **41**: pp. 361–364, 1980.

[193] J. Vannimenus, G. Toulouse, and G. Parisi. "Study of a simple hypothesis for the mean-field theory of spin-glasses". *Journal de Physique* **42**: pp. 565–571, 1981.

[194] M. Mézard, G. Parisi, and M. Virasoro. "Random free energies in spin glasses". *Journal de Physique Lettres* **46**: pp. 217–222, 1985.

[195] L. R. Ford and D. R. Fulkerson. "Maximal flow through a network". In: *Classic papers in combinatorics*. Springer, 2009. Pp. 243–248.

List of Figures

List of Tables